# Targeted Lipid Nanoparticles for Retinal Drug Delivery

Dissertation to obtain the Degree of Doctor of Natural Sciences
(Dr. rer. nat.)
From the Faculty of Chemistry and Pharmacy
University of Regensburg


Presented by
**Marilena Bohley**
from Coburg (Germany)

August 2021

Marilena Bohley

# Targeted Lipid Nanoparticles for Retinal Drug Delivery

# Targeted Lipid Nanoparticles for Retinal Drug Delivery

Dissertation to obtain the Degree of Doctor of Natural Sciences
(Dr. rer. nat.)
From the Faculty of Chemistry and Pharmacy
University of Regensburg


Presented by
**Marilena Bohley**
from Coburg (Germany)

August 2021

This work was carried out from July 2017 until July 2021 at the Department of Pharmaceutical Technology at the University Regensburg.

The thesis was prepared under supervision of Prof. Dr. Achim Göpferich.


| | |
|---|---|
| Doctoral application submitted on: | 05.08.2021 |
| Date of examination: | 14.10.2021 |
| Examination board: | |
| Chairman: | Prof. Dr. Sigurd Elz |
| 1st Expert: | Prof. Dr. Achim Göpferich |
| 2nd Expert: | Prof. Dr. Ernst Tamm |
| 3rd Examiner: | Prof. Dr. Joachim Wegener |

*To my dear ones*

‘*be less curious about people and more curious about ideas*’

*Marie Curie*

# Table of contents


| | | |
|---|---|---|
| **Chapter 1** | Introduction<br>The retinal pigment epithelium: An emerging therapeutic target | 9 |
| **Chapter 2** | Goals of the Thesis | 43 |
| **Chapter 3** | Intracellular availability of poorly soluble drugs from lipid nanocapsules | 51 |
| **Chapter 4** | Design of dye and superparamagnetic iron oxide nanoparticle loaded lipid nanocapsules with dual detectability in vitro and in vivo | 85 |
| **Chapter 5** | Targeted Lipid Nanoparticles for the Treatment of Neovascular Ocular Diseases | 115 |
| **Chapter 6** | Summary and Conclusion | 156 |
| **Appendix** | Abbreviations | 165 |
| | Curriculum Vitae | 169 |
| | List of Publications | 170 |
| | Acknowledgements | 171 |
| | Statement in Lieu of an Oath | 173 |

# Chapter 1

---

# The retinal pigment epithelium:

# An emerging therapeutic target

# Abstract

The major culprit for the initiation and progression of various sight threatening diseases are malfunctions of the retinal pigment epithelium (RPE). In this review, we shed light on the underestimated cell monolayer in terms of its role in health and disease and explain why a paradigm shift towards targeted RPE therapy is needed to overcome drawbacks and limitations of current treatment options. A comprehensive overview is given of the possible routes to reach the RPE and challenges faced by drug delivery to the RPE are discussed. More so, we highlight different successful nanoparticle approaches, and further provide insights for rational nanoparticle design principles for targeted RPE drug delivery.

# 1 The RPE's importance for vision

Besides cancer, blindness is the most dreaded disease worldwide (*1*). More than 50% of the ocular diseases causing partial or complete blindness, including retinitis pigmentosa, posterior uveitis, proliferative vitreoretinopathy, posterior uveitis, age-related macular degeneration, diabetic retinopathy and retinopathy of prematurity are associated with inherited or acquired malfunctions of the retinal pigment epithelium (RPE) (*2*). The RPE is not only involved in almost all pathologic events and thus an extraordinary contributor to the induction and progression of these diseases, but crucial for normal retinal and visual function. The importance of the RPE, however, contrasts sharply with the inconspicuousness of the simple cell monolayer that is interposed between the choriocapillaris and the neurosensory retina (Fig. 1) (*3*).

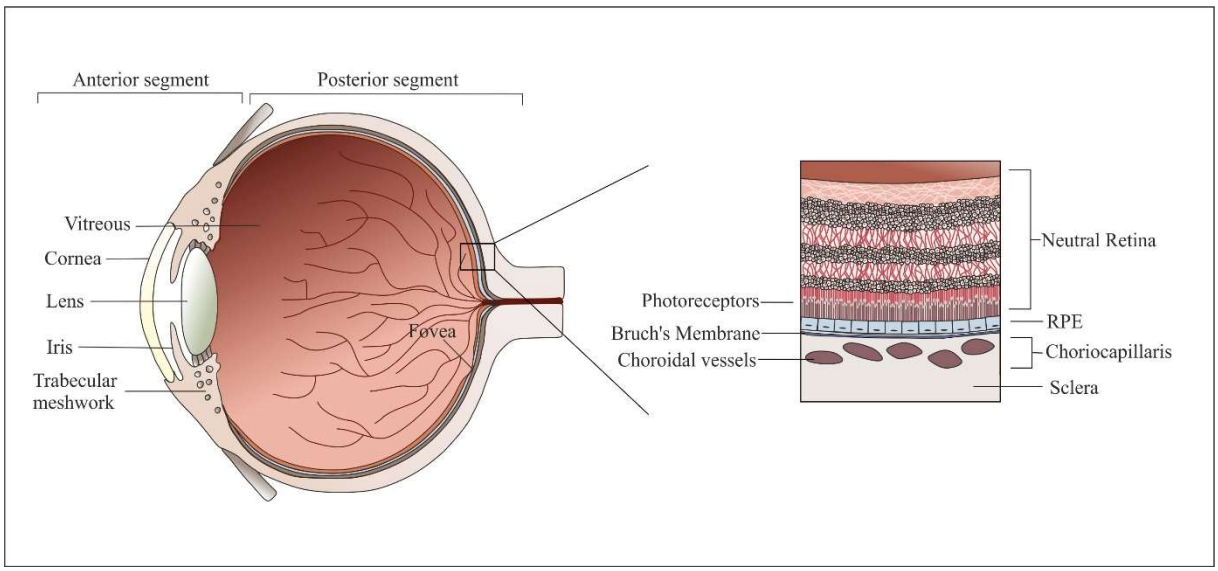


***Figure 1.*** *The anterior segment of the eye, consisting of the cornea, iris and trabecular meshwork, is separated from the posterior segment by the lens. The posterior segment consists primarily of the vitreous, retina, retinal pigment epithelium (RPE), Bruch's Membrane and choriocapillaris. The RPE is localized in the posterior eye at the interface between the neural retina and choriocapillaris.*

By virtue of its location and in its quest for optimal retinal function, the RPE exhibits a polarized structure with the cuboidal RPE cells being structurally and functionally asymmetric (Fig. 2). On the photoreceptor facing, apical side, the RPE emits long microvilli for the interaction with photoreceptor outer segments and interphotoreceptor extracellular matrix (*4*). On the basal side, the RPE faces Bruch's Membrane (BM), a multilayered extracellular matrix structure that separates the RPE from the fenestrated choroid, therefore building an

interface for nutrient and signaling molecule exchange between retina and blood stream. For efficient adsorption and secretion from and to the blood stream, the basal membrane of RPE cells is embellished with numerous infoldings which increase the overall surface area (Fig. 2) (*3–5*). The polarized structure of the RPE is preserved by tight junctions, leading to the formation of a tight epithelium, and therefore creating a barrier for the free passage of molecules and ions into and out of the retina (*6*).

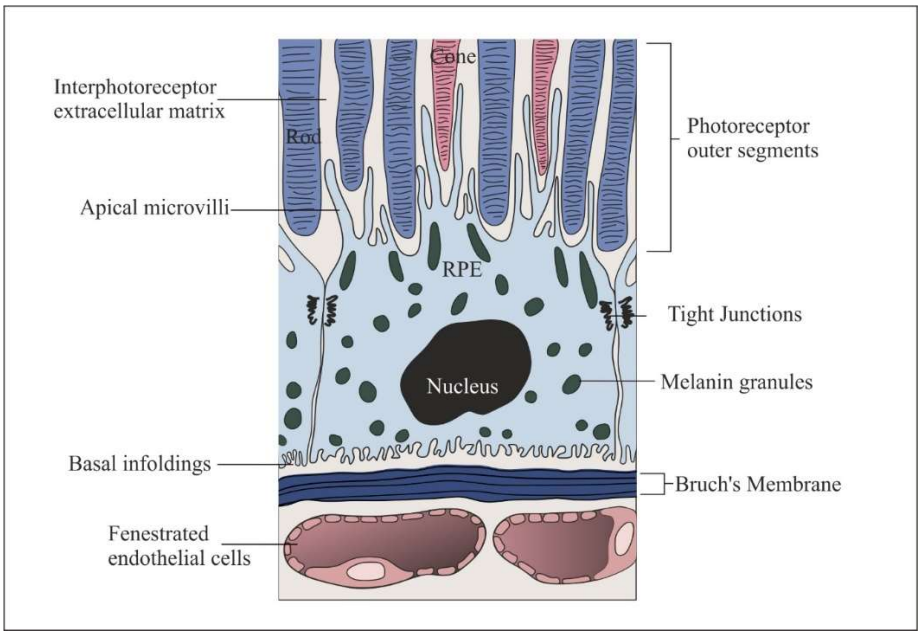


***Figure 2.*** *RPE cell polarity and structure. On the apical side RPE cells emit microvilli facing the photoreceptor outer segments and interphotoreceptor extracellular matrix. On the basal side, RPE cells exhibit infoldings towards the Bruch's Membrane that separated RPE from the fenestrated endothelium of the choriocapillaris. Tight junctions between neighboring RPE cells preserve the polarized structure of the RPE and enable the strict control of nutrients and fluids into the retina.*

As photoreceptors lack direct blood supply, RPE cells must manage and control the bi-directional transport of ions and molecules to and from the photoreceptor layer (Fig. 3). Specialized transport proteins in the apical and basal RPE cell membrane enable the supply of nutrients to the highly metabolic active photoreceptors as well as the removal of waste products and water. With an asymmetric distribution and regulation of these mechanisms, RPE cells control the passage of ions like $Cl^-$, $K^+$, $Na^+$ and $HCO_3^-$ to and from the retina and thus regulate cell membrane polarization and hyperpolarization, fluid transport and pH (Fig. 3). By being responsible for maintaining the volume and chemical composition of the subretinal space, the RPE exhibits a function crucial for phototransduction (*7*). In addition to the transcellular transport of ions and water, RPE cells absorb and transport various nutrients from the blood to the photoreceptors using membrane transporters present on both the apical and basolateral

surface. To nourish the photoreceptors, RPE cells absorb, glucose, different amino acids including taurine, alanine, glutamine and leucine, and fatty acids like docosahexaenoic acid from the blood stream and deliver it to the photoreceptors (Fig. 3) (*3*).

Together, the trans-RPE transport is coordinated by a variety of asymmetrically distributed channels and transporters regulating the retinal microenvironment and further providing the overall framework for a functioning retinal system (*2*).

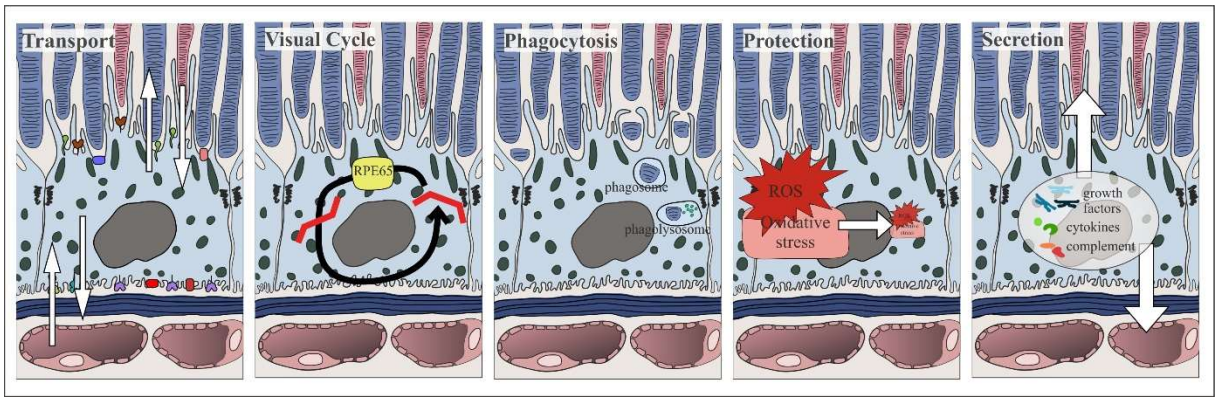


***Figure 3.*** *By virtue of their location and function as retinal caretakers, RPE cells: 1) Manage the transport of nutrients, ions, water and waste products from the blood to the retina and vice versa. 2) Control the release, processing, transport and uptake of retinal (visual cycle). 3) Phagocytose and recycle shed photoreceptor outer segments. 4) Protecting the retina against ROS and oxidative damage. 5) Preserve retinal cell function and homeostasis as well as immune privilege of the eye by producing and secreting various growth factors, cytokines and complements.*

Another key function of the RPE is the release, transport, processing, and uptake of vitamin A (all-trans retinal), known as visual cycle (Fig. 3) (*8*). The first step in the process of vision is absorption of light energy by photoreceptor visual pigments (rhodopsin in rods and cone-opsins in cones). Subsequently, the activation of visual pigment induces a change in the conformation of the chromophore: from 11-cis retinal to all-trans retinal. Since photoreceptors are unable to convert all-trans retinal back to 11-cis retinal, it is transferred to RPE cells for recycling. RPE cells internalize the all-trans retinal, reconvert it into its 11-cis isomer and deliver it back to the photoreceptors (*9*). This metabolic process of continuous visual pigment regeneration after light activation is key to maintain light sensitivity. In addition to vitamin A transport and recycling, RPE cells preserve intraretinal vitamin A levels by using specific retinol-binding proteins to take it up from the blood stream (*10, 11*).

The process of vision, that requires continuous light exposure of photosensitive molecules, is accompanied by photo-oxidative damage of proteins and lipids in the photoreceptor outer segments. Hence, to maintain excitability of photoreceptors and ensure proper visual function,

photoreceptor outer segments undergo a constant renewal process. In humans, photoreceptor outer segments are completely renewed every 11 days (*5*). In this regeneration process, new photoreceptor outer segments are constantly assembled from the connecting cilium, while the old segments are shed and subsequently phagocytosed by the RPE (Fig. 3). Mechanistically, the phagocytotic processes of RPE cells resemble the recognition and elimination of apoptotic cells by macrophages (*12*). However, even though a vast number of putative receptor molecules have been identified, including mannose-6-phosphate receptor, melatonin receptors MT1 and MT2, megalin receptor, scavenger receptor CD36, $\alpha_v\beta_5$ integrin, MerTK, a transmembrane tyrosine kinase receptor and a number of glycoproteins expressed on the RPE surface, signaling mechanisms for segment binding and ingestion are still not fully understood (*13*). Upon receptor mediated ingestion, the phagosome merges with a lysosome, where numerous lysosomal enzymes digest proteins, polysaccharides, lipids, and nucleic acids. The resulting end products are afterwards either recycled or disposed into the blood stream via the choroid (*8*). Since the segments are rich in lipids, the transport and recycling of docosahexaenoic acid (DHA) and cholesterol are particularly important. While the transport mechanism of DHA back to the photoreceptors is still unclear, cholesterol is disposed either apically or basally via ABCA1 transporters and therefore fosters the formation of basolateral and apical cholesterol depositions (drusen) (*5, 14*).

The combination of constant light exposure, high oxygen levels caused by the choroids' extraordinary high blood perfusion (*15*), and high levels of metabolic activity provoke creation of reactive oxygen species (ROS) and processes of photo-oxidation. Subsequently leading to oxidative damage of proteins, DNA and lipids (*2*). In order to protect the retina against ROS and to minimize oxidative damage, the RPE provides three staggered defense strategies. The first is the absorption and filtering of light by pigments like melanin. The second relies on the on-demand neutralization of ROS by enzymatic (superoxide dismutase and catalase) and non-enzymatic antioxidants (glutathione, ascorbate, a-tocopherol, carotenoids, melanin). Finally, the third line of defense is the repair or replacement of damaged DNA, lipids, and proteins, in case that oxidative damage was inevitable (*3, 8*). With these defense lines, the RPE preserves not only itself, but the integrity and function of neighboring cells.

Additionally, as retinal caretaker, the RPE provides numerous growth factors and cytokines that are essential for the functional integrity of the retina and the choroid (Fig. 3) (*16, 17*). These include pigment epithelium-derived factor (PEDF), vascular endothelial growth factor (VEGF), fibroblast growth factors (FGF-1, FGF-2, and FGF-5), insulin-like growth factor-I (IGF-I), ciliary neurotrophic factor (CNTF), platelet-derived growth factor (PDGF), lens epithelium-derived growth factor (LEDGF), tumor necrosis factor α (TNF-α), transforming growth factor-β (TGF-β), and various interleukins (IL) (*8*). While PEDF is a neuroprotective and antiangiogenic factor, that protects neurons against hypoxia induced apoptosis, inhibits

endothelial cell proliferation and stabilizes the choroid (*18, 19*), VEGF is an angiogenic factor and prevents endothelial cell apoptosis, leads to the stabilization of endothelial fenestrations and is essential for the integrity of the choroid. Additionally, VEGF acts as a survival factor for various retinal cells, including Müller cells, astrocytes, ganglion cells, glial cells and RPE cells themselves (*20*). Another angiogenic factor is the growth promoting factor FGF, that induces proliferation and differentiation of endothelial cells, fibroblasts, epithelial cells and smooth muscle cells (*8*). However, even though, many of these peptides are constitutively expressed and it is known that changes in their expression play crucial roles in all retinal diseases, the sensitive interactions between growth factor expression and retinal homeostasis are still not fully understood (*2*).

Furthermore, the RPE is essential for establishing and maintaining the immune privilege of the eye by being part of the blood-retinal barrier separating the retina from the bloodstream. As an immune privileged tissue, circulating immune cells are under normal physiological conditions not able to enter the retina in order to deal with endogenous insults. Nevertheless, the retina exhibits a unique immune defense system against exogenous and endogenous insults consisting of retinal immune cells (microglia, perivascular macrophages, and dendritic cells) and the complement system. The complement system, an important part of the innate immune system, comprises over 30 proteins and protein fragments that complement antibodies and phagocytes aiming to inactivate pathogens. Even though it is constantly active at a low-level, activation via either the classical or alternative pathway is needed to obtain substantial immune responses (*21, 22*). By producing anti-inflammatory and pro-inflammatory cytokines that play an important role in the development of immune and inflammatory responses, RPE cells are able to activate immune cells and stimulate inflammatory responses (*16, 22*). Moreover, RPE cells appear, besides retinal microglia, to be the major sources of retinal complement, thus, controlling both parts of the ocular defense system (*22*).

On the pro-inflammatory site, IL-1 is one of the most potent multifunctional cell activators, stimulating immune cells and other cell types, subsequently activating immune and inflammatory responses. IL-6 has similar activities as IL-1 and both can have synergistic effects. While TNF-α exclusively exhibits potent pro-inflammatory potential, the properties of TGF-β, whether inflammatory or immunosuppressive are concentration dependent (*23*). Finally, it is noteworthy to mention that, in case of IL-1, IL-6, IL-15, TNF-α, TGF-β, FGF, IGF-1, VEGF and PDGF, RPE cells do not only express the ligand but the corresponding receptor, indicating autocrine regulation. In addition to the autocrine effects, RPE-derived cytokines affect various other cells in the posterior eye, including vascular endothelial cells and Müller cells and further influence complement production by the RPE (*3, 8, 13, 23*).

## 2 The RPE changes with age

Since the RPE is a non-regenerative tissue, a number of irreversible structural and functional changes occur as it ages, affecting RPE cell function as well as adjacent cells and tissues like the BM (Fig. 4) (*24*).

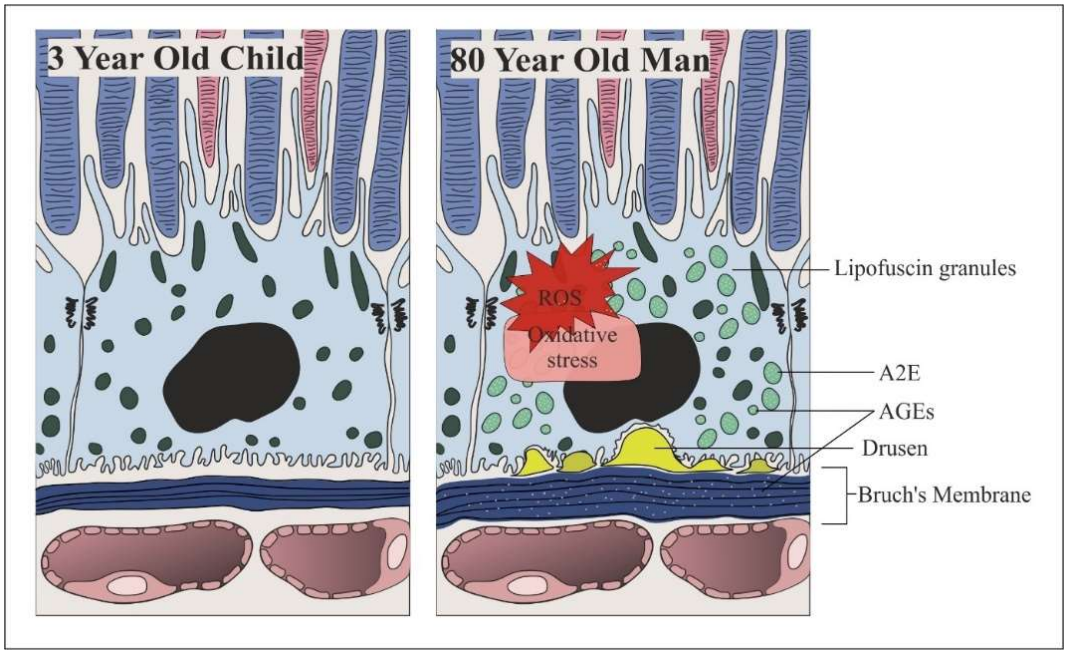


***Figure 4.*** *The RPE of a young child has a homogenous distribution of melanin granules, a Bruch's Membrane without deposits, and preserved retinal function. With age, RPE cell pigmentation changes by simultaneously loosing melanin granules while accumulating phototoxic A2E containing lipofuscin granules. Increased levels of ROS and oxidative stress lead to the formation of advanced glycosylation end products (AGEs), subsequently damaging DNA and cell membranes and causing inflammation, RPE cell dysfunction and degeneration. In addition to age-related changes of RPE cells, Drusen (extracellular matrix depositions containing lipids, AGEs and complement components) between the RPE and BM emerge and the accumulation of drusen and debris within the BM further induces BM thickening.*

One of the main changes with age is the significant change in RPE cell pigmentation due to the loss of electron dense melanin granules and the accumulation of lipofuscin granules within lysosomal compartments (residual bodies) (Fig. 4) (*2*). As the accumulation of residual bodies is part of normal lysosomal aging (*25*) and the RPE has an highly active lysosomal system, aging RPE cells accumulate vast numbers of residual bodies, filling up almost the entire cytoplasm by the 5$^{th}$ decade of life (Fig. 4) (*26*). The problem with that is not only the clogging of the RPE cell cytoplasm, but the massive amounts of lipofuscin, particularly A2E (pyridinium bis-retinoid N-retinylidene-N-retinylethanolamine), as A2E is highly phototoxic.

By generating ROS and inducing oxidative changes, lipofuscin compromises lysosomal function, DNA integrity, causes lipid peroxidation and finally, in combination with the congestion of the cytoplasm, results in RPE dysfunction (*27*). Another reason for elevated levels of oxidative stress and the resulting accumulation of oxidative damages is the age-associated decline of enzymatic and non-enzymatic antioxidants, like catalase, a $H_2O_2$ degrading enzyme, and the antioxidants a-tocopherol, lutein and zeaxanthin (*28*). As the RPE-photoreceptor complex is continuously exposed to high oxygen levels and energy and therefore generally prone to oxidative damages, these changes have tremendous impact on the impairment of RPE function over time (*8*). The consequence of continuous oxidative stress and the decline in oxidative damage defense efficacy is the occurrence and accumulation of AGEs (Fig. 4). AGEs, mainly located within the BM and in lipofuscin granules, are capable to covalently react with other biomolecules, leading to the formation of aggregates and further compromising lysosomal enzyme activity and function (*29*). Furthermore, AGEs effect growth factor levels by elevating PDGF production in RPE cells, VEGF production in RPE as well as endothelial cells and therefore induce proliferation of the latter (*30–32*). Thus, accumulation of AGEs in the RPE and BM may not only contribute to age-related RPE dysfunction but to the initiation and progression of pathologic mechanisms (*33*).

In addition to direct structural and functional alterations of RPE cells, the area around the RPE also changes with age. One of the most prominent changes is the formation of drusen, above or beneath the RPE, on or within the BM (Fig. 4). Drusen are depositions of extracellular materials, comprising a mixture of various lipids, including apolipoprotein B and E, esterified and unesterified cholesterol, polysaccharides, glycosaminoglycans and proteins (*34, 35*). Moreover, drusen contain several proteins associated with inflammation and/or the complement system including C-reactive protein, immunoglobulin G, vitronectin, clusterin and complement components (C) C3, C5, C9 (*13*). Over time, the accumulation of drusen and debris within the BM, which is accompanied by increased levels of phospholipids, triglycerides, fatty acids, and free cholesterol, changes the BM structure significantly (Fig. 4) (*36*). These compositional changes do not only hamper the diffusion permeability of ions and molecules across the membrane but induce immune responses by complement pathway activation and further impair RPE cell adhesion. Therefore, they contribute to RPE and photoreceptors dysfunction and are complicit in the onset and progression of age-related ocular diseases (*37–39*).

However, while the interdependency of aging and age-related ocular diseases is inevitable, the precise dissociation between normal age-relate and pathological changes is complex. For though many risk factors and pathologic characteristics emerge from age-related changes of the RPE and BM, ageing is a highly variable process based on a combination of both genetic and environmental factors, predisposing only certain individuals to develop age-related ocular

diseases. Thus, age-related changes of the RPE may lead to RPE dysfunction and visual impairment, but not necessarily to pathologic conditions (*2, 24*).

# 3 The RPE's role in retinal diseases

Due to its importance in retinal functions, disturbance of the physiologic function of the RPE (Fig. 3), whether through genetic disorders, chronic dysfunction or age-related decline, are associated with visual impairment and vision loss (*40*). Hence, depending on the type and extent of malfunction, etiologically different retinal diseases emerge, affecting RPE, photoreceptor, and endothelial cells.

Malfunctioning of the visual cycle causes several types of photoreceptor and RPE degeneration, clinically ranging from moderate visual impairment to severe blindness. The primary causes of visual cycle impairment are RPE gene defects reducing the function of enzymes involved in the visual cycle reaction cascade and thereby hampering or interrupting the recycling of 11-cis retinal (7). One of the gene defects leading to severe retinopathy are mutations that impair the function of the key regulatory protein RPE65 (Fig. 3). The impairment of RPE65 function causes a lack of chromophore and at the same time elevated levels of phosphorylated opsin, resulting in photoreceptor dysfunction and degradation (*41*). Therefore, RPE65 mutations provide an example for RPE associated gene defects affecting both RPE and photoreceptor function and further highlight the importance of the functional interplay of RPE and photoreceptors (*13*). This interdependency is also reflected by the fact that the inability of the RPE to phagocytose the shed photoreceptors segments causes photoreceptor degeneration and alterations of RPE (*3*). Hereditary diseases affecting the visual cycle or photoreceptor phagocytosis are referred to as retinitis pigmentosa. Today, there are no approved therapeutic approaches available able to stop the pathogenesis and restore vision. As retinitis pigmentosa is a mechanistically, genetically, and clinically very heterogenous disease, there can't be "one fits all" standard therapeutic approach. However, increasing knowledge of causal genes and associated impairment of biochemical mechanisms led to the identification of targets and the development of novel drugs, which now only need to be delivered to the affected RPE or photoreceptor cells (*42*).

Besides ensuring proper photoreceptor function, the ability of the RPE to secrete growth factors ensures choriocapillaris integrity and further protects various other retinal cells, including Müller cells, astrocytes, and ganglion cells. However, dysregulation of growth factor secretion, therefore, is a driving force of the pathogenesis of retinal diseases (*8*). The major culprit for causing pathologic endothelial cell proliferation is VEGF, which is primarily expressed by RPE cells. However, while RPE cells produce and secrete physiologic VEGF levels in order to preserve normal retinal cell function, various extracellular stimuli induce VEGF secretion, resulting in pathologic VEGF levels.

These stimuli include growth factors like IGF-1, TNF-α, the integrin ligand vitronectin, hypoxia, hyperglycemia and AGEs. It is furthermore noteworthy to mention, that exaggerated VEGF production and secretion do not only affect endothelial cells, but due to autocrine mechanisms, RPE cells and can even induce RPE cell proliferation. VEGF effects on endothelial and RPE cells are further enforced by the equilibrium shift of VEGF and PEDF, as PEDF is not only a key coordinator of retinal neuronal and vascular function, but the physiologic counterpart of VEGF. Besides VEGF and PEDF, another growth factor with major influence on RPE and endothelial cells is TGF-β. Even though, the multitude of effects are concentration dependent and yet not fully understood, the dysregulation of TGF-β expression can cause cell proliferation and has additionally been shown to induce immune responses (*8*).

In addition to growth factors, RPE cells secrete cytokines, FasL, adhesion molecules, major histocompatibility complex (MHC) molecules and many if not all components and regulators of the complement cascade (*23*). To date, it is also known that under physiologic conditions, retinal innate immune cells (including microglia, perivascular macrophages, and a small population of dendritic cells) and the complement system undergo a low-grade activation, named parainflammation, which is crucial to maintain retinal homeostasis. In contrast, under pathologic conditions, the parainflammatory response is dysregulated and develops into detrimental chronic inflammation. Thus, complement activation in the retina, attributed to RPE cells, is a pivotal part of chronic inflammation and further contributes significantly to the pathology of all retinal diseases associated with inflammation. Although, the initial triggers of these retinal diseases may differ, the following retinal immune response is based on the same mechanisms (*43*). With the complement factors H, I and B rapidly activating the alternative pathway and C2, C3 and C5 activating the classical pathway, both inducing inflammation and immune responses (*22*).

Therefore, malfunctions and dysregulation of the secretory function of the RPE are implicated in all retinal disease, often causing multifactorial pathogenesis associated with exuberant cell proliferation, inflammation, and immune system activation.

### 3.1 Posterior uveitis

Posterior uveitis is a chronic inflammatory condition that affects the choroid and the retina and causes devastating vision loss if left untreated. Being triggered by autoimmune disorders, the pathogenesis is mainly driven by complement activation. Current treatment of uveoretinitis is based on the unspecific reduction of inflammation and infections through local or systemic administration of immunosuppressants and corticosteroids which are often associated with severe adverse effects such as cataract and glaucoma. Thus, there is an urgent need to develop cell specific approaches that counteract the destructive inflammation in an more effective and safer manner (*44*).

### 3.2 Proliferative vitreoretinopathy

Proliferative vitreoretinopathy (PVR) is a severe complication of retinal detachment and the primary cause of retinal reattachment surgery failure. Under normal circumstances, RPE cells do not undergo mitosis, however, under some pathologic conditions like retinal detachment und retinitis pigmentosa, RPE cells proliferate and migrate. Triggered by the detachment of the neural retina and the breakdown of the blood-retinal-barrier (BRB), RPE cells cannot be kept in place, dislocate and convert into proliferating fibroblast-like cells (*13*). These cells generate peri-retinal fibrotic membranes with contractile properties, subsequently causing retinal wrinkling, detachment, and blindness. Even though the exact pathomechanism of PVR remains unclear, RPE cells are generally regarded as the major culprit for both the initiation and progression of the disease, as it is known that cytokines and growth factors, most notably TGF-β, PDGF, VEGF, IL-1, IL-6, IL-8 and IL-10 stimulate the proliferation and migration of RPE cells (*45*). To date, the only treatment option for advanced PVR is surgery. However, as the treatment can be accompanied by irreversible damage, poor prognosis of visual acuity and is repeatedly required, there is an urgent need for less invasive treatment options allowing earlier intervention or even prophylaxis (*46*). Currently, there a several clinical trials ongoing including oral and intravitreal use of approved drugs like isotretinoin, colchicine for oral administration and intravitreal methotrexate, 5-fluorouracil, low molecular weight heparin, Avastin, and decorin. However, even though the cellular culprit is known and effective drugs are available, yet there is no RPE specific approach (*47*).

### 3.3 Age-related macular degeneration

Age-related macular degeneration (AMD) is a complex and multifactorial disease leading to progressive degeneration of the macula. AMD is the most common cause of irreversible blindness in developed countries, currently affecting over 196 million people and predicted to rise to 288 million by 2040 (*48*). According to the disease progression, AMD can be divided into two stages: early and late stage AMD. The early stage AMD is characterized by the appearance of drusen formed between RPE and BM (Fig. 4), clinically accompanied by mild and asymptomatic visual impairment. The disease then progresses into one of the late stages, dry AMD (also named geographic atrophy) or wet AMD (also named neovascular AMD). Dry AMD is characterized by RPE cell degeneration, subsequently leading to the impairment of photoreceptor and RPE function as well as photoreceptor degradation. As of now, there is no treatment for dry AMD.

Accounting for two thirds of all late stages, wet AMD is characterized by choroidal neovascularization, the abnormal blood vessel growth of the choriocapillaris. The newly formed, leaky blood vessels sprout and invade the neutral retina, destructing retinal tissue, the BRB and therefore causing sudden or gradual vision loss (*49*). Today's standard therapy for

wet AMD relies on the treatment of pathologic neovascularization using intravitreal anti-VEGF agents. However, even though the anti-VEGF treatment has shown great success in reducing abnormal vessel growth and leakage and therefore alleviating vision loss, the therapy is accompanied by severe side effects and serious drawbacks. Recently, a long-term study revealed that patients eventually lose the vision gained from previous anti-VEGF therapy as they struggle in sustaining frequent invasive and costly intravitreal injections. More so, the invasive intervention increases the risks of severe complications, including inflammation, vitreous hemorrhage, glaucoma, retinal detachment, and retinal degeneration, especially with repeated uses over time (*50, 51*). However, as the therapy only relies on symptomatic suppression of choroidal neovascularization without taking the multifactorial, RPE-related pathomechanism into account, clinical success is limited and long-term effects of rigorous VEGF suppression in the retina are still not fully assessed (*52*).

Even though reasons for retinal damage and vision loss differ fundamentally between wet and dry AMD, it is now known that inflammation and immune response, particularly the complement system play crucial roles in the pathogenesis of both forms (*22*). Recent studies suggest that the complement system, and in particular the alternative pathway may be dysregulation in all AMD patients (*53*). Moreover, current experimental studies have demonstrated that that inhibition of complement activation via either systemic or local routes can suppress laser-induced choroidal neovascularization (*22*). These findings underpin not only the contribution but the significance of inflammation and immune responses to the pathology of AMD and more so, pave the way for radically new approaches for the treatment of AMD.

### 3.4 Diabetic retinopathy

Diabetic retinopathy (DR) is the most frequently occurring complication of diabetes mellitus and year after year ranking among the leading causes of blindness. Since diabetes is currently affecting over 463 million people and being predicted to affect 700 million people by 2045, the prevalence of DR will expand as well (*54*). DR is a chronic, progressive disease affecting retinal vessels and the neural retina. The disease can be classified into two stages, the early, nonproliferative DR and progressed, proliferative DR. Clinically, early stages are characterized by microaneurysms, hard exudates, hemorrhages, and cotton-wool spots in the fundus region of the retina. The progression of DR is driven by ischemic conditions and growth factor dysregulation which subsequently induce endothelial cell proliferation and thus retinal neovascularization (*55*). These newly formed vessels may leak fluid causing diabetic macular oedema and/or severe hemorrhages, ultimately leading to retinal detachment and destruction of the neural retina. In addition to vascular damage, there is growing evidence that inflammation and immune responses play crucial roles in the pathogenesis, especially in the

onset and early disease stages. Even though the exact underling mechanisms causing retinal cell degeneration are yet not fully understood, oxidative stress and inflammation are known to be detrimental key factors and even may represent the inciting factors leading to the complex pathology of DR (*56*). Since the role of the complement system in DR pathogenesis and especially how the complement system is activated in the diabetic eye, is still not fully understood, the clinical predictive or therapeutic value of targeting the complement system remains to be elucidated (*22*).

In general, there are different treatment options for the different stages of DR, ranging from maintaining blood glucose, blood pressure and blood lipid levels to laser therapy and intravitreal anti-VEGF treatments. However, especially the treatment of late stage (proliferative) DR remains a major challenge as current therapies have significant drawbacks and lack therapeutic efficacy. Laser therapy is accompanied by severe side effects like visual impairment (visual field constriction, night blindness, color vision changes) up to sudden blindness, inadvertent laser burn, macular edema exacerbation, acute glaucoma, and retinal detachment. Anti-VEGF therapy indeed demonstrated remarkable clinical benefits in DR patients regarding the inhibition of vessel proliferation, however, the majority of patients failed to achieve significant visual improvement and intravitreal injections further bear the risk of serious side effects and complications (see *Age-related macular degeneration*) (*57*). Therefore, there is an urgent need for the development of RPE specific therapeutic approaches, that include the multifactorial pathology and allow to counteract inflammation and immune response.

### 3.5 Retinopathy of prematurity

Retinopathy of prematurity (ROP) is a multifactorial retinal disease affecting premature infants. ROP is characterized by exaggerated and uncontrolled retinal vessel growth, inflammation, and retinal cell degeneration of the immature retina. Mechanistically, the suppression of growth factors due to hyperoxia and loss of the maternal-fetal interaction stop physiologic retinal vessel development. Subsequently, the increasingly metabolically active, yet poorly vascularized retina becomes hypoxic and therefore triggers growth factor and cytokine secretion (VEGF, IGF-1, FGF-2, IL-1β, TNF-α, and IL-6). While abnormal neovascularization results in severe retinal detachment and permanent visual loss, inflammation is considered a key contributor to the overall pathogenesis of ROP, including choroidal, photoreceptor and RPE degeneration (*58, 59*). In contrast to the crucial role of neovascularization and inflammation, the influence of the complement system on the pathogenesis is still not fully elucidated. However, as it is known that deficiencies in complement components and complement receptors can induce pathological angiogenesis and further provoke macrophages

and RPE cells to express high amounts of growth factors and cytokines, the complement system is very likely involved (*22*).

Although precise control of oxygen administration to preterm infants can reduce the risk for developing ROP, ROP is still one of the leading causes of childhood blindness worldwide. Reasons for this are increased survival rates of infants with extremely low gestational ages and/or birthweights and the increased unmonitored treatment of preterm infants with 100% oxygen in developing countries (*58*). Once ROP has developed, laser or intravitreal anti-VEGF therapy can be used to counteract retinal neovascularization. While laser ablation may itself reduce visual field, induce myopia, and only is indicated for the treatment of very advanced forms of ROP, anti-VEGF therapy, has been shown success in reducing neovascularization and halting the progression of ROP. However, treating preterm infants with anti-VEGF agents poses serious risks, including endophthalmitis, pulmonary hypoplasia, and stroke, as well as hemorrhage, cataract and retinal detachments which may occur up to a year after initial injection (*60*). Rigorous suppression of VEGF in the eye further affects the physiologic functions of non-vascular cells including photoreceptors, neurons, Müller, ciliary body and RPE cells, therefore risking off-target cell dysfunction, degradation and apoptosis (*58*). More so, since the VEGF blockage alone cannot eliminate pathological angiogenesis completely, thereby underscoring the multifactorial nature of the disease, novel less destructive and more causal approaches are needed.

Taken together, the RPE is vital for sight and disorders or dysfunctions of the inconspicuous cell monolayer are involved in a vast number of ocular diseases, all causing visual impairment and vision loss (*3*). By continuously increasing the knowledge about the RPEs' contribution to the maintenance of retinal homeostasis and its implication in the pathogenesis and pathomechanisms of retinal diseases, the RPE emerges as a tremendously attractive target for the treatment of various ocular diseases.

# 4 Drug delivery to the RPE

The extensive research on degenerative retinal diseases led to a fundamental knowledge of pathologic processes and interdependencies. This thorough understanding in turn, furthered the identification of new drug targets and paved the way for the development of new therapeutic entities. More so, the identification of the RPE as a major culprit/key player in the pathogenesis of various ocular diseases led to the development of drugs designed to specifically interfere with the RPE, chemically ranging from small molecules to nucleic acids (*61*). However, the development of active compounds alone is not enough, as it must also be considered how to deliver them to the RPE. Since sufficient drug delivery to the posterior eye

remains a significant challenge, drug delivery to the RPE is the real bottleneck for the development of efficient RPE therapeutics.

### 4.1 Barriers on the way to the RPE

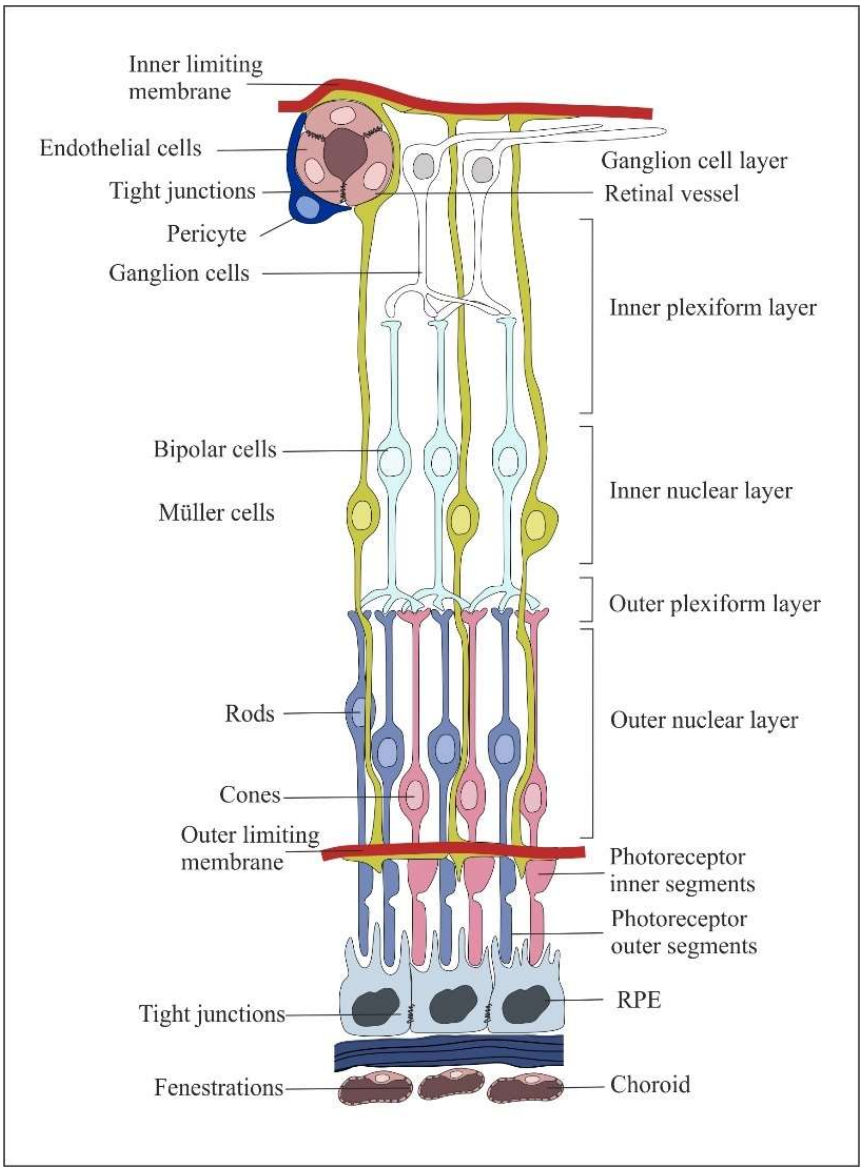


***Figure 5.*** *Layers of the neural retina: outer nuclear layer, outer plexiform layer, inner nuclear layer, inner plexiform layer, and ganglion cell layer. Blood-retinal barrier (BRB): while outer BRB is formed by RPE cells, inner BRB is built by retinal endothelial cells, pericytes and Müller cells. Layers that may restrict movement of molecules and nanoparticles are the outer limiting membrane (OLM), phagocytosing Müller cells and the inner limiting membrane (ILM).*

Drug delivery to the posterior eye is a very challenging task as the retina is protected by the BRB. The BRB consists of two different parts (Fig. 5): The outer and inner BRB. While the outer BRB is built by endothelial cells of the choroid (fenestrated with diaphragms) and the

adjacent RPE with its tight junctions. The inner BRB is formed by endothelial cells of non-fenestrated retinal vessels which are additionally surrounded by pericytes and Müller cells (*6*). Besides contributing to the inner BRB, Müller cells play a major role in the formation of the outer and inner limiting membrane and therefore shield the neuroretina from the vitreous towards the RPE (Fig. 5) (*61, 62*). The inner limiting membrane (ILM), is built up by the end feet of Müller cells and an extracellular matrix of collagen and glycosaminoglycans, forming a negatively charged barrier. While small molecular drugs can diffuse freely through the ILM, the ILM can hinder the transport of macromolecules, biologics, and nanoparticles. However, the qualitative and quantitative barrier function, including cut-off sizes are still unknown and variations of the ILM due to age or diseases like diabetes do further complicate permeability predictions (*63*). The same also applies to the outer limiting membrane (OLM) formed by adherent and tight junctions between Müller cells and the inner segments of photoreceptor cells (*64*). To date, the size limit and barrier role of the OLM are not fully elucidated and there are only few studies investigating the permeation of small molecules, macromolecules and nanoparticles through the OLM (*65*).

Since there are two different ways to address the RPE either from the basal or the apical side, a molecule or nanoparticle must overcome at least one of the challenging barriers to successfully reach the RPE. While upon intravitreal administration, ILM, OLM and Müller cells are the biggest obstacles, upon systemic administration, only the choroid and BM hinder reaching the RPE.

Systemic administrations, especially via intravenous (i.v.) and oral routes can therefore be used to transport drugs and nanoparticles to the RPE, if those are able to extravasate from the fenestrated choroidal vessels and cross the BM. Since the roles of choroid and BM as barriers to small molecules and neutral macromolecules are negligible (*66*), the distribution of a drug from the blood stream to the RPE mainly depends on the free drug concentration in plasma and distribution between systemic circulation and the eye (*67*). In addition to factors generally influencing drug distribution, the drug may reveal enhanced accumulation in the RPE, way higher than expected or calculated (*67*), due to melanin binding (*68*). Even though there is evidence that preferably lipophilic and basic substances bind to melanin, melanin binding is very difficult to predict. However, melanin binding can significantly influence pharmacokinetics and further increase drug accumulation in RPE. More so, melanin binding can even prolong drug effects, especially when the drug is released gradually from the melanin depot (*68, 69*). Although systemic administration is beneficial in terms of simplicity and patient compliance it can be associated with systemic side effects and toxicity, limiting the practical application. Therefore, very high doses are needed to achieve therapeutic drug levels in the posterior eye, even though bioavailability of the drug is high. Thus, only few drugs with wide therapeutic indices, such as antibiotics, antivirals, and cytostatics are used in clinical

practice, while most other drugs result in sub-therapeutic drug levels or lead to severe systemic side effects (*70, 71*).

To overcome the challenge of sub-therapeutic drug levels, systemic side effects and toxicity, drugs can be administered directly into the vitreous. Today, intravitreal drug injections are the method of choice in retinal drug delivery and extensively used for both clinical and scientific treatment of retinal diseases (*72*). In contrast to systemic delivery, intravitreal injections bear the advantages of relatively low drug doses, reasonable bioavailability, and reduced systemic adverse effects (*73*). Mechanistically, immediately following injection, drugs distribute into the vitreous and to the surrounding ocular tissues, while at the same time the elimination of the drugs starts. Drug elimination takes place via drug transport over the BRB and drug removal via the aqueous humor outflow, both handing the drug over to systemic circulation (*74*). Because of the fast and highly efficient elimination processes, half-lives of small molecules in the vitreous are typically very short (1 - 10 h). On the contrary, due to the inability of larger molecules to cross the BRB, half-lives of macromolecules and proteins are drastically prolonged. Thus, drug elimination is molecular weight-dependent: the higher the molecular weight, the slower the elimination (*75*). However, as the molecular weight of most drugs is under 500 Da, predicted half-lives are rarely longer than 30 h (*76*). In clinically settings, acceptable treatment intervals can therefore only be achieved because strong fluctuations in the drug levels are accepted. Thus, in the case of anti-VEGF proteins (bevacizumab, ranibizumab, aflibercept), the treatment intervals of 4 - 8 weeks are only feasible because these antibodies and soluble receptors have intravitreal half-lives of several days, are highly potent compounds showing sufficient effects even at very low concentrations and are tolerated at relatively high doses. In fact, the vitreal anti-VEGF drug concentrations show about 100-fold changes during one treatment. As the half-lives of small molecules and many other protein drugs are much shorter and their therapeutic indices are narrower, their dosing intervals would be way too short to be practicable (*47*).

Taken together, both systemic and intravitreal delivery of drugs to the RPE bear a high potential for the treatment of RPE associated diseases. However, suffering from serious drawbacks that question the applicability, especially in the context of treating chronic, progressive diseases.

# 5 Nanoparticles for enhanced drug delivery to the RPE

Due to the specific short comings of drug delivery to the RPE, regardless of the administration route, the use of nanotechnology obviously offers tremendous potential for drug delivery to the RPE. Nanoparticles can improve the solubility of poorly water-soluble drugs and protect the drug from degradation, that is especially valuable for the transport of very sensitive cargos being negatively affected by environmental conditions, such as DNA and RNA.

Additionally, nanoparticles can be designed to cross biological barriers, increase the bioavailability, residence time, and cellular uptake of the drug. Ideally, nanoparticles would allow for efficient, RPE-specific drug delivery, followed by a sustained release of the cargo (*77*). In recent years, even though tremendous effort was made to tackle the challenges of drug delivery to the posterior eye (*47*), yet no far-reaching successes have been achieved, particularly not with regard to RPE specific drug delivery. To that end, this review will focus on biological and pharmacological facts that must be considered for the development of either intravitreal or systemic nanotherapeutics and further highlight the most promising approaches.

### 5.1 Intravitreal Nanoparticle Approaches

By virtue of maximizing drug delivery efficacy and with lessons learned from general poor delivery efficacy to the target using systemic administration, intravitreal administration seemed to be the most obvious and easiest solution to tackle drug delivery problems (*73*). In practice, however, it is not as straight forward as it seems, as upon intravitreal administration, nanoparticles must not only diffuse though the vitreous but move through the whole sensory retina to finally reach the RPE.

Upon intravitreal injection, nanoparticle distribution in the vitreous is mainly driven by diffusion, as the vitreous is composed of approximately 99% water and 1% collagen and hyaluronan. The collagen fibers and hyaluronan molecules form an extensive meshwork in the vitreous, with pore sizes around 550 nm (*65*). Therefore, owing to the negative charge carried by hyaluronan, only negatively or neutrally charged particles with sizes below 500 nm diffuse freely in vitreous. After successful passage through the vitreous, nanoparticles face the ILM, OLM and the adjacent Müller cells. Since most nanoparticles exceed estimated ILM and OLM pore sizes of 10 - 20 nm (*74, 78*) and there are controversial studies showing both, the retention of nanoparticles on these barriers as well as nanoparticles with sizes far above 10 nm being able to overcome the barriers (*79*), ILM and OLM should not be underestimated and should be addressed in the nanoparticles design (*65*). Besides limiting membranes, another obstacle on the nanoparticles' way to the RPE are Müller cells. Müller cells, spanning all retinal layers from the vitreal border to the photoreceptors, are phagocytosing glial cells. Under physiologic conditions, Müller cells are responsible for the homeostatic and metabolic support of retinal neurons, the composition of the extracellular space fluid, provide trophic and anti-oxidative support for photoreceptors and neurons and further regulate the tightness of the BRB (*80*). By virtue of their function as contributors to the defense against endogenous and exogenous insults, they can eliminate nanoparticles via receptor mediated endocytosis and phagocytosis. Upon internalization of foreign materials, Müller cells can produce and secrete proinflammatory cytokines, especially when intrinsically activated by damages or pathogens

associated with retinal disease. Additionally, Müller cells can allow the entry of plasma proteins, recruit plasma immune system components, therefore induce inflammation and overrule the immune privilege of the eye (*81*). As a consequence, intravitreal nanoparticles for the therapy of retinal diseases not only bear the risk of being taken up by Müller cells as part of the normal reaction to foreign objects and being internalized and eliminated by invading macrophages but triggering additional immune responses (*65*). However, even though nanoparticles can be designed to show low immunogenicity, as for example PEG coated lipid nanoparticles, they can reveal high accumulation and Müller glia cells and finally fail to reach the RPE (*82*).

By virtue of their physiological functions, Müller cells ingest and degrade nanoparticles, even stealthy nanoparticles, coated with hyaluronic acid or albumin, and thereby present a major obstacle for to reach the RPE (*74*). Considering the function and importance of Müller cells, off-target accumulation is very common phenomenon and can have serious consequences and should therefore be evaluated critically. Besides Müller cells, various other retinal cells are able to internalize nanoparticles, including ganglion cells, bipolar cells and photoreceptor cells. Therefore, most intravitreal nanoparticle approaches lack RPE cell specific (*65, 83, 84*). The apparent preference for RPE cells, however, mainly relies on the phagocytic nature of the RPE which easily takes up both endogenous material such as photoreceptor outer segments as well as exogenous material (*78, 85*). Currently, there are no intravitreal approaches available specifically targeting RPE cells. However, there are resent approaches trying to solve this problem. Using RPE specific targeting moieties (*86*) or cleavable linkers (*87*) could potentially enhance RPE cell specific nanoparticle uptake or specific drug release and therefore reduce off-target effects of nanotherapeutics.

**Table 1.** *Intravitreal nanoparticle approaches for drug delivery to the RPE.*

| NP | Material | Size* [nm] | ZP [mV] | Cargo | NP Accumulation | Ref. | Observation Period |
|---|---|---|---|---|---|---|---|
| DNA-NP | 10 kDa polyethylene glycol-substituted polylysine (CK30PEG) | Rods; Diameter 8 – 11 Length ~200 | -1 ± 2 | pscCBA-GFP; pEPI-S/MAR; pEPI-S/MAR | RPE, photoreceptors and other retinal cells | (*78*) | 15 d |
| HAS-NP | human serum albumin (±hexamethylenediamine) | Anionic: ~114 Cationic: ~175 nm | -23.73 ± 3.03 +11.7 ± 7.2 | - | Müller cells, RPE cells, other retinal cells around retinal vascular structures | (*79*) | 5 h |

| | | | | | | | |
|---|---|---|---|---|---|---|---|
| PLA-NP | polylactide | 120 - 160 | -60 | Rh-6G (Rh); Nile red (Nr) | RPE cells, other retinal cells | (*85*) | 28 d |
| CeO2-NPs (nano-ceria) | cerium oxide nanoparticles | - | - | - | Photoreceptors, RPE cells, Müller cells, bipolar cells, ganglion cells | (*88*) (*89*) (*90*) | - 90 d 60 d |
| PEG-LPH-NP | PEGylated liposome-protamine-hyaluronic acid nanoparticles | ~132 | +20 | siRNA | Ganglion cells, bipolar cells, Müller cells, photoreceptors, RPE cells | (*91*) | 24 h |
| AuNP | gold nanoparticles | 20 | - | - | all retinal cells, endothelial cells | (*92*) | - |
| Oligo-chitosan-DNA polyplex | oligochitosan /pCMS-EGFP polyplexes | 200 - 312 | +10 | - | Ganglion cells, Müller cells, RPE, other retinal cells | (*93*) | 72 h |
| MNP-rVEGF | Carboxylic acid-stabilised iron oxide nanoparticles / recombinant VEGF | ~130 | -34.7 ± 2.21 | - | RPE, Choroid, other retinal cells | (*86, 94*) | 72 h |
| PLA/PLA-PEO-NP | polylactic acid/polylactic acid-polyethylene oxide nanoparticles | 302 - 367 | -38.26 ± 1.42 | integrin-antagonist peptide: C16Y | ganglion cells, Müller cells photoreceptor, RPE cells, other retinal cells | (*95*) | 3 d |
| HA-LCS-NP | hyaluronan-modified core-shell liponanoparticles | ~320 | -25 | - | RPE, ganglion cells, Müller cells, other retinal cells | (*96*) | 7 d |
| PEG-b-PCL micelles | poly(ethylene glycol)-block-poly(ε-caprolactone) micelles | ~55 | -1.39 ± 0.23 | Desatinib | RPE, other retinal cells | (*97*) | 28 d |
| DNA–SLN | dextran–protamine–DNA - solid lipid nanoparticles | 200 - 270 | +3 | pCMS-EGFP plasmid; pCEP4-RS1 plasmid | Müller cells, ganglion cells, RPE cells | (*98*) | 72 h |

*NP: nanoparticle; ZP: Zeta potential; *spherical unless otherwise stated*

Even if nanoparticles reach the RPE, however, the drug delivery and availability in RPE cells is not guaranteed, as another crucial point is the discrepancy of nanoparticle vs. drug presence. Although there are multiple studies revealing the presence of nanoparticles in the vitreous or retina for days or even weeks after intraocular administration, the drug fate remains to be unknown (*74*). There are still too few studies investigating the distribution and kinetics of both drug and drug carrier, the few, however, revealed a significant difference in drug vs. particle presence and elimination. Since drug release from the nanoparticle can be much faster than particle elimination from the vitreous and clearance of small molecules from the inner eye is extremely fast, drawn conclusions might be incorrect and of limited informative value (*74, 85, 99*). Thus, not only nanoparticle accumulation, including retinal off-target distribution, but drug content in the target tissue should be assessed to finally evaluate the success of the drug delivery system. However, even though intravitreal delivery of nanoparticles is a common and highly promising approach for drug delivery to the RPE, there are more considerable challenges than might initially appear. Since, even though nanoparticles manage to cross the two limiting membranes on their way to the RPE, they often lack cell specific accumulating in the retina and can therefore initiate inflammatory responses and reveal serious off-target effects. However, by crossing theses membranes, they usually reach the RPE and due to the tissues' phagocytic nature, accumulate in the target cells. For the design of successful, efficient, and safe intravitreal nanoparticles approaches, it therefore is mandatory to successively address the challenges presented by limiting membranes, Müller cells and consider elimination processes.

### 5.2 Intravenous Nanoparticle Approaches

The other option to target the RPE is from the basal side via the choroidal vasculature using systemically applied nanoparticles. Although to date there are only very few nanoparticle approaches using this route to the RPE (*72*), it has several advantages over intravitreal injections. Besides the simplicity and non-invasive character of systemic administration, the feasibility is given by the physiology of the eye, as the choroidal blood flow is one of the highest in the human body and the choroid being in immediate proximity to the RPE (*99*). However, even though choroidal vessels are leaky, provide rapid transport of solutes and small molecules and have fenestrations with pore sizes of 60 – 80 nm diameter, it is a common misconception that there is free transport of nanoparticles and macromolecules to the RPE (*100*). In fact, fenestrations are spanned by diaphragms with pore sizes of approx. 6 nm, restricting the transport of macromolecules to the RPE. However, as the RPE-photoreceptor complex depends on nutrient supply from the blood stream, transport occurs either via diffusion through the fenestrations or transcellularly, mediated by caveolae or coated pits (*100*). Upon extravasation from the choroidal blood stream, nanoparticles must only diffuse through the

extracellular matrix of the BM to finally reach the target cells. Thus, nanoparticles do not need to distinguish between the different cell types in the retina and do not need to escape phagocytoses by Müller cells. More so, since RPE cells have a high phagocytosis activity, they are prone to efficiently recognize and subsequently internalize nanoparticles. Therefore, the accessibility of the RPE depends mainly on the fact that nanoparticles extravasate from the choroidal blood stream. While, for instance, inorganic RGD-(arginine–glycine–aspartic acid)-modified nanoparticles revealed accumulation in the choroid but no enrichment in the RPE after systemic administration (*101*), RGD-modified lipid nanoparticles, liposomes as well as poly-(lactide-co-glycolide) (PLGA) nanoparticles where shown to efficiently extravasate from the choroid and accumulate in the RPE (*102*). Thus, indicating that nanocarrier composition plays a crucial role for targeting the RPE by affecting blood extravasation. Furthermore, indicating that choroidal extravasation must necessarily be considered and addressed during nanoparticles design. In addition to nanoparticle composition, another crucial parameter is size. Since very small dendrimers, as well as inorganic gold nanoparticles were not only shown to extravasate from the choroid and reach the RPE but pass through the BRB and are therefore able to reach various cells in the neural retina (*103, 104*).

**Table 2.** *Intravenous nanoparticle approaches for drug delivery to the RPE.*

| NP | Material | Size* [nm] | ZP [mV] | Cargo | NP Accumulation | Ref. | Observation Period |
|---|---|---|---|---|---|---|---|
| AuNP | gold nanoparticles | 50<br>20 | -<br>- | -<br>- | all retinal layers, including neurons, endothelial cells, glial cells, RPE cells | (*105*)<br>(*103*) | 21 d<br>1 d |
| BSA-A647 / BSA-GNP | Alexa647 conjugated to Bovine serum albumin / Bovine serum albumin conjugated to gold nanoparticles | 2.3<br>12.1 | -12.1<br>-18.0 | - | RPE cells, photoreceptors | (*100*) | 4 h |
| D-Cy5 | generation-4 hydroxyl poly-amidoamine (D-Cy5) dendrimers | 4.87 ±0.20 | 6.63 ±0.24 | - | Müller cells microglia macrophages RPE cells | (*104*) | 21 d |

| | | | | | | | |
|---|---|---|---|---|---|---|---|
| RGD-Tf-Flt23K-PLGA-NP | Transferrin-RGD (arginine–glycine–aspartic acid) functionalized poly-(lactide-co-glycolide) nanoparticle | 419.2 ±6.3 | –11.2 ±1.15 | Flt23K plasmid | Photoreceptors RPE cells endothelial cells | (*102*) | 48 h |
| 8D3-PIL | monoclonal antibody (mAb) to the transferrin receptor (TfR) functionalized pegylated immune-liposomes (PIL) | - | - | pSV-β-galactosidase;pGfa-lacZ | Ganglion cells Müller cells RPE cells | (*106*) | 48 h |

*NP: nanoparticle; ZP: Zeta potential; *spherical unless otherwise stated*

However, for most nanoparticles that have shown to reach the RPE, the exact transport mechanism remains to be elucidated and further research is needed to fully understand the processes of choroidal blood extravasation and extracellular matrix crossing in order to progressively address and leverage these mechanisms.

Due to the heterogeneity of particle composition, size, charge, and targeting ligands, unfortunately, no general conclusions can be drawn for the design of nanoparticles for targeted drug delivery to the RPE. However, besides considering blood extravasation and BM-crossing, addressing, and mimicking nutrient pathways seem to be utterly beneficial. As RPE cells are responsible for the transport of various nutrients and waste products from the blood to the photoreceptors and vice versa, they exhibit a multitude of transporters and receptors, usually localized either on the apical or basal side. Depending on the route of administration, diverse receptors can be targeted in order to facilitate intracellular and cell specific nanoparticle enrichment. As addressing transporters and receptors dramatically influences drug delivery and bioavailability and thus therapeutic efficacy, active targeting bears the potential to facilitate RPE accumulation independent from the chosen administration route (*3*). For example, functionalization of the nanoparticle surface with transferrin, RGD or both increased RPE delivery of nanoparticles when compared to nonfunctionalized nanoparticles. Additionally, liposomes and PLGA nanoparticles functionalized with either transferrin or transferrin and RGD were shown to efficiently transfect RPE cells after systemic administration in mice (*102, 107*). And LDL-mimicking CsA loaded RGD-modified lipid nanoparticles accumulated in the RPE and revealed comprehensive therapeutic effects in a mouse model of retinopathy of prematurity after one single intravenous injection (Chapter 5). These approaches indicate the enormous therapeutic potential of systemically administered

nanoparticles for the efficient, safe and patient friendly treatment of diseases with RPE association, irrespective of the chosen drug, including small molecules, antibodies, oligonucleotides, genes, and growth factors.

# 6 Concluding remarks

With the constantly increasing understanding of RPE biology the role of the RPE as retinal caretaker and key player in various retinal diseases is gaining more and more attention. The resulting emerging appreciation of the RPE as attractive target for drug therapy facilitates the development of novel drugs and drug delivery systems. Thus, during the last few years some initial developments have been made opening unprecedented possibilities for targeted RPE drug delivery. However, drug delivery to the neuroretina, and even more so, the RPE, still bears major challenges, including efficacy and cell specificity. Hence, future research is needed to gain a better understanding of the limitations and obstacles for drug delivery to the RPE in order to subsequently design drug delivery systems that comprehensively address these challenges. If researchers mange to overcome these limitations and successfully delivery therapeutics to the RPE, targeted RPE therapy has the potential to revolutionize the current treatment landscape of retinal diseases.

# References


1. J. D. Steinmetz, et al., Causes of blindness and vision impairment in 2020 and trends over 30 years, and prevalence of avoidable blindness in relation to VISION 2020. *The Lancet Global Health* **9**, e144-e160 (2021).
2. M. Boulton, P. Dayhaw-Barker, The role of the retinal pigment epithelium. *Eye (London, England)* **15**, 384–389 (2001).
3. P. S. Caceres, E. Rodriguez-Boulan, Retinal pigment epithelium polarity in health and blinding diseases. *Current opinion in cell biology* **62**, 37–45 (2020).
4. V. L. Bonilha, Retinal pigment epithelium (RPE) cytoskeleton in vivo and in vitro. *Experimental eye research* **126**, 38–45 (2014).
5. T. Storm, T. Burgoyne, C. E. Futter, Membrane trafficking in the retinal pigment epithelium at a glance. *Journal of Cell Science* **133** (2020).
6. M. Díaz-Coránguez, C. Ramos, D. A. Antonetti, The inner blood-retinal barrier. *Vision research* **139**, 123–137 (2017).
7. S. Wimmers, M. O. Karl, O. Strauss, Ion channels in the RPE. *Progress in retinal and eye research* **26**, 263–301 (2007).
8. O. Strauss, The retinal pigment epithelium in visual function. *Physiological reviews* **85**, 845–881 (2005).
9. R. R. Rando, The biochemistry of the visual cycle. *Chemical reviews* **101**, 1881–1896 (2001).
10. M. Zhong, R. Kawaguchi, B. Costabile, Y. Tang, J. Hu, G. Cheng, M. Kassai, B. Ribalet, F. Mancia, D. Bok, H. Sun, Regulatory mechanism for the transmembrane receptor that mediates bidirectional vitamin A transport. *Proceedings of the National Academy of Sciences of the United States of America* **117**, 9857–9864 (2020).
11. R. Kawaguchi, J. Yu, J. Honda, J. Hu, J. Whitelegge, P. Ping, P. Wiita, D. Bok, H. Sun, A membrane receptor for retinol binding protein mediates cellular uptake of vitamin A. *Science (New York, N.Y.)* **315**, 820–825 (2007).
12. A. Aderem, D. M. Underhill, Mechanisms of phagocytosis in macrophages. *Annual review of immunology* **17**, 593–623 (1999).
13. J. R. Sparrrow, D. Hicks, C. P. Hamel, The Retinal Pigment Epithelium in Health and Disease. *CMM* **10**, 802–823 (2010).
14. S. J. Fliesler, L. Bretillon, The ins and outs of cholesterol in the vertebrate retina. *J. Lipid Res.*, jlr.R010538.
15. A. Bill, G. O. Sperber, Control of retinal and choroidal blood flow. *Eye (London, England)* **4 ( Pt 2)**, 319–325 (1990).
16. P. A. Campochiaro, S. F. Hackett, S. A. Vinores, Growth factors in the retina and retinal pigmented epithelium. *Progress in retinal and eye research* **15**, 547–567 (1996).
17. H. Tanihara, M. Inatani, Y. Honda, Growth factors and their receptors in the retina and pigment epithelium. *Progress in retinal and eye research* **16**, 271–301 (1997).
18. G. L. King, K. Suzuma, Pigment-epithelium-derived factor—a key coordinator of retinal neuronal and vascular functions. *The New England journal of medicine* **342**, 349–351 (2000).
19. D. W. Dawson, O. V. Volpert, P. Gillis, S. E. Crawford, H. Xu, W. Benedict, N. P. Bouck, Pigment epithelium-derived factor. *Science* **285**, 245–248 (1999).
20. K. M. Ford, M. Saint-Geniez, T. Walshe, Zahr, P. A. D'Amore, Expression and role of VEGF in the adult retinal pigment epithelium. *Investigative Ophthalmology & Visual Science* **52**, 9478–9487 (2011).
21. I. Benhar, A. London, M. Schwartz, The privileged immunity of immune privileged organs. *Frontiers in immunology* **3**, 296 (2012).

22. H. Xu, M. Chen, Targeting the complement system for the management of retinal inflammatory and degenerative diseases. *European Journal of Pharmacology* **787**, 94–104 (2016).
23. G.M. Holtkamp, A. Kijlstra, R. Peek, A.F. de Vos, Retinal Pigment Epithelium-immune System Interactions. *Progress in retinal and eye research* **20**, 29–48 (2001).
24. V. L. Bonilha, Age and disease-related structural changes in the retinal pigment epithelium. *Clinical Ophthalmology (Auckland, N.Z.)* **2**, 413–424 (2008).
25. Y. S. Rajawat, Z. Hilioti, I. Bossis, Aging. *Ageing research reviews* **8**, 199–213 (2009).
26. L. Feeney-Burns, C. L. Gao, M. Tidwell, Lysosomal enzyme cytochemistry of human RPE, Bruch's membrane and drusen. *Invest. Ophthalmol. Vis. Sci.* **28**, 1138–1147 (1987).
27. J. R. Sparrow, M. Boulton, RPE lipofuscin and its role in retinal pathobiology. *Experimental eye research* **80**, 595–606 (2005).
28. S. C. Saccà, C. A. Cutolo, D. Ferrari, P. Corazza, C. E. Traverso, The Eye, Oxidative Damage and Polyunsaturated Fatty Acids. *Nutrients* **10** (2018).
29. J. T. Handa, N. Verzijl, H. Matsunaga, A. Aotaki-Keen, G. A. Lutty, J. M. te Koppele, T. Miyata, L. M. Hjelmeland, Increase in the advanced glycation end product pentosidine in Bruch's membrane with age. *Invest. Ophthalmol. Vis. Sci.* **40**, 775–779 (1999).
30. A. Klettner, Oxidative stress induced cellular signaling in RPE cells. *Front Biosci* **S4**, 392–411 (2012).
31. L. Sun, T. Huang, W. Xu, J. Sun, Y. Lv, Y. Wang, Advanced glycation end products promote VEGF expression and thus choroidal neovascularization via Cyr61-PI3K/AKT signaling pathway. *Scientific reports* **7**, 14925 (2017).
32. S. Hoffmann, U. Friedrichs, W. Eichler, A. Rosenthal, P. Wiedemann, Advanced glycation end products induce choroidal endothelial cell proliferation, matrix metalloproteinase-2 and VEGF upregulation in vitro. *Graefe's archive for clinical and experimental ophthalmology = Albrecht von Graefes Archiv fur klinische und experimentelle Ophthalmologie* **240**, 996–1002 (2002).
33. J. V. Glenn, A. W. Stitt, The role of advanced glycation end products in retinal ageing and disease. *Biochimica et biophysica acta* **1790**, 1109–1116 (2009).
34. G. S. Hageman, R. F. Mullins, Molecular composition of drusen as related to substructural phenotype. *Molecular Vision* **5**, 28 (1999).
35. S. R. Russell, R. F. Mullins, B. L. Schneider, G. S. Hageman, Location, substructure, and composition of basal laminar drusen compared with drusen associated with aging and age-related macular degeneration. *American journal of ophthalmology* **129**, 205–214 (2000).
36. A. C. Bird, Bruch's membrane change with age. *British Journal of Ophthalmology* **76**, 166–168 (1992).
37. A. A. Hussain, C. Starita, A. Hodgetts, J. Marshall, Macromolecular diffusion characteristics of ageing human Bruch's membrane. *Experimental eye research* **90**, 703–710 (2010).
38. R. Fernandez-Godino, Alterations in Extracellular Matrix/Bruch's Membrane Can Cause the Activation of the Alternative Complement Pathway via Tick-Over. *Advances in experimental medicine and biology* **1074**, 29–35 (2018).
39. R. Fernandez-Godino, K. M. Bujakowska, E. A. Pierce, Changes in extracellular matrix cause RPE cells to make basal deposits and activate the alternative complement pathway. *Human molecular genetics* **27**, 147–159 (2018).
40. S. Fuhrmann, C. Zou, E. M. Levine, Retinal pigment epithelium development, plasticity, and tissue homeostasis. *Experimental eye research* **123**, 141–150 (2014).
41. S. M. Gu, D. A. Thompson, C. R. Srikumari, B. Lorenz, U. Finckh, A. Nicoletti, K. R. Murthy, M. Rathmann, G. Kumaramanickavel, M. J. Denton, A. Gal, Mutations in RPE65 cause autosomal recessive childhood-onset severe retinal dystrophy. *Nature genetics* **17**, 194–197 (1997).

42. D. T. Hartong, E. L. Berson, T. P. Dryja, Retinitis pigmentosa. *The Lancet* **368**, 1795–1809 (2006).
43. M. Chrzanowska, A. Modrzejewska, M. Modrzejewska, New insight into the role of the complement in the most common types of retinopathy-current literature review. *International journal of ophthalmology* **11**, 1856–1864 (2018).
44. J. V. Forrester, Intermediate and posterior uveitis. *Chemical immunology and allergy* **92**, 228–243 (2007).
45. G. A. Limb, B. C. Little, A. Meager, J. A. Ogilvie, R. A. Wolstencroft, W. A. Franks, A. H. Chignell, D. C. Dumonde, Cytokines in proliferative vitreoretinopathy. *Eye (London, England)* **5 ( Pt 6)**, 686–693 (1991).
46. J.C. Pastor, E.R. de La Rúa, F. Martı´n, Proliferative vitreoretinopathy. *Progress in retinal and eye research* **21**, 127–144 (2002).
47. Q. Li, J. Weng, S. N. Wong, W. Y. Thomas Lee, S. F. Chow, Nanoparticulate Drug Delivery to the Retina. *Molecular pharmaceutics* (2020).
48. J. Rezapour, A. K. Schuster, S. Nickels, C. A. Korb, H. Elbaz, T. Peto, M. Michal, T. Münzel, P. S. Wild, J. König, K. Lackner, A. Schulz, N. Pfeiffer, M. E. Beutel, Prevalence and new onset of depression and anxiety among participants with AMD in a European cohort. *Scientific reports* **10**, 4816 (2020).
49. R. D. Jager, W. F. Mieler, J. W. Miller, Age-related macular degeneration. *The New England journal of medicine* **358**, 2606–2617 (2008).
50. F. G. Holz, R. Tadayoni, S. Beatty, A. Berger, M. G. Cereda, R. Cortez, C. B. Hoyng, P. Hykin, G. Staurenghi, S. Heldner, T. Bogumil, T. Heah, S. Sivaprasad, Multi-country real-life experience of anti-vascular endothelial growth factor therapy for wet age-related macular degeneration. *The British journal of ophthalmology* **99**, 220–226 (2015).
51. N. Ferrara, A. P. Adamis, Ten years of anti-vascular endothelial growth factor therapy. *Nature reviews. Drug discovery* **15**, 385–403 (2016).
52. Jong, P. T. V. M. de, Age-related macular degeneration. *The New England journal of medicine* **355**, 1474–1485 (2006).
53. J. R. Sparrow, K. Ueda, J. Zhou, Complement dysregulation in AMD. *Molecular aspects of medicine* **33**, 436–445 (2012).
54. C. Sabanayagam, R. Banu, M. L. Chee, R. Lee, Y. X. Wang, G. Tan, J. B. Jonas, E. L. Lamoureux, C.-Y. Cheng, B. E. K. Klein, P. Mitchell, R. Klein, C. M. G. Cheung, T. Y. Wong, Incidence and progression of diabetic retinopathy. *The Lancet Diabetes & Endocrinology* **7**, 140–149 (2019).
55. C. Hernández, A. Simó-Servat, P. Bogdanov, R. Simó, Diabetic retinopathy. *Journal of endocrinological investigation* (2017).
56. A. P. Adamis, Is diabetic retinopathy an inflammatory disease? *British Journal of Ophthalmology* **86**, 363–365 (2002).
57. Quresh Mohamed, Management of Diabetic Retinopathy - A Systematic Review. *Clinician's Corner*, 902–916 (2007).
58. A. Hellstrom, L. E. Smith, O. Dammann, Retinopathy of prematurity. *The Lancet* **382**, 1445–1457 (2013).
59. J. C. Rivera, M. Holm, D. Austeng, T. S. Morken, T. E. Zhou, A. Beaudry-Richard, E. M. Sierra, O. Dammann, S. Chemtob, Retinopathy of prematurity. *Journal of neuroinflammation* **14**, 165 (2017).
60. S. Fouzdar Jain, H. H. Song, S. N. Al-Holou, L. A. Morgan, D. W. Suh, Retinopathy of prematurity. *Clinical Ophthalmology (Auckland, N.Z.)* **12**, 1003–1009 (2018).
61. E. Himawan, P. Ekström, M. Buzgo, P. Gaillard, E. Stefánsson, V. Marigo, T. Loftsson, F. Paquet-Durand, Drug delivery to retinal photoreceptors. *Drug discovery today* **24**, 1637–1643 (2019).

62. M. A. Fields, L. V. Del Priore, R. A. Adelman, L. J. Rizzolo, Interactions of the choroid, Bruch's membrane, retinal pigment epithelium, and neurosensory retina collaborate to form the outer blood-retinal-barrier. *Progress in retinal and eye research* **76**, 100803 (2020).
63. T. L. Jackson, R. J. Antcliff, J. Hillenkamp, J. Marshall, Human retinal molecular weight exclusion limit and estimate of species variation. *Invest. Ophthalmol. Vis. Sci.* **44**, 2141–2146 (2003).
64. A. H. Bunt-Milam, J. C. Saari, I. B. Klock, G. G. Garwin, Zonulae adherentes pore size in the external limiting membrane of the rabbit retina. *Invest. Ophthalmol. Vis. Sci.* **26**, 1377–1380 (1985).
65. X. Huang, Y. Chau, Intravitreal nanoparticles for retinal delivery. *Drug discovery today* **24**, 1510–1523 (2019).
66. E. Ramsay, M. Hagström, K.-S. Vellonen, S. Boman, E. Toropainen, E. M. del Amo, H. Kidron, A. Urtti, M. Ruponen, Role of retinal pigment epithelium permeability in drug transfer between posterior eye segment and systemic blood circulation. *European Journal of Pharmaceutics and Biopharmaceutics* **143**, 18–23 (2019).
67. K.-S. Vellonen, E.-M. Soini, E. M. del Amo, A. Urtti, Prediction of Ocular Drug Distribution from Systemic Blood Circulation. *Molecular pharmaceutics* **13**, 2906–2911 (2016).
68. A.-K. Rimpelä, M. Reinisalo, L. Hellinen, E. Grazhdankin, H. Kidron, A. Urtti, E. M. del Amo, Implications of melanin binding in ocular drug delivery. *Advanced drug delivery reviews* **126**, 23–43 (2018).
69. P. Jakubiak, F. Lack, J. Thun, A. Urtti, R. Alvarez-Sánchez, Influence of Melanin Characteristics on Drug Binding Properties. *Molecular pharmaceutics* **16**, 2549–2556 (2019).
70. P. M. Hughes, O. Olejnik, J.-E. Chang-Lin, C. G. Wilson, Topical and systemic drug delivery to the posterior segments. *Advanced drug delivery reviews* **57**, 2010–2032 (2005).
71. D. H. Geroski, H. F. Edelhauser, Drug delivery for posterior segment eye disease. *Invest. Ophthalmol. Vis. Sci.* **41**, 961–964 (2000).
72. T. R. Thrimawithana, S. Young, C. R. Bunt, C. Green, R. G. Alany, Drug delivery to the posterior segment of the eye. *Drug discovery today* **16**, 270–277 (2011).
73. H. M. Kim, S. J. Woo, Ocular Drug Delivery to the Retina. *Pharmaceutics* **13** (2021).
74. E. M. del Amo, A.-K. Rimpelä, E. Heikkinen, O. K. Kari, E. Ramsay, T. Lajunen, M. Schmitt, L. Pelkonen, M. Bhattacharya, D. Richardson, A. Subrizi, T. Turunen, M. Reinisalo, J. Itkonen, E. Toropainen, M. Casteleijn, H. Kidron, M. Antopolsky, K.-S. Vellonen, M. Ruponen, A. Urtti, Pharmacokinetic aspects of retinal drug delivery. *Progress in retinal and eye research* **57**, 134–185 (2017).
75. I. P. Kaur, S. Kakkar, Nanotherapy for posterior eye diseases. *Journal of controlled release : official journal of the Controlled Release Society* **193**, 100–112 (2014).
76. H. Kidron, E. M. del Amo, K.-S. Vellonen, A. Urtti, Prediction of the vitreal half-life of small molecular drug-like compounds. *Pharmaceutical Research* **29**, 3302–3311 (2012).
77. P. Couvreur, Nanoparticles in drug delivery. *Advanced drug delivery reviews* **65**, 21–23 (2013).
78. R. A. Kelley, S. M. Conley, R. Makkia, J. N. Watson, Z. Han, M. J. Cooper, M. I. Naash, DNA nanoparticles are safe and nontoxic in non-human primate eyes. *International journal of nanomedicine* **13**, 1361–1379 (2018).
79. H. Kim, S. B. Robinson, K. G. Csaky, Investigating the movement of intravitreal human serum albumin nanoparticles in the vitreous and retina. *Pharmaceutical Research* **26**, 329–337 (2009).

80. A. Reichenbach, A. Bringmann, New functions of Müller cells. *Glia* **61**, 651–678 (2013).
81. J.W. Streilein, N. Ma, H. Wenkel, T. Fong Ng, P. Zamiri, Immunobiology and privilege of neuronal retina and pigment epithelium transplants. *Vision research* **42**, 487–495 (2002).
82. R. C. Ryals, S. Patel, C. Acosta, M. McKinney, M. E. Pennesi, G. Sahay, The effects of PEGylation on LNP based mRNA delivery to the eye. *PloS one* **15**, e0241006 (2020).
83. A. Koirala, R. S. Makkia, S. M. Conley, M. J. Cooper, M. I. Naash, S/MAR-containing DNA nanoparticles promote persistent RPE gene expression and improvement in RPE65-associated LCA. *Human molecular genetics* **22**, 1632–1642 (2013).
84. Z. Han, S. M. Conley, M. I. Naash, Gene therapy for Stargardt disease associated with ABCA4 gene. *Advances in experimental medicine and biology* **801**, 719–724 (2014).
85. J.-L. Bourges, S. E. Gautier, F. Delie, R. A. Bejjani, J.-C. Jeanny, R. Gurny, D. BenEzra, F. F. Behar-Cohen, Ocular Drug Delivery Targeting the Retina and Retinal Pigment Epithelium Using Polylactide Nanoparticles. *Invest. Ophthalmol. Vis. Sci.* **44**, 3562–3569 (2003).
86. M. Giannaccini, L. Pedicini, G. de Matienzo, F. Chiellini, L. Dente, V. Raffa, Magnetic nanoparticles. *Scientific reports* **7**, 43092 (2017).
87. M. Bhattacharya, S. Sarkhel, J. Peltoniemi, R. Broadbridge, M. Tuomainen, S. Auriola, A. Urtti, Differentially cleaving peptides as a strategy for controlled drug release in human retinal pigment epithelial cells. *Journal of controlled release : official journal of the Controlled Release Society* **251**, 37–48 (2017).
88. A. Tisi, V. Flati, S. Delle Monache, L. Lozzi, M. Passacantando, R. Maccarone, Nanoceria Particles Are an Eligible Candidate to Prevent Age-Related Macular Degeneration by Inhibiting Retinal Pigment Epithelium Cell Death and Autophagy Alterations. *Cells* **9** (2020).
89. L. L. Wong, S. Barkam, S. Seal, J. F. McGinnis, Temporal Distribution Patterns of Alexa Fluor 647-Conjugated CeNPs in the Mouse Retina After a Single Intravitreal Injection. *Advances in experimental medicine and biology* **1185**, 125–130 (2019).
90. A. Tisi, M. Passacantando, L. Lozzi, R. Maccarone, Cerium oxide nanoparticles reduce the accumulation of autofluorescent deposits in light-induced retinal degeneration. *Experimental eye research* **199**, 108169 (2020).
91. H.-a. Liu, Y.-l. Liu, Z.-z. Ma, J.-c. Wang, Q. Zhang, A lipid nanoparticle system improves siRNA efficacy in RPE cells and a laser-induced murine CNV model. *Invest. Ophthalmol. Vis. Sci.* **52**, 4789–4794 (2011).
92. J. H. Kim, M. H. Kim, D. H. Jo, Y. S. Yu, T. G. Lee, J. H. Kim, The inhibition of retinal neovascularization by gold nanoparticles via suppression of VEGFR-2 activation. *Biomaterials* **32**, 1865–1871 (2011).
93. G. Puras, J. Zarate, M. Aceves, A. Murua, A. R. Díaz, M. Avilés-Triguero, E. Fernández, J. L. Pedraz, Low molecular weight oligochitosans for non-viral retinal gene therapy. *European journal of pharmaceutics and biopharmaceutics : official journal of Arbeitsgemeinschaft fur Pharmazeutische Verfahrenstechnik e.V* **83**, 131–140 (2013).
94. M. Giannaccini, M. Giannini, M. P. Calatayud, G. F. Goya, A. Cuschieri, L. Dente, V. Raffa, Magnetic nanoparticles as intraocular drug delivery system to target retinal pigmented epithelium (RPE). *International journal of molecular sciences* **15**, 1590–1605 (2014).
95. H. Kim, K. G. Csaky, Nanoparticle-integrin antagonist C16Y peptide treatment of choroidal neovascularization in rats. *Journal of controlled release : official journal of the Controlled Release Society* **142**, 286–293 (2010).
96. L. Gan, J. Wang, Y. Zhao, D. Chen, C. Zhu, J. Liu, Y. Gan, Hyaluronan-modified core-shell liponanoparticles targeting CD44-positive retinal pigment epithelium cells via intravitreal injection. *Biomaterials* **34**, 5978–5987 (2013).

97. Q. Li, X. Qian, H. Y. Li, K. L. Lai, Q. Gao, W. Y. T. Lee, Safety assessment of polymeric micelles as an ophthalmic drug delivery system for intravitreal administration of dasatinib. *International journal of pharmaceutics* **596**, 120226 (2021).
98. D. Delgado, A. del Pozo-Rodríguez, M. Á. Solinís, M. Avilés-Triqueros, B. H. F. Weber, E. Fernández, A. R. Gascón, Dextran and protamine-based solid lipid nanoparticles as potential vectors for the treatment of X-linked juvenile retinoschisis. *Human gene therapy* **23**, 345–355 (2012).
99. A. Urtti, Challenges and obstacles of ocular pharmacokinetics and drug delivery. *Advanced drug delivery reviews* **58**, 1131–1135 (2006).
100. M. Nakanishi, R. Grebe, I. A. Bhutto, M. Edwards, D. S. McLeod, G. A. Lutty, Albumen Transport to Bruch's Membrane and RPE by Choriocapillaris Caveolae. *Invest. Ophthalmol. Vis. Sci.* **57**, 2213–2224 (2016).
101. R. Henning, A. Ohlmann, J. Staffel, K. Pollinger, A. Haunberger, M. Breunig, F. Schweda, E. R. Tamm, A. Goepferich, Multivalent nanoparticles bind the retinal and choroidal vasculature. *Journal of Controlled Release* **220**, 265–274 (2015).
102. S. R. Singh, H. E. Grossniklaus, S. J. Kang, H. F. Edelhauser, B. K. Ambati, U. B. Kompella, Intravenous transferrin, RGD peptide and dual-targeted nanoparticles enhance anti-VEGF intraceptor gene delivery to laser-induced CNV. *Gene Therapy* **16**, 645 (2009).
103. J. H. Kim, J. H. Kim, K.-W. Kim, M. H. Kim, Y. S. Yu, Intravenously administered gold nanoparticles pass through the blood-retinal barrier depending on the particle size, and induce no retinal toxicity. *Nanotechnology* **20**, 505101 (2009).
104. S. P. Kambhampati, A. J. M. Clunies-Ross, I. Bhutto, M. K. Mishra, M. Edwards, D. S. McLeod, R. M. Kannan, G. Lutty, Systemic and Intravitreal Delivery of Dendrimers to Activated Microglia/Macrophage in Ischemia/Reperfusion Mouse Retina. *Invest. Ophthalmol. Vis. Sci.* **56**, 4413–4424 (2015).
105. R. Singh, J. C. Batoki, M. Ali, V. L. Bonilha, B. Anand-Apte, Inhibition of choroidal neovascularization by systemic delivery of gold nanoparticles. *Nanomedicine : nanotechnology, biology, and medicine* **28**, 102205 (2020).
106. C. Zhu, Y. Zhang, W. M. Pardridge, Widespread expression of an exogenous gene in the eye after intravenous administration. *Invest. Ophthalmol. Vis. Sci.* **43**, 3075–3080 (2002).
107. Y. Zhang, F. Schlachetzki, J. Y. Li, R. J. Boado, W. M. Pardridge, Organ-specific gene expression in the rhesus monkey eye following intravenous non-viral gene transfer. *Molecular Vision* **9**, 465–472 (2003).

# Chapter 2

# Goals of the Thesis

Positive patient outcomes rely heavily on the ability to direct drugs to a specific site. Conventional drug therapy often results in subtherapeutic concentrations at the target site as most drugs distribute broadly through the patient. To overcome limitations presented by conventional drug therapy, nanoparticle-based drug delivery systems emerged as suitable vehicles to enhance on-site drug availability. More so, nanoparticles have been proven to be advantageous at solubilizing therapeutic cargos, prolonging the circulation lifetimes of drugs, and altering their biodistribution. Consequently, nanotherapeutics offer tremendous potential for improving targeted delivery of therapeutics ranging from small molecules to complex modalities such as RNA and DNA (*1, 2*). However, despite a century of perpetual discovery and development, nanotherapeutics still lack therapeutic efficacy in a broad range of indications including oncologic, inflammatory and ocular diseases. One major challenge that has been discussed repeatedly in the field (*3, 4*) is the incapability of nanoparticles to enrich *en masse* at the site of interest: The inability to reach target sites has been associated with a lack of clinical efficacy and safety, therefore leaving the therapeutic potential of various highly promising drugs untapped (*5*).

Therefore, the goal of this work was to develop nanotherapeutics targeting the retina to ultimately unleash the full potential of various drugs in ocular diseases.

As basic nanoparticulate drug carrier, lipid nanocapsules (LNCs) were used in this study. LNCs are important drug delivery systems given their biocompatibility, capability to encapsulate a broad range of drugs, and ease of preparation with favorable particle characteristics like precise control of particle size and narrow size distribution (*6*). Importantly, the encapsulation of lipophilic drugs can overcome physicochemical constraints limiting the therapeutic efficacy, such as low aqueous solubility and high plasma protein binding (*7*). Enhancing solubility by encapsulation into nanoparticles, however, does not automatically entail enhancement of intracellular drug availability. Fundamental reasons for the failure of site-specific drug release from the drug delivery system, are either the 'loss' of significant amounts of cargo already on the way to the target or limited intracellular release of the drug from the carrier (*8*). Therefore, to elucidate the relationship between intracellular availability and biological efficacy, lipophilic drugs were encapsulated into LNCs and *in vitro* effects of the nanotherapeutic were evaluated, accordingly (**Chapter 3**). Cyclosporin A (CsA) and Itraconazole (It), were used as model compounds given their therapeutic potential for the treatment of retinal diseases. To optimize cellular uptake of nanoparticles and further enable intracellular drug delivery, drug loaded LNCs were modified with an αvβ3 integrin-specific ligand cyclo(-Arg-Gly-Asp-D-Phe-Cys) (RGD), facilitating the internalization into endothelial and RPE cells (*9, 10*). The nanoparticle formulations were characterized for their physicochemical characteristics including size, polydispersity index, zeta potential and drug load. Additionally, their ability to be taken up and transport drugs into the target cells was investigated through flow cytometry and confocal laser

scanning microscopy. Subsequently, the therapeutic efficacy of the nanoparticles compared to free drugs and untreated control was elucidated by investigating inhibitory effects on endothelial cell proliferation, vascular endothelial growth factor expression, and tube formation.

As LNCs generally lack detectability in biological environments, labeling of LNCs is necessary for assessing their *in vitro* and *in vivo* performance. It is for this reason that fluorescent tags are usually introduced to the LNC core. This allows quick and easy quantification of the nanoparticles and enable visualization, localization and tracking of LNCs after *in vivo* or *in vitro* application (*11*). In order to additionally gain high resolution visualization via transmission electron microscopy (TEM) and further enable quantification using inductively coupled plasma optical emission spectroscopy (ICP-OES) (*12*), LNCs loaded simultaneously with fluorescent dye and superparamagnetic iron oxide nanoparticles (SPIONs) (*13*) were designed (**Chapter 4**). These dually labelled LNCs (Dual LNCs) were designed to be concomitantly visualizable via fluorescence and transmitted light imaging after either the internalization by cells *in vitro* or *in vivo* administration. Dual LNCs were analyzed and compared with fluorescent dye labeled LNCs (Dye LNCs) and SPION loaded LNCs (SPION LNCs) regarding physicochemical properties, colloidal stability, particle integrity and biocompatibility. Additionally, SPION content of Dual LNCs was determined using ICP-OES analysis. Furthermore, as special focus was laid on the enhancement of *in vivo* detectability, visibility of Dual LNCs in tissues after systemic administration to mice was examined using both optical microscopy and TEM.

Nanoparticle formulations are generally optimized based on *in vitro* performance and characteristics. Poor *in vivo - in vitro* correlation, however, can result in paradox outcomes and formulations often fail to successfully deliver drugs to the target site *in vivo (1, 3)*. In **Chapter 5** it was investigated whether systemically administered, drug-loaded RGD-LNCs overcome the obstacles of limited and unspecific target tissue enrichment, enhance on-site bioavailability and exhibit therapeutic efficacy for the treatment of retinal diseases. First, the ability of RGD-LNCs to reach and enrich in retinal pigment epithelial (RPE) and retinal endothelial cells was determined in healthy mice through quantitative and qualitative biodistribution studies. Additionally, cell specific nanoparticle enrichment and cellular residence time was assessed through fluorescence microcopy. Furthermore, to elucidate the mechanism underlying target cell enrichment and further shed light on the route RGD-LNCs take to reach RPE cells, TEM imaging was used. After investigating target cell specific enrichment in the retina of healthy mice, the therapeutic potential of CsA loaded RGD-LNCs compared to free CsA was assessed using a mouse model of retinopathy of prematurity (*14*). Effects of the intravenous CsA RGD-LNC therapy on pathologic neovascularization and inflammation were determined through immunohistochemistry, ELISA, real-time RT-qPCR

and fluorescence microscopy methods. Anti-angiogenic efficacy was assessed by determining suppression of retinal neovascularization, vascular endothelial growth factor (VEGF) and VEGF receptor expression in either the retina or RPE-choroid complex. Additionally, anti-inflammatory potential was investigated by examining glia cell reactivity and pro-inflammatory cytokine expression.

In summary, the overall goal of this work was to develop a nanotherapeutic able to overcome limitations presented by insufficient and unspecific target tissue enrichment to ultimately enhance on-site bioavailability and exhibit therapeutic efficacy for the treatment of retinal diseases.

# References


1. N. Bertrand, J.-C. Leroux, The journey of a drug-carrier in the body. *Journal of controlled release: official journal of the Controlled Release Society* **161**, 152–163 (2012).
2. Z. Zhao, A. Ukidve, J. Kim, S. Mitragotri, Targeting Strategies for Tissue-Specific Drug Delivery. *Cell* **181**, 151–167 (2020).
3. E. Blanco, H. Shen, M. Ferrari, Principles of nanoparticle design for overcoming biological barriers to drug delivery. *Nat Biotechnol* **33**, 941–951 (2015).
4. K. Park, Facing the truth about nanotechnology in drug delivery. *ACS nano* **7**, 7442–7447 (2013).
5. K. Park, The beginning of the end of the nanomedicine hype. *Journal of controlled release: official journal of the Controlled Release Society* **305**, 221–222 (2019).
6. N. T. Huynh, C. Passirani, P. Saulnier, J. P. Benoit, Lipid nanocapsules: a new platform for nanomedicine. *International journal of pharmaceutics* **379**, 201–209 (2009).
7. J. Qi, J. Zhuang, Y. Lu, X. Dong, W. Zhao, W. Wu, In vivo fate of lipid-based nanoparticles. *Drug discovery today* **22**, 166–172 (2017).
8. S. Behzadi, V. Serpooshan, W. Tao, M. A. Hamaly, M. Y. Alkawareek, E. C. Dreaden, D. Brown, A. M. Alkilany, O. C. Farokhzad, M. Mahmoudi, Cellular uptake of nanoparticles. *Chemical Society reviews* **46**, 4218–4244 (2017).
9. M. Friedlander, C.L. Thehsfeld, M. Sugita, M. Fruttiger, M.A. Thomas, S. Chang, D.A. Cheresh, Involvement of integrins alphavbeta3 and alphavbeta5 in ocular neovascular diseases. *Proceeding of the National Academy of Sience* **1996**, 9764–9769.
10. K. Markó, M. Ligeti, G. Mezo, N. Mihala, E. Kutnyánszky, E. Kiss, F. Hudecz, E. Madarász, A novel synthetic peptide polymer with cyclic RGD motifs supports serum-free attachment of anchorage-dependent cells. *Bioconjugate chemistry* **19**, 1757–1766 (2008).
11. G. Bastiat, C. O. Pritz, C. Roider, F. Fouchet, E. Lignieres, A. Jesacher, R. Glueckert, M. Ritsch-Marte, A. Schrott-Fischer, P. Saulnier, J.-P. Benoit, A new tool to ensure the fluorescent dye labeling stability of nanocarriers. *Journal of controlled release : official journal of the Controlled Release Society* **170**, 334–342 (2013).
12. X. Ma, A. Gong, B. Chen, J. Zheng, T. Chen, Z. Shen, A. Wu, Exploring a new SPION-based MRI contrast agent with excellent water-dispersibility, high specificity to cancer cells and strong MR imaging efficacy. *Colloids and Surfaces B: Biointerfaces*, 44–49 (2015).
13. E. Luque-Michel, V. Sebastian, A. Larread, C. Marquina, M. J. Blanco-Priet, Co-encapsulation of superparamagnetic nanoparticles and doxorubicin in PLGA nanocarriers. *European Journal of Pharmaceutics and Biopharmaceutics* **145**, 65–75 (2019).
14. K. M. Connor, N. M. Krah, R. J. Dennison, C. M. Aderman, J. Chen, K. I. Guerin, P. Sapieha, A. Stahl, K. L. Willett, L. E. H. Smith, Quantification of oxygen-induced retinopathy in the mouse. *Nature protocols* **4**, 1565–1573 (2009).

# Chapter 3

# Intracellular availability of poorly soluble drugs from lipid nanocapsules

Published in

*European Journal of Pharmaceutics and Biopharmaceutics*

2019, 139, 23-32

This chapter was published as: *M. Bohley, A. Haunberger, A. Goepferich, Intracellular availability of poorly soluble drugs from lipid nanocapsules. European Journal of Pharmaceutics and Biopharmaceutics 139, 23–32 (2019)*

# Abstract

Lipid nanocapsules (LNCs) are extensively used as drug carrier systems, due to their small size distribution, biocompatibility, and ease of preparation. They are especially useful for lipophilic drugs to overcome physicochemical constraints that limit their efficacy, such as low solubility in aqueous media. The aim of this work was to investigate the relationship between the intracellular availability of poorly soluble drugs delivered via LNCs and their biological efficacy in cells *in vitro*. Cyclosporin A (CsA) with a $\log P_{Oct}$ = 4.3 and Itraconazole (It) with a $\log P_{Oct}$ = 6.2 served as model lipophilic compounds, as they are highly promising candidates for the treatment of neovascular ocular diseases. Due to their lipophilic properties and the resulting preference for the oily core of LNCs, high encapsulation efficiencies were achieved. Drug-loaded LNCs with particle sizes around 50 nm were grafted with an αvβ3 integrin ligand (RGD) to optimize cellular uptake by human dermal microvascular endothelial cells. Even though RGD-LNCs showed excellent internalization, they exhibited insufficient inhibitory effects *in vitro* regarding endothelial cell proliferation, vascular endothelial growth factor expression, and tube formation in contrast to free drugs. This loss of efficacy could be explained by negligible intracellular availability of the poorly soluble drugs from LNCs.


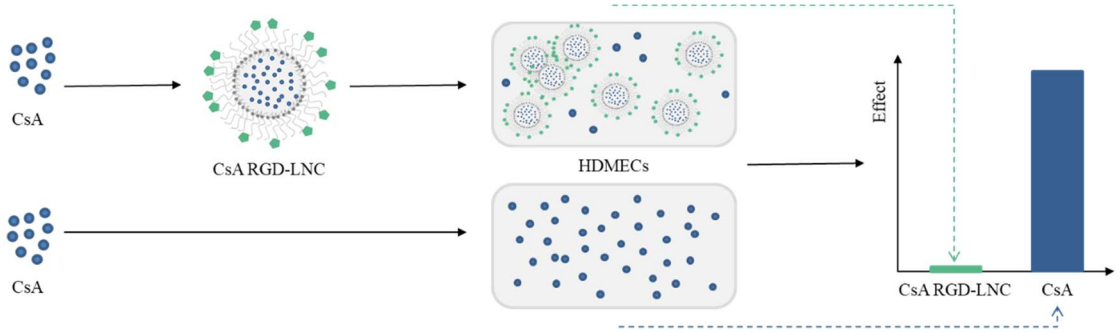

# 1 Introduction

Lipid nanocapsules (LNCs) are widely used as delivery systems, especially for poorly soluble drugs. This extensive use can be explained by their narrow size distributions with achievable sizes between 25 and 100 nm, biocompatible nature, simplicity of preparation, and capacity to encapsulate a broad range of drugs with various solubility characteristics (*1*). LNCs usually consist of an oily core made of medium-chain triglycerides, surrounded by a mixture of lecithin and a PEGylated surfactant. Their formulation is commonly based on the phase-inversion temperature phenomenon of emulsions leading to LNC formation with good mono-dispersity (*2*). In light of these advantages, we have chosen LNCs as a delivery system for lipophilic antiangiogenic drugs for the treatment of neovascular ocular diseases.

Neovascular ocular diseases, in particular exudative age-related macular degeneration (wet AMD) and proliferative diabetic retinopathy (DR), are associated with pronounced choroidal or intraretinal neovascularization, during which the blood vessels become leaky and begin to sprout (*3*). With the observation that blood vessel proliferation and hyperpermeability are the major underlying pathomechanisms (*4, 5*), vascular endothelial growth factor (VEGF) was identified as a key regulator of these processes (*6, 7*). Currently, VEGF is well known to be of paramount significance for the regulation of angiogenesis (*8*), blood vessel permeability, and the creation of endothelial cell fenestrations (*9, 10*). As a consequence, today's standard therapy for the treatment of neovascular ocular diseases are intravitreal anti-VEGF antibody injections (*11*). Even though this therapeutic concept has shown great success, there are numerous drawbacks and side effects that accompany continuous anti-VEGF therapy. Blocking the VEGF signaling pathway completely results in blocking all the positive VEGF effects as well (*12*). The biological VEGF effects in the retina are not limited to endothelial cells, where the effects are undesired, because VEGF receptors are expressed on a number of other cell types such as Müller cells, astrocytes, photoreceptors, and retinal pigment epithelial cells (*13, 14*). Clinically, rigorous suppression of omnipresent VEGF levels manifests in a decrease of choroid thickness (*15*). Epidemiologically, the risk of contracting geographic atrophy increases under long-term anti-VEGF antibody therapy and is accompanied by massive local cell death of retinal pigment epithelium cells and photoreceptors (*16*).

With AMD and DR being two of the leading causes of blindness globally (*17, 18*) and the limitations of continuous and rigorous VEGF knockdown in the retina, there is an urgent need for the development of a new therapeutic concept. Therefore, we developed antiangiogenic drug-loaded LNCs that allow for choroidal endothelium-specific anti-VEGF therapy. Ideally, this therapy would spare all cell types in the retina that suffer from general VEGF deprivation. Therefore, αvβ3 integrins were chosen as a promising target for selective nanoparticle delivery because their expression is limited to very few cell types and they are significantly over-

expressed during neovascularization (*19*). In the case of αvβ3 integrin, it is preferentially expressed by proliferating endothelial cells (*20–22*). Additionally, integrins stand out due to their high rates of receptor-mediated endocytosis, which could facilitate the intracellular delivery of targeted nanoparticles (*23, 24*).

Therefore, the highly potent and αvβ3 integrin-specific ligand cyclo(-Arg-Gly-Asp-D-Phe-Cys) (RGD) was attached to the LNC surface to target proliferating endothelial cells (*25, 26*). For intracellular anti-VEGF therapy, two highly appealing drugs were chosen: Cyclosporin A (CsA) and Itraconazole (It). They are already well known and widely used as an immunosuppressant and an antifungal drug, respectively. Besides their current scope of application, both interfere with the VEGF signaling pathway at different intracellular sites.

CsA is able to suppress the intracellular VEGF signaling pathway (*27*) and alleviates endothelial cell sprouting and proliferation *in vitro* (*28, 29*). Additionally, CsA counteracts the TGFβ-related increase of VEGF production in retinal pigment epithelial cells (*30*), which is the main source of VEGF in the retina (*31*). Furthermore, CsA possesses anti-inflammatory potential and decreases interleukin-1β levels. In addition, CsA repairs damage to the blood-retina-barrier in an animal model of diabetes (*32*). VEGF receptor type 2 (VEGF-R2) glycosylation and intracellular trafficking is not only inhibited by CsA, but also by It (*33*), and the same applies to endothelial cell proliferation (*34*). According to Nacev, et al., the drugs exert synergistic effects (*28*).

CsA has been shown to significantly, but moderately alleviate progression of diabetic retinopathy after oral administration to transplantation patients, demonstrating its high therapeutic potential but suffer from an insufficient availability in the ocular vasculature (*35–37*).

We have designed targeting nanocarriers loaded with CsA and a combination of CsA and It to overcome this lack of intracellular availability and concomitantly reduce side effects. The aim of this work was to elucidate whether an appropriate intracellular availability of CsA and It could be achieved by using LNCs as carrier systems for the poorly soluble drugs. The intracellular availability was investigated by comparing the inhibitory efficacy of CsA and a combination of CsA and It encapsulated in LNCs or as free drugs, on endothelial cell proliferation, VEGF-receptor expression, and tube formation.

# 2 Materials and Methods

## 2.1 Materials

Cyclosporin A (CsA) was obtained from Pharma Stulln GmbH (Stulln, Germany). Itraconazole (It) was purchased from Fagron GmbH (Barsbüttel, Germany). Kolliphor® HS15 was obtained from BASF. Lipoid® S75-3 was obtained from Lipoid GmbH (Ludwigshafen, Germany). Miglyol® 812 (MCT) was purchased from Caesar & Loretz GmbH (Hilden, Germany). NaCl was obtained from Merck (Darmstadt, Germany). 3,3'-Dioctadecyloxacarbocyanine-perchlorate (DiO) and 1,1'-Dioctadecyl-3,3,3',3'-tetramethylindocarbocyanine-perchlorate (DiI) were purchased from Invitrogen (Thermo Fisher Scientific, Waltham, MA, USA). Purified water was obtained from a MilliQ System from Millipore (Schwalbach, Germany). Dulbecco's Phosphate Buffered Saline (DPBS) was obtained from Gibco® Life Technologies (Thermo Fisher Scientific, Waltham, MA, USA). Cyclosporine D (CsD) was a generous gift from Prof. Dr. F. Kees (University of Regensburg, Germany). Methanol and dichloromethane, analytical standard, were purchased from Merck (Darmstadt, Germany). 1,2-Distearoyl-sn-glycero-3-phosphoethanolamine-N[maleimide(polyethyleneglycol)-2000] (ammonium salt) (DSPE-PEG2000-maleimide) and 1,2-Distearoyl-sn-glycero-3-phosphoethanolamine-N-[methoxy(polyethylene glycol)-2000] (ammonium salt) (DSPE-mPEG2000) were purchased from Avanti Polar Lipids Inc. (Alabaster, AL, USA) and cyclo(-Arg-Gly-Asp-D-Phe-Cys) acetate salt (RGD) from Bachem Distribution Service GmbH (Weil a. Rhein, Germany).
Fetal Calf Serum (FCS) was purchased from Biowest (Nuaillé, France). Recombinant Human Vascular Endothelial Growth Factor (VEGF)-165, APC anti-human CD309 (VEGF-R2) Antibody and APC Mouse IgG1, κ Isotype Ctrl Antibody were obtained from BioLegend UK Ltd. (London, UK). 3-(4,5-Dimethyl-2-thiazolyl)-2,5-diphenyl-2H-tetrazolium bromide (MTT) and Sodium dodecyl sulfate (SDS) were purchased from AppliChem (Darmstadt, Germany). Leibovitz's L-15, Trypsin-EDTA (0.25%) and Calcein-AM were obtained from Life Technologies (Thermo Fisher Scientific, Waltham, MA, USA). Propidium iodide was purchased from Sigma-Aldrich (Taufkirchen, Germany). Matrigel® Matrix was obtained from Corning (Amsterdam, Netherlands).

## 2.2 Cell Culture

Human Dermal Microvascular Endothelial Cells (HDMECs) were purchased from PromoCell GmbH (Heidelberg, Germany) and cultured in Endothelial Cell Growth Medium MV (GM) and Endothelial Cell Basal Medium MV (BM), purchased from PromoCell GmbH (Heidelberg, Germany). HDMECs were exclusively used in low passage numbers ranging from 4 to 6. Furthermore, it was ensured that confluence levels were below 80% in every experiment.

### 2.3 Preparation of Lipid Nanocapsules

LNCs were prepared according to a modified protocol originally based on the work of Heurtault et al. (*2*). In short, 887.5 mg Kolliphor® HS15, 30 mg Lipoid® S75-3, 415 mg MCT, 12 mg NaCl and 655.8 mg water were subjected to three cycles of progressive heating and cooling between 90 and 60°C. To quantify particles after modification and purification, fluorescent dyes (DiI or DiO 1.5% (w/w)) were added to the initial mixture. During the last cycle, an irreversible shock was induced by dilution with 5 ml water at the phase inversion temperature, leading to the formation of stable LNCs. Afterwards, additional magnetic stirring was applied for 5 min at room temperature. The final dispersion was filtered through a 0.22 µm regenerated cellulose (RC) membrane for sterilization and stored at room temperature in the dark.
To prepare drug-loaded LNCs, 35.3 mg CsA were dissolved in MCT and particles were prepared as described above. For It encapsulation, 0.1 mg was dissolved in dichloromethane and added to the mixture of MCT, Kolliphor, Lipoid, and NaCl. Dichloromethane was then evaporated at 75°C for 30 min. Afterwards, the water was added, and the first heating cycle was initiated.

### 2.4 Drug Loading Studies

Free non-encapsulated drug was separated from the LNCs by ultrafiltration using an Amicon® Ultra-4 MWCO 10 kDa centrifugal filter (Merck, Germany), as described by others (*38, 39*). 2 g of freshly prepared LNC dispersion were centrifuged for 30 min at 4000 *g*. The resulting filtrate was weighed, and the retentate weight adjusted to 2 g with water. After that, 20 µl of sample was diluted 5000-fold with methanol and ultrasonicated for 30 min to disrupt the particles and extract the drug, which was quantified by UHPLC-MS, as previously described (*40*). Briefly, CsD was used as an internal standard, and a calibration curve was made with CsA in blank LNC methanol solution, prepared as described above. Samples were analyzed in triplicate and the mean ± SD was calculated (mg of CsA per g of LNC dispersion). The encapsulation efficiency was determined (experimental drug payload/theoretical drug payload).

### 2.5 RGD-Peptide grafting on LNCs

First, peptides were coupled to the amphiphilic DSPE-PEG2000-maleimide using conjugation chemistry between the thiol group present on the cyclic structure of the peptide and the maleimide (*41*). Next, the conjugate or DSPE-mPEG2000 was inserted in the shell of the LNCs by post-insertion method (*42*). Modified LNCs were dialyzed against DPBS overnight using Spectra/Por® Float-A-Lyzer® G2 MWCO 300 kDa (Sigma-Aldrich, Germany) and subsequently centrifuged twice (15 min, 4000 *g*) using an Amicon® Ultra-4 MWCO 100 kDa centrifugal filter (Merck, Germany) for further purification.

## 2.6 Characterization of LNCs

Dynamic light scattering (DLS) was used to determine the Z-average particle diameter and the polydispersity index (PDI) of LNCs using a Zetasizer®Nano ZEN 3600 (Malvern Instruments, Worcestershire, UK). All batches were diluted in 10% DPBS and were analyzed in triplicate.

## 2.7 Cellular Uptake Studies

Flow Cytometry studies were performed on 24-well plates using DiO-labeled LNCs. 50,000 cells/well were seeded and incubated overnight in GM. GM was then aspirated, the cells were washed with DPBS and afterwards incubated with different LNC dispersions (0.6 mg/ml) for 45 min at 37°C. The cells were then washed with DPBS, detached from the well surfaces, washed again and re-dispersed in DPBS. Immediately prior to the measurement they were stained with propidium iodide to exclude damaged cells during analysis. The cells were analyzed using a BD FACS Calibur™ fluorescent-activated flow cytometer with BD CellQuest™ software (BDBiosciences, Heidelberg, Germany). Fluorescence was excited at 488 nm and recorded with a FL1 530/30 (DiO-LNCs) bandpass filter and a FL3 670 nm (PI) long pass filter. 10,000 cells were measured in each sample and untreated cells were used as internal control. Data was analyzed with Flowing Software (Turku Centre of Biotechnology, Finland). The population of viable cells was gated, and the mean fluorescence intensity was analyzed.

For Confocal Laser Scanning Microscopy, 20,000 cells/well were seeded in 8-well µ-slides (ibidi, Planegg, Germany) and incubated overnight. Cells were washed with DPBS, LNC samples (0.6 mg/ml) were added and incubated for 45 min at 37°C. Afterwards, cells were washed twice, covered with Leibovitz's Medium supplemented with 10% FCS and examined with a confocal microscope LSM 510 Meta (Zeiss, Oberkochen, Germany), using a Plan-Apochromat 63x/1.4 oil objective. Fluorescence was excited at 488 nm with an argon laser, and emission was recorded with a 505 nm long pass filter. Images were captured and analyzed using ZEN (Zeiss, Oberkochen, Germany).

## 2.8 MTT Assay

To determine cellular proliferation and viability, the MTT assay after Mosmann and Buttke, et al. (*43, 44*) was adapted. In short, 4,000 cells/well were seeded in 96-well plates and incubated overnight to allow the cells to adhere. Then the GM was replaced by various dilutions of VEGF (5 – 100 ng/ml), CsA (1.0 – 25 µg/ml), It (0.1 – 2.5 µg/ml), CsA/It in a ratio of 10:1 (1.0/0.1 – 25/2.5 µg/ml), CsA RGD-LNC, CsA+It RGD-LNC, or RGD-LNC (0.6 g/ml) in BM supplemented with 2% FCS. The cells were incubated at 37°C for 24 h, and then drug-containing medium was removed, and the cells were washed with DPBS. 0.63 mg/ml MTT solution (in 75% GM and 25% DPBS) was added to each well with a subsequent incubation over 4 h. Afterwards, MTT solution was aspirated carefully and 10% SDS solution was added.

The cells were further incubated overnight in the dark at room temperature. Lastly, the degree of proliferation was ascertained by measuring the absorbance at 570 nm on a microplate reader (FLUOstar Omega, BMG Labtech). Absorbance values were used to calculate the proliferation rate by referring to untreated control cells with a proliferation value of 100%.

### 2.9 Cell Cycle Analysis

Cell Cycle Analysis by flow cytometry was performed as previously described (*45–48*), to determine the percentage of cells in the $G_{0/1}$-, S- and $G_2$- Phases after DNA staining with propidium iodide. In short, 1 million cells were seeded in T75 culture flasks and incubated in GM overnight. Afterwards the GM was aspirated, the cells were washed with DPBS and samples (25 µg/ml CsA, 1.0/0.1 µg/ml CsA/It and 0.6 mg/ml CsA RGD-LNCs or CsA/It RGD-LNCs) in BM with 10 ng/ml VEGF were added. After an incubation period of 24 h, the samples were aspirated, the cells were washed, pelletized and washed twice again. 1 million cells per sample were transferred to a falcon tube, centrifuged again, resuspended in DPBS, and stored on ice for 5 min. Next, methanol was added under continuous stirring to dilute samples to 70% methanol and the cells were fixed for a minimum of 12 h. After the fixation process, the cells were washed with DPBS again and resuspended in 425 µl DPBS. 50 µl RNAse (Qiagen, Venio, Netherlands) (1 mg/ml) were added and incubated at 37°C for 20 min. Thereafter 25 µl propidium iodide (1 mg/ml) were added and samples were measured by flow cytometry with 50,000 counts/sample. Fluorescence was excited at 488 nm with an argon laser and emission was recorded with a FL3 670 nm (PI) long pass filter. Analysis and quantification were performed using ModFit LT (Verity Software House, Maine, USA).

### 2.10 VEGF-Receptor-2 Expression

To investigate the effect of drug-loaded LNCs and free drugs on VEGF-R2 expression, flow cytometry was used. For that 50,000 cells/well were seeded in a 24-well plate and grown in GM overnight. Thereafter, the cells were washed with DPBS and samples (25 µg/ml CsA, 1.0/0.1 µg/ml CsA/It and 0.6 mg/ml CsA RGD-LNCs or CsA/It RGD-LNCs) in BM containing 10 ng/ml VEGF were added and incubated for 24 h. Then, they were washed again, pelletized, and resuspended in cell staining buffer (DPBS supplemented with 5% FCS). APC anti-human CD309 (VEGF-R2) Antibody and APC Mouse IgG1, κ Isotype Ctrl Antibody were added to untreated and treated cells. After an incubation of 20 min on ice in the dark, the cells were pelletized again and washed twice with cell staining buffer before analysis. 10,000 events per sample were measured using flow cytometry. Fluorescence was excited at 635 nm, and emission was recorded with a FL4 661/8 nm (APC) bandpass filter. Data was analyzed by using mean fluorescence intensity, excluding mean fluorescence values obtained by isotype control, using Flowing Software (Turku Centre of Biotechnology, Finland).

### 2.11 Tube Formation Assay

Tube Formation Assays were performed to test antiangiogenic potency (*49*) of LNCs and free drugs on HDMECs, according to previously published methods (*50*). Briefly, a 96-well plate was coated with 50 µl Matrigel® per well. HDMECs were stained with Calcein-AM and adjusted to 1 million cells/ml. 1 ml of cell dispersion per sample was pelletized in Eppendorf tubes, resuspended in 25 µg/ml CsA, 1.0/0.1 µg/ml CsA/It and 0.6 mg/ml CsA RGD-LNCs or CsA/It RGD-LNCs and 10,000 cells/well were seeded gently on Matrigel®. The cells were examined after 2, 4, 6, 8, 10, and 24 h for tube formation using an inverted microscope LSM 510 Meta (Zeiss, Oberkochen, Germany) with a 5x objective, 488 nm laser, Ph1 (phase contrast). Quantification of tube networks was performed by using Angiogenesis Analyzer for ImageJ (*51*). As quantification parameters, the percentage reduction of nodes and the total tube length were used.

### 2.12 Statistical Analysis

All data are indicated as means ± SD of at least three independent experiments. The statistical analysis was performed using GraphPad Prism 6 and by using one-way ANOVA (unless otherwise stated). Significant differences were indicated as: *($P < 0.05$), **($P < 0.01$), *** ($P < 0.001$) and **** ($P < 0.0001$) related to control unless otherwise stated.

# 3 Results

### 3.1 Drug Loading studies

The poorly water-soluble drug CsA was dissolved in the oil phase prior to preparation. High encapsulation efficiencies were achieved with values of 67% and a drug payload of 34.1 mg/g LNC (Table 1). Similar behavior can be expected for It, due to its even lower water solubility compared to CsA (*52, 53*).

| | Drug payload [mg/g LNC] | Encapsulation efficiency [%] | Zeta Potential [mV] |
|---|---|---|---|
| CsA LNCs | 34.1 ± 0.7 | 66.8 ± 1.2 | - 2.26 ± 0.73 |

**Table 1.** Zeta potential [mV], drug payload [mg/g LNC dispersion] and encapsulation efficiency [%] with standard deviation of three independent batches. Drug payload and encapsulation efficiency characterized by HPLC-MS with a correlation coefficient $r^2 = 0.995$.

No significant differences could be detected in terms of drug payload and encapsulation efficiency between the batches, indicating that the manufacturing process of drug-loaded LNCs

is very reproducible. Nevertheless, there is a considerable amount of non-encapsulated CsA that presumably does not appear in a free state in the aqueous phase because there were no detectable amounts of free CsA in the filtrate after purification (data not shown).

## 3.2 Particle characterization

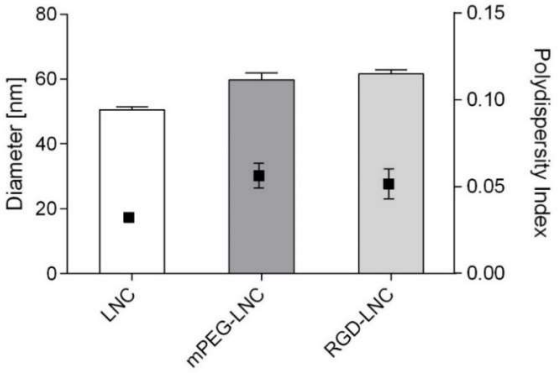


**Figure 1.** Size (bars) and size distribution (polydispersity, black squares) measured in 10% DPBS at 25°C.

It is well known that particle size is a key factor in cellular uptake of nanoparticles and that uptake increases with decreasing particle diameter up to an optimal point. In general, for nanoparticles with diameters below 100 nm, good cellular uptake has been shown, while the optimal size for cellular internalization seems to be 50 nm (*54*). Although, the size is only one factor that affects cellular internalization of nanocarriers (*55*). Another important physicochemical property regarding cellular uptake is the surface charge. Increased cellular internalization can be achieved by an enhancement of surface charge, either positive or negative, while extensive charges might lead to lysosomal escape or lysosome co-localization (*56*). Based on this knowledge, we prepared LNCs with a diameter of approximately 50 nm and a slightly negative zeta potential.

Size and polydispersity index (PDI) of blank LNCs as well as peptide-grafted LNCs are presented in Figure 1. Encapsulation of drugs or dyes did not change these characteristics (data not shown), as described by others (*57*). On the contrary, DSPE-mPEG or DSPE-PEG-RGD inserted after encapsulation increased the size of LNCs by an average of 10 nm, while PDI remained relatively low, indicating effective attachment of the peptides. For all formulations, the polydispersity index was < 0.07, which demonstrates narrow size distributions of all preparations.

## 3.3 Cellular Uptake Studies

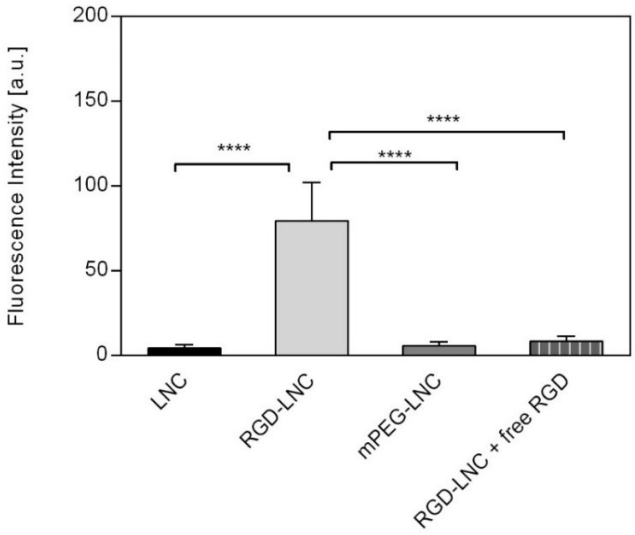


**Figure 2.** Mean fluorescence intensity of cells incubated with 0.6 mg/ml of modified, DiO loaded LNCs for 45 min incubation time at 37°C.

Internalization of modified and unmodified LNCs was evaluated *in vitro* by using flow cytometry (FACS) (Fig. 2) and confocal microscopy (Supplements S1). The FACS analysis revealed excellent cellular uptake of RGD-LNCs, whereas uptake of unmodified LNCs or mPEG-LNCs was negligible. The significantly higher internalization of RGD-LNCs confirmed the interaction between the RGD peptide and $\alpha_v\beta_3$ integrins on the cell surface of endothelial cells, as previously reported (*58*). This is additionally supported by the fact that there is a significant decrease of the fluorescent values when free RGD is added and $\alpha_v\beta_3$ integrins are saturated with free ligand. This clearly demonstrates active uptake of RGD-LNCs via $\alpha_v\beta_3$ integrin receptors and reveals that a targeting ligand on the shell of LNCs is needed to achieve satisfactory internalization.

Confocal laser scanning microscopy (CLSM) was used to confirm the excellent cellular uptake revealed by FACS analysis and to determine whether the LNCs were cell-surface bound or internalized. The CLSM pictures confirmed the results from the flow cytometry experiments (Supplements S1). Like the untreated cells (A), cells treated with LNCs (B) or mPEG-LNCs (D) showed no measurable fluorescence. Dense, bright fluorescence can be observed in the cytosolic region of the cells treated with RGD-LNCs (excluding the nucleus which showed less fluorescence) (C). This suggests that the RGD-LNCs were internalized rather than bound to the cell membrane. The internalization of RGD-LNCs was inhibited by the addition of free RGD during the incubation, indicating specific receptor-mediated uptake (E).

With both standard methods for the investigation of cellular uptake, we found that RGD-LNCs can interfere functionally with the $\alpha_v\beta_3$ integrin *in vitro*. This indicates that the coupling and

post-insertion process was successful and resulted in efficient recognition of the integrin receptors on the cell surface. Additionally, the results show that a targeting ligand is essential for achieving a sufficient uptake of LNCs, as non-modified LNCs were not taken up into the cells. Furthermore, the results reflect the great potential of RGD-LNCs for effectively and specifically delivering drugs into endothelial cells. Contrary to previous findings in the literature, we could not detect that LNCs or mPEG-LNCs were actively or passively internalized by cells with the experimental conditions we used (*59, 60*).

### 3.4 Evaluation of cell proliferation

Firstly, an MTT assay was used to determine the ability of CsA and It to hamper cell proliferation *in vitro* both in the presence and absence of VEGF. VEGF is a growth factor with high angiogenic potential due to its stimulation of endothelial cell proliferation and its inhibition of endothelial cell apoptosis (*61*). Therefore, the effect of different concentrations of free drugs (CsA, It, It+CsA) with and without addition of VEGF on HDMECs was investigated. Performing the same experiment with and without growth factor revealed whether the inhibitory effects of CsA and It are VEGF-dependent.

To determine the optimum VEGF concentration for HDMECs, different concentrations were used (Supplements S2). We found that 10 ng/ml was the most effective VEGF concentration for cell proliferation, which is in accordance with previous findings (*62*). This concentration was subsequently used in all other *in vitro* experiments.

Interestingly, we saw that freshly prepared, drug free, unmodified LNCs showed major toxic effects on HDMECs (Supplements S3). This toxicity could be avoided by using the same purification processes used after post-insertion of the targeting peptide, indicating that toxicity was probably due to free components from the manufacturing process, which could be removed by dialysis and centrifugation.

The ratio of CsA to It was kept at 10:1, as it has been shown to be the ratio with the highest synergistic effect according to Nacev, et al. (*28*).

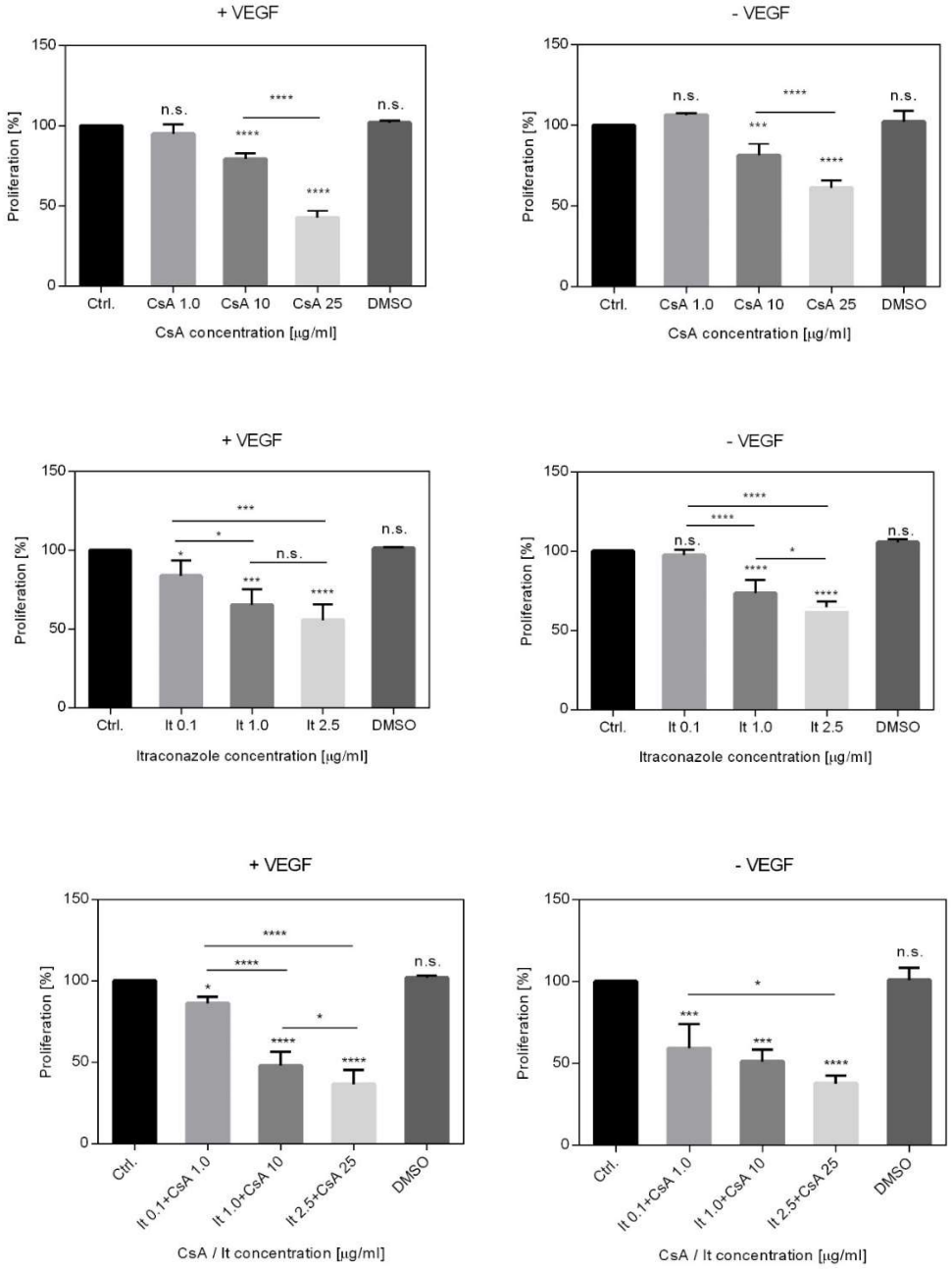


**Figure 3.** MTT assay showing the proliferation rate (%) relative to untreated cells as control. All experiments were carried out with HDMECs that were incubated for a 24 h period. Drugs were dissolved in DMSO, which was used as a control in the experiments. Cells were incubated with 1.0, 10, 25 µg/ml CsA, 0.1, 1.0, 2.5 µg/ml It, and It 0.1 + CsA 1.0, It 1.0 + CsA 10, It 2.5 + CsA 25 µg/ml. All experiments were performed with and without addition of 10 ng/ml VEGF.

All treatment groups showed dose dependent inhibition profiles (Fig. 3). Especially in the case of free CsA the inhibitory effect on cell proliferation is greater in the presence of VEGF, indicating, that there is a massive VEGF-dependency of the CsA efficacy.

CsA 25 (25 µg/ml) represents the greatest possible loading that can be reached in LNCs containing MCT as the oily core when using LNC concentrations of 0.6 mg/ml for *in vitro* experiments. With these conditions, it is excellent to see that there is such a strong reduction in proliferation, especially when VEGF is present. In the case of free It, our observations were similar. There is dose dependence, and the inhibitory effects on cell proliferation are also greater in the presence of VEGF, so it can be assumed that It acts in a VEGF-dependent manner as well. However, only 0.1 mg It could be encapsulated in the LNCs, resulting in a concentration of approx. 0.1 µg/ml It when using 0.6 mg/ml LNC dispersion. Still, we investigated the effects of 1.0 µg/ml It and 2.5 µg/ml It on cell proliferation as well, to determine if higher loading would reveal in higher efficacy. Nevertheless, in the presence of VEGF, 1.0 µg/ml It showed a statistically significant inhibitory effect on the proliferation rate.

Statistically significant inhibitory effects and dose dependency could also be seen for the combination of both drugs. Paradoxically, the observed extent of inhibition is, in the case of combining both drugs, stronger when there is no VEGF present. Unfortunately, the previously described (*28*) synergistic effect of combined CsA and It did not beat the efficacy of higher concentrations of CsA used alone. With these results, CsA 25 was selected as the most promising concentration, which was used in comparison with CsA 1.0 / It 0.1. This combination of the two drugs in a 10:1 ratio represents the highest possible concentration achievable.

Having confirmed that free CsA and CsA combined with It inhibit HDMEC proliferation and that these cells take up RGD-LNCs, we loaded these drugs into LNCs and tested them for their inhibitory effects on cell proliferation (Fig. 4).

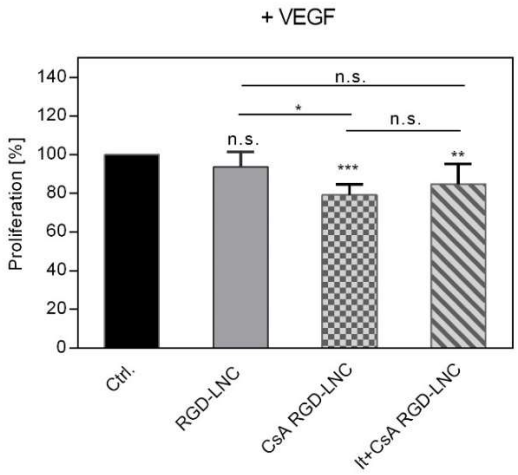


**Figure 4.** MTT assay showing the proliferation rate (%) relative to untreated cells as control. HDMECs were incubated for a 24 h period with either 0.6 mg/ml of targeted RGD-modified LNCs (RGD-LNCs), CsA-loaded RGD-LNCs (CsA RGD-LNC), or It- and CsA-loaded RGD-LNCs (It+CsA RGD-LNCs).

The MTT assay was performed using the same protocol as that used to evaluate the inhibitory potential of free CsA and It but yielded different results. CsA RGD-LNCs and It+CsA RGD-LNCs induced significant decreases in proliferation rate compared to the untreated control, but to smaller extends than free drug. Free CsA decreased the proliferation rate by 50%, while CsA RGD-LNCs only achieved a reduction of 20%. The degree of inhibition caused by It+CsA RGD-LNCs was minor, with no statistically significant differences from RGD-LNCs or CsA RGD-LNC. In contrast, the inhibitory efficiency of CsA RGD-LNCs was significant compared to RGD-LNCs. Drug-free RGD-LNCs showed no effect on the proliferation rate, confirming the cytocompatibility of the particles, as observed previously (supplemental information S3). Unexpectedly, free CsA had a highly efficient inhibitory effect on the proliferation rate of HDMECs but loading it into RGD-LNCs caused a loss of efficiency. The same trend could be seen for the combination of both drugs, despite the effects of free combined drugs being lower anyway.

To confirm the results of the MTT assay with another independent method, cell cycle analysis was performed to determine the inhibitory effect on cell proliferation of drug-loaded RGD-LNCs. To this end, flow cytometry was used to monitor the nuclear content of a cell and its changes during proliferation (*48*). The goal was to determine whether RGD-LNCs loaded with CsA or the combination of It+CsA were able to decrease the number of cells in the S-phase, when DNA is replicated, and trap these cells in the $G_{0/1}$-phase (*63*). Accordingly, HDMECs were incubated with free drugs or drug-loaded RGD-LNCs as in the MTT assays.

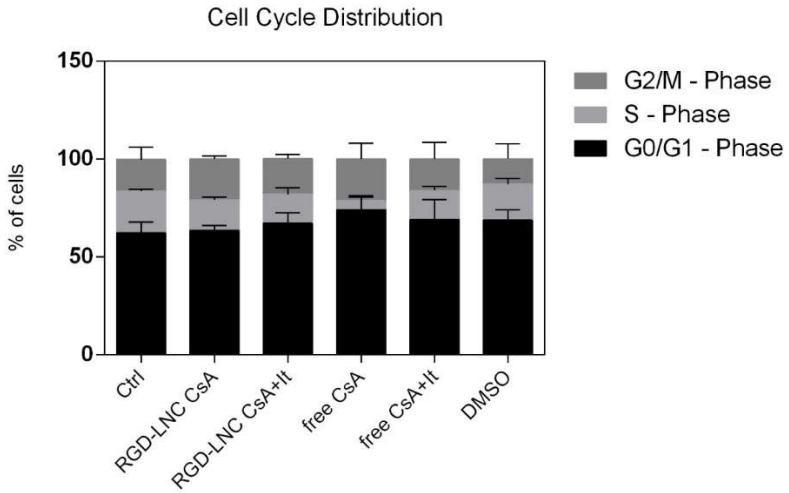


**Figure 5A.** Cell cycle distribution for HDMECs using 25 µl propidium iodide (1 mg/ml) and 50 µl RNAse (1 mg/ml) for DNA-staining. HDMECs were treated with 10 ng/ml VEGF with addition of free CsA (25 µg/ml), free CsA + It (1.0 + 0.1 µg/ml), 0.6 mg/ml CsA-loaded RGD-LNCs (CsA RGD-LNC), or 0.6 mg/ml CsA- and It-loaded RGD-LNCs (CsA+It RGD-LNCs) for 24 h at 37°C. Free drugs were dissolved in DMSO, which was used as a control in the experiments.

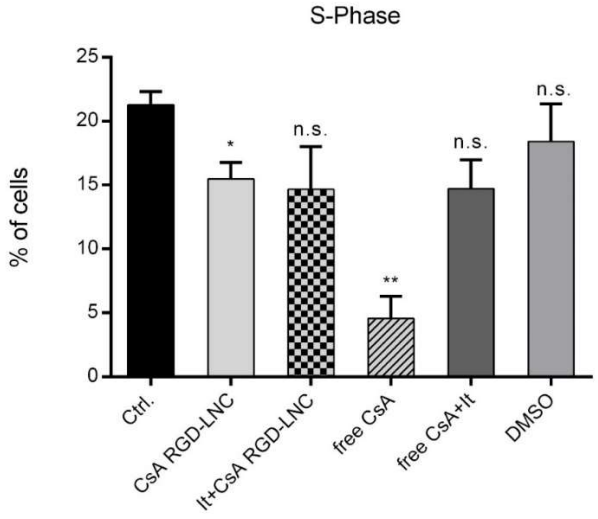


**Figure 5B.** Further Analysis of the average S-phase fraction, referring to Fig. 5A.

Figure 5A shows the overlay graphs of all phases of the cell cycle. There was a slight increase in the number of cells in the $G_{0/1}$-phase for CsA and It loaded RGD-LNCs. Free CsA showed the highest increase of cells in the $G_{0/1}$-phase. There were no significant differences among samples regarding the $G_2$/M-phase. Figure 5B gives more detailed insight into the S-phase, as the proportion of cells in this phase gives the most relevant readout. CsA-loaded RGD-LNCs had a statistically significant effect on cell cycle distribution, although they did not reach the efficacy of free CsA.

These results match the results obtained from the MTT assay, indicating that the efficacy of drug-loaded RGD-LNCs lags behind that of free drugs, despite RGD-LNCs having excellent targeting to and internalization in HDMECs (see Fig. 2 and Supplements S1). An explanation for this phenomenon could be poor intracellular bioavailability of the drugs from the LNCs, due to their high lipophilicity and solubility in the oily core. It cannot be due to the drugs, because they revealed excellent biological effects when dissolved in DMSO.

## 3.5 VEGF-Receptor-2 Expression

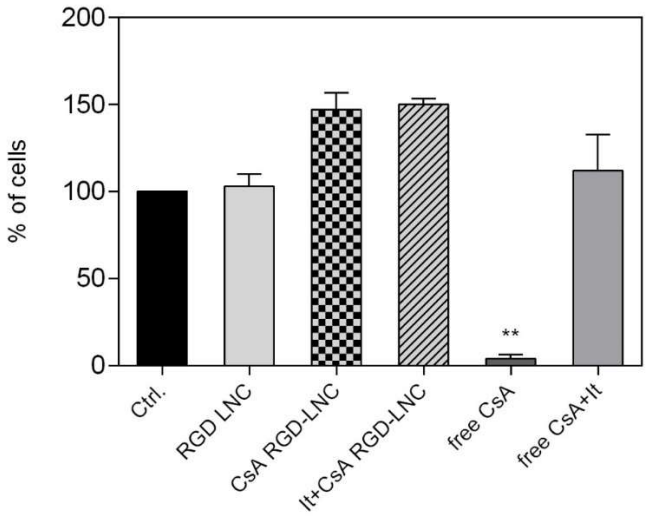


**Figure 6.** Expression of VEGF-R2 in HDMECs, stained with anti-human CD309 (VEGF-R2) antibody. Effects of free CsA (25 µg/ml), free CsA + It (1.0 + 0.1 µg/ml) and 0.6 mg/ml drug-free RGD-LNCs, 0.6 mg/ml CsA-loaded RGD-LNCs (CsA RGD-LNC) or 0.6 mg/ml CsA- and It-loaded RGD-LNCs (CsA+It RGD-LNCs) on surface expression of VEGF-R2 after an incubation period of 24 h relative to control (untreated cells). Cells were additionally treated with 10 ng/ml VEGF.

VEGF-Receptor 2 (VEGF-R2) mediates the biological effects of VEGF, which is well known as a key regulator of pathological angiogenesis (*64*). Reduction on the expression levels of VEGF-R2 has been discovered for both CsA and It (*27, 34*). To determine if free drugs or drug-loaded RGD-LNCs can reduce VEGF-R2 expression, we made *in vitro* evaluations with HDMECs and anti-human CD309 (VEGF-R2) antibody. Nonspecific binding of the CD309 antibody was investigated by using mouse IgG1 antibody as the isotype control. Fluorescence values resulting from non-specific binding were subtracted from all samples, including untreated cells.

Figure 6 displays that unloaded RGD-LNCs did not change VEGF-R2 expression values, as would be expected. Free CsA again reveals great efficacy, as it is able to eliminate expression almost completely. On the contrary, expression levels seemed to increase after treatment with drug-loaded RGD-LNCs, but not significantly compared to control.

This shows once again that CsA at the chosen concentration is a highly promising drug candidate for the treatment of neovascular diseases and that CsA encapsulation in LNCs leads to a massive loss of efficacy. For the combination of both drugs, similar observations could not be made. This is probably due to the low concentrations (0.1 µg/ml It and 1.0 µg/ml CsA) used, as even the free drugs showed no statistically relevant effect on VEGF-R2 expression.

## 3.6 Tube Formation Assay

Besides cell proliferation and VEGF-receptor expression, *in vitro* angiogenesis can be assessed by the tube formation assay (*27*). This assay has the highest explanatory power regarding the process of angiogenesis besides *in vivo* experiments. The tube formation assay involves not only one parameter like proliferation rate or receptor expression, but the complex interaction of different processes within cells while building new structures, including cell adhesion, migration, protease activity, and tubule formation (*65*). When HDMECs were seeded on a matrix, they built capillary-like structures (tubes) within a time frame of 24 h, with a maximum reached after 8 h of incubation (Fig. 7).

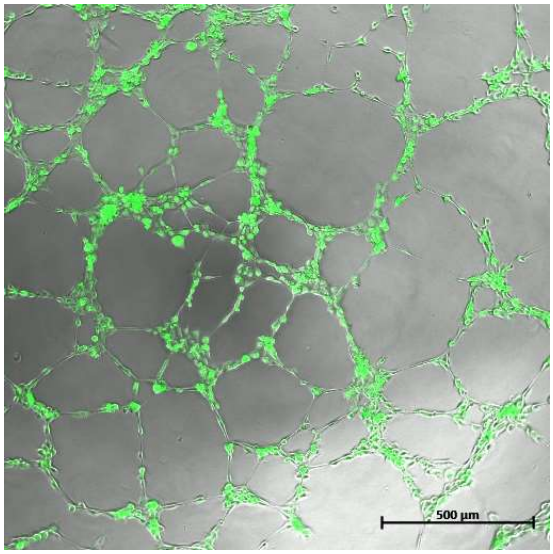


**Figure 7.** Confocal Image (with a 5x objective, excited at 488 nm with an argon laser, emission recorded at 505 nm with a long pass filter) of Calcein-AM stained HDMECs, treated with BM (control) after an incubation period of 8 h at 37°C.

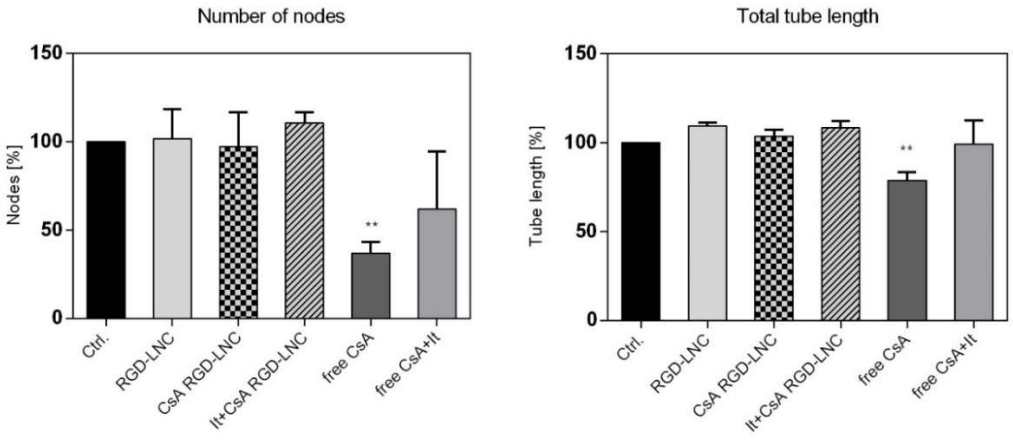


**Figure 8.** Quantification of tube formation by HDMECs after treatment with free CsA (25 µg/ml), free CsA + It (1.0 + 0.1 µg/ml) or 0.6 mg/ml of RGD-LNCs, CsA-loaded RGD-LNCs (CsA RGD-LNC) or CsA- and It-loaded RGD-LNCs (It+CsA RGD-LNCs) in presence of 10 ng/ml VEGF, relative to control (untreated cells). Number of nodes and total tube length relative to control (untreated cells) was determined after an incubation period of 8 h.

Free CsA exhibited marked inhibitory effects on the formation of tube-like structures by HDMECs, visible by significant reduction of the number of nodes and total tube length compared to untreated cells (Fig. 8). Drug-free RGD-LNCs showed no influence on the tube formation, as expected. Contrary to what would be expected, drug-loaded RGD-LNCs (CsA RGD-LNC and It+CsA RGD-LNC) had no effect on the tube formation. The combination of both free drugs revealed a slight effect on the number of nodes, whereas there was no detectable effect on the total tube length.

These results displayed a lack of inhibitory potential of drug-loaded RGD-LNCs on tube formation of HDMECs. This correlates with our previous experiments and shows that the anti-angiogenic potential of free drugs is lost once they are incorporated into this nanoparticle system. We hypothesize that the high lipophilicity of both drugs and their dissolution in the lipophilic core of the nanoparticle lead to poor intracellular availability and concomitant loss of biological efficacy.

# 4 Discussion

In this study, anti-angiogenic effects of CsA- or CsA+It-loaded in RGD-grafted LNCs were assessed *in vitro* using proliferating microvascular endothelial cells. We could demonstrate that targeted RGD-LNCs showed optimal physicochemical properties regarding size, PDI, and encapsulation efficiency, as well as excellent cellular uptake upon binding to the $\alpha_v\beta_3$ integrin expressed by endothelial cells. However, we saw no anti-angiogenic effects for CsA- or CsA+It-loaded LNCs, contrary to the effects displayed by the free drugs, especially CsA.

We hypothesize that this is due to the low intracellular escape of the poorly water-soluble drugs from the LNCs.

In the literature, very few studies can be found regarding the *in vitro* release or bioavailability of drugs from LNCs. LNCs are commonly used to overcome the poor water solubility of drugs like Ibuprofen (*66*), Quercetin, (-)-Epigallocatechin gallate (*57*), lipophilic radionuclides (*67*), methotrexate (*68*), ivermectin (*69*), Paclitaxel (*70*), Amiodarone (*71*), and antipsychotic drugs like promazine, chlorpromazine, thioridazine, trifluoperazine, triflupromazine, and chlorprothixene (*38*). In one of the few studies that report drug release kinetics for LNCs, *in vitro* release was only observed for promazine and chlorpromazine, while very lipophilic drugs like thioridazine, trifluoperazine, triflupromazine, and chlorprothixene were not discharged from LNCs (*38*). In the case of amiodarone, satisfactory release characteristics could only be achieved by pH adjustment and the addition of blank LNCs to the release medium as an acceptor phase (*71*). In another study, in which ibuprofen was taken as a model drug and encapsulated in LNCs, first order release kinetics were observed (*66*). A problem with this result is the low $\log P_{Oct}$ value for ibuprofen of 1.2 (*72*) that hardly reflects a lipophilic drug.

In contrast to drug delivery applications where release is desired, the firm immobilization of lipophilic compounds in LNCs may be an advantage in some cases such as when dyes or radiolabels are used for diagnostic purposes. Highly lipophilic indocarbocyanines like DiD, DiI and DiO, for example, did not leach from the particles even when oil was used as a lipophilic acceptor phase (*73*). Lipophilic $^{99m}$Tc-oxine incorporated in the lipid core of LNCs remained inside the particles even when submitted to aggressive release conditions such as dialysis. This made the labeled nanoparticles an ideal tool to evaluate LNC biodistribution *in vivo* (*74*).

In summary, these results raise doubts as to whether it is possible to improve the intracellular bioavailability of poorly soluble drugs by the encapsulation into lipid nanoparticles. A definite advantage of the technology is that the drug can be dissolved in the lipid phase of a particle, allowing for perfect dispersion in an aqueous medium. That such particles can be taken up by cells has been proven in numerous studies (*75*). However, what seems to be an advantage for the production of drug-loaded LNCs might be a handicap when it comes to intracellular drug release. Thus, it cannot be taken for granted that the encapsulated amount of drug corresponds to the amount of drug that is readily available inside cells. The active, available amount of drug seems to be dependent mainly on the drug-lipid interaction and the partitioning of the drug between the oily core of LNCs and the surrounding aqueous phase (*38*). We should, however, not forget that dissolution is a time dependent process, and that the kinetics of intracellular release must be considered as well. In our experiments, the time scale of observation was approximately 24 h which does not rule out the possibility that the drug might become available when observing release over longer time periods. Whether such slow kinetics would

be able to elicit the desired biological effects, however, needs to be scrutinized on a case-by-case basis.

# 5 Conclusion

CsA- and CsA+It-loaded, RGD-grafted LNCs were prepared successfully. Even though RGD-LNCs showed excellent cell internalization properties, we were not able to achieve satisfactory biological effects with drug-loaded RGD-LNCs *in vitro* compared to free drug. This observed lack of efficacy can be explained by the poor intracellular availability of lipophilic drugs from LNCs. If this observation holds true for our drug-particle combination only or if it is a more general trend remains to be seen. As a result, the intracellular release of drugs from LNCs should be investigated more carefully in future studies. Such studies could clarify if the ease of drug encapsulation in LNCs comes at the expense of limited biological drug efficacy.

# References


1. N. T. Huynh, C. Passirani, P. Saulnier, J. P. Benoit, Lipid nanocapsules: a new platform for nanomedicine. *International journal of pharmaceutics* **379**, 201–209 (2009).
2. B. Heurtault, P. Saulnier, B. Pech, A Novel Phase Inversion-Based Process for the Preparation of Lipid Nanocarriers. *Pharmaceutical Research*, 875–880 (2002).
3. H. Grossniklaus, R. Green, Choroidal neovascularization. *American journal of ophthalmology* **137**, 496–503 (2004).
4. G. A. Peyman, J. Koziol, Age-related macular degeneration and its management. *Journal of Cataract & Refractive Surgery* **14**, 421–430 (1988).
5. T. Murata, T. Ishibashi, A. Khalil, Y. Hata, H. Yoshikawa, H. Inomata, Vascular Endothelial Growth Factor Plays a Role in Hyperpermeability of Diabetic Retinal Vessels. *Ophthalmic Res* **27**, 48–52 (1995).
6. L. P. Aiello, R.L. Avery, P.G. Arrigg, B.A. Keyt, H.D. Jampel, S.T. Shah, L.R. Pasquale, H. Thieme, M.A. Iwamoto, J.E. Park, H.V. Nguyen, L.M. Aiello, N. Ferrara, G.L. King, Vascular Endothelial Growth Factor in Ocular Fluid of Patients with Diabetic Retinopathy and Other Retinal Disorders. *New England Journal of Medicine*, 1480–1486 (1994).
7. J.-P. Tong, W.-M. Chan, D. T. L. Liu, T. Y. Y. Lai, K.-W. Choy, C.-P. Pang, D. S. C. Lam, Aqueous humor levels of vascular endothelial growth factor and pigment epithelium-derived factor in polypoidal choroidal vasculopathy and choroidal neovascularization. *American journal of ophthalmology* **141**, 456–462 (2006).
8. M. Klagsbrun, S. Soker, VEGF/VPF: the angiogenesis factor found? *Current Biology*, 699–702 (1993).
9. D.R. Senger, S.J. Galli, A.M. Dvorak, Tumor Cells Secrete a Vascular Permeability Factor That Promotes Accumulation of Ascites Fluid. *Sience*, 983–985 (1983).
10. W.G. Roberts, G.E. Palade, Increased microvascular permeability and endothelial fenestration induced by VEGF. *Journal of Cell Sience*, 2369–2379 (1995).
11. L. P. Aiello, E. A. Pierce, E. D. Foley, H. Takagi, H. Chen, L. Riddle, N. Ferrara, G. L. King, L. E. Smith, Suppression of retinal neovascularization in vivo by inhibition of vascular endothelial growth factor (VEGF) using soluble VEGF-receptor chimeric proteins. *Proceedings of the National Academy of Sciences* **92**, 10457–10461 (1995).
12. T. Kamba, B. Y. Y. Tam, H. Hashizume, A. Haskell, B. Sennino, M. R. Mancuso, S. M. Norberg, S. M. O'Brien, R. B. Davis, L. C. Gowen, K. D. Anderson, G. Thurston, S. Joho, M. L. Springer, C. J. Kuo, D. M. McDonald, VEGF-dependent plasticity of fenestrated capillaries in the normal adult microvasculature. *American journal of physiology. Heart and circulatory physiology* **290**, H560-76 (2006).
13. M. Saint-Geniez, A. S. R. Maharaj, T. E. Walshe, B. A. Tucker, E. Sekiyama, T. Kurihara, D. C. Darland, M. J. Young, P. A. D'Amore, Endogenous VEGF is required for visual function. *PloS one* **3**, e3554 (2008).
14. J. M. Rosenstein, J. M. Krum, New roles for VEGF in nervous tissue—beyond blood vessels. *Experimental neurology* **187**, 246–253 (2004).
15. K. Sayanagi, Transient choroidal thinning after intravitreal bevacizumab injection for myopic choroidal neovascularization. *Clip Experiment Ophthalmol* (2011).
16. J. Grunwald, E. Daniel, J. Huang, G. Ying, M. Maguire, C. Toth, G. Jaffe, S. Fine, B. Blodi, M. Klein, A. Martin, S. Hagstrom, D. Martin, Risk of geographic atrophy in the comparison of age-related macular degeneration treatments trials. *Ophthalmology* **121**, 150–161 (2014).
17. J. B. Evans, B. A. Syed, New hope for dry AMD? *Nature reviews. Drug discovery* **12**, 501–502 (2013).
18. C. Hernández, A. Simó-Servat, P. Bogdanov, R. Simó, Diabetic retinopathy. *Journal of endocrinological investigation* (2017).
19. K. Hodivala-Dilke, alphavbeta3 integrin and angiogenesis. *Current opinion in cell biology* **20**, 514–519 (2008).

20. M. Friedlander, C.L. Thehsfeld, M. Sugita, M. Fruttiger, M.A. Thomas, S. Chang, D.A. Cheresh, Involvement of integrins alphavbeta3 and alphavbeta5 in ocular neovascular diseases. *Proceeding of the National Academy of Sience* **1996**, 9764–9769.
21. R.B. Brem, S.G. Robbins, D.J. Wilson, L.M. ORourke, Immunolocalization of integrins in the human retina. *Investigative Ophthalmology & Visual Science*, 3466–3474 (1994).
22. S.G. Robbins, R.B. Brem, D.J. Wilson, L.M. ORourke, Immunolocalization of integrins in proliferative retinal membranes. *Invest. Ophthalmol. Vis. Sci.*, 3475–3485 (1994).
23. A. Arjonen, J. Alanko, S. Veltel, J. Ivaska, Distinct recycling of active and inactive β1 integrins. *Traffic* **13**, 610–625 (2012).
24. P. Caswell, J. Norman, Endocytic transport of integrins during cell migration and invasion. *Trends in cell biology* **18**, 257–263 (2008).
25. X. Liu, W. Cui, B. Li, Z. Hong, Targeted therapy for glioma using cyclic RGD-entrapped polyionic complex nanomicelles. *International journal of nanomedicine* **7**, 2853–2862 (2012).
26. K. Markó, M. Ligeti, G. Mezo, N. Mihala, E. Kutnyánszky, E. Kiss, F. Hudecz, E. Madarász, A novel synthetic peptide polymer with cyclic RGD motifs supports serum-free attachment of anchorage-dependent cells. *Bioconjugate chemistry* **19**, 1757–1766 (2008).
27. P. Rafiee, J. Heidemann, H. Ogawa, N.A. Johnson, P.J. Fisher, M.S. Li, M.F. Otterson, C.P. Johnson, D.G. Binion, Cyclosporin A differentially inhibits multiple steps in VEGF induced angiogenesis in human microvascular endothelial cells through altered intracellular signaling. *Cell Communication and Signaling*, 1–22 (2004).
28. B. A. Nacev, J. O. Liu, Synergistic inhibition of endothelial cell proliferation, tube formation, and sprouting by cyclosporin A and itraconazole. *PloS one* **6**, e24793 (2011).
29. C. Esposito, A. Fornoni, F. Cornacchia, N. Bellotti, G. Fasoli, A. Foschi, I. Mazzucchelli, T. Mazzullo, L. Semeraro, A. Dal Canton, Cyclosporine induces different responses in human epithelial, endothelial and fibroblast cell cultures. *Kidney international* **58**, 123–130 (2000).
30. Z.-M. Bian, S. G. Elner, V. M. Elner, Regulation of VEGF mRNA expression and protein secretion by TGF-beta2 in human retinal pigment epithelial cells. *Experimental eye research* **84**, 812–822 (2007).
31. O. Strauss, The retinal pigment epithelium in visual function. *Physiological reviews* **85**, 845–881 (2005).
32. A. Carmo, J. G. Cunha-Vaz, A. P. Carvalho, M. C. Lopes, Effect of cyclosporin-A on the blood-retinal barrier permeability in streptozotocin-induced diabetes. *Mediators of inflammation* **9**, 243–248 (2000).
33. B. A. Nacev, P. Grassi, A. Dell, S. M. Haslam, J. O. Liu, The antifungal drug itraconazole inhibits vascular endothelial growth factor receptor 2 (VEGFR2) glycosylation, trafficking, and signaling in endothelial cells. *The Journal of biological chemistry* **286**, 44045–44056 (2011).
34. C. R. Chong, J. Xu, J. Lu, S. Bhat, D. J. Sullivan, J. O. Liu, Inhibition of angiogenesis by the antifungal drug itraconazole. *ACS chemical biology* **2**, 263–270 (2007).
35. R. Giannarelli, A. Coppelli, M. Sartini, M. Aragona, U. Boggi, F. Vistoli, G. Rizzo, S. Del Prato, F. Mosca, P. Marchetti, Effects of pancreas-kidney transplantation on diabetic retinopathy. *Transplant international : official journal of the European Society for Organ Transplantation* **18**, 619–622 (2005).
36. V. C. Chow, R. P. Pai, J. R. Chapman, P. J. O'connell, R. D. Allen, P. Mitchell, B. J. Nankivell, Diabetic retinopathy after combined kidney-pancreas transplantation. *Clin Transplant* **13**, 356–362 (1999).
37. I.A. Pearce, B. Ilango, R.A. Sells, D. Wong, Stabilisation of diabetic retinopathy following simultaneous pancreas and kidney transplant. *British Journal of Ophthalmol*, 736–740 (2000).
38. H. Nehme, P. Saulnier, A. A. Ramadan, V. Cassisa, C. Guillet, M. Eveillard, A. Umerska, Antibacterial activity of antipsychotic agents, their association with lipid nanocapsules and its impact on the properties of the nanocarriers and on antibacterial activity. *PloS one* **13**, e0189950 (2018).

39. A. Umerska, N. Matougui, A.-C. Groo, P. Saulnier, Understanding the adsorption of salmon calcitonin, antimicrobial peptide AP114 and polymyxin B onto lipid nanocapsules. *International journal of pharmaceutics* **506**, 191–200 (2016).
40. C. Luschmann, J. Tessmar, S. Schoeberl, O. Strauss, C. Framme, K. Luschmann, A. Goepferich, Developing an in situ nanosuspension. *European Journal of Pharmaceutical Sciences* **50**, 385–392 (2013).
41. M. Brinkley, A brief survey of methods for preparing protein conjugates with dyes, haptens and crosslinking reagents. *Bioconjugate chemistry* **3**, 2–13 (2002).
42. T. Perrier, P. Saulnier, F. Fouchet, N. Lautram, J.-P. Benoît, Post-insertion into Lipid NanoCapsules (LNCs): From experimental aspects to mechanisms. *International journal of pharmaceutics* **396**, 204–209 (2010).
43. T. Mosmann, Rapid colorimetric assay for cellular growth and survival. *Journal of Immunological Methods* **65**, 55–63 (1983).
44. T. M. Buttke, J. A. McCubrey, T. C. Owen, Use of an aqueous soluble tetrazolium/formazan assay to measure viability and proliferation of lymphokine-dependent cell lines. *Journal of Immunological Methods* **157**, 233–240 (1993).
45. P. N. Dean, J. W. Gray, F. A. Dolbeare, The analysis and interpretation of DNA distributions measured by flow cytometry. *Cytometry* **3**, 188–195 (1982).
46. P. Pozarowski, Z. Darzynkiewicz, in *Checkpoint controls and cancer, Volume 2: Activation and regulation protocols*, A. H. Schönthal, Ed. (Human Press, Totowa, N.J, 2004), pp. 301–311.
47. I. Nicoletti, G. Migliorati, M. C. Pagliacci, F. Grignani, C. Riccardi, A rapid and simple method for measuring thymocyte apoptosis by propidium iodide staining and flow cytometry. *Journal of Immunological Methods* **139**, 271–279 (1991).
48. R. Nunez, DNA measurement and cell cycle analysis by flow cytometry. *Current issues in molecular biology* **3**, 67–70 (2001).
49. I. Arnaoutova, J. George, H. K. Kleinman, G. Benton, The endothelial cell tube formation assay on basement membrane turns 20. *Angiogenesis* **12**, 267–274 (2009).
50. K. L. DeCicco-Skinner, G. H. Henry, C. Cataisson, T. Tabib, J. C. Gwilliam, N. J. Watson, E. M. Bullwinkle, L. Falkenburg, R. C. O'Neill, A. Morin, J. S. Wiest, Endothelial cell tube formation assay for the in vitro study of angiogenesis. *Journal of visualized experiments : JoVE*, e51312 (2014).
51. C. A. Schneider, W. S. Rasband, K. W. Eliceiri, NIH Image to ImageJ. *Nature Methods* **9**, 671 EP - (2012).
52. I. Zaghloul, R.J. Ptachcinski, G.J. Burckart, Blood Protein Binding of Cyclosporine in Transplant Patients. *Clinical Research: Immunosuppressive Drugs*, 240–242 (1987).
53. K. De Beule, Itraconazole: pharmacology, clinical experience and future development. *International Journal of Antimicrobial Agents*, 175–181 (1996).
54. S. E. A. Gratton, P. A. Ropp, P. D. Pohlhaus, J. C.r. Luft, V. J. Madden, M. E. Napier, J. M. DeSimone, The effect of particle design on cellular internalization pathways. *Proceedings of the National Academy of Sciences of the United States of America* **105**, 11613–11618 (2008).
55. K. Kettler, K. Veltman, D. van de Meent, A. van Wezel, A. J. Hendriks, Cellular uptake of nanoparticles as determined by particle properties, experimental conditions, and cell type. *Environmental Toxicology and Chemistry* **33**, 481–492 (2014).
56. P. Foroozandeh, A. A. Aziz, Insight into Cellular Uptake and Intracellular Trafficking of Nanoparticles. *Nanoscale Research Letters* **13** (2018).
57. A. Barras, A. Mezzetti, A. Richard, S. Lazzaroni, S. Roux, P. Melnyk, D. Betbeder, N. Monfilliette-Dupont, Formulation and characterization of polyphenol-loaded lipid nanocapsules. *International journal of pharmaceutics* **379**, 270–277 (2009).
58. J. Choi, E. Rustique, M. Henry, M. Guidetti, V. Josserand, L. Sancey, J. Boutet, J.-L. Coll, Targeting tumors with cyclic RGD-conjugated lipid nanoparticles loaded with an IR780 NIR dye. *International journal of pharmaceutics* **532**, 677–685 (2017).

59. S. Hirsjärvi, C. Belloche, F. Hindré, E. Garcion, J.-P. Benoît, Tumour targeting of lipid nanocapsules grafted with cRGD peptides. *European journal of pharmaceutics and biopharmaceutics : official journal of Arbeitsgemeinschaft fur Pharmazeutische Verfahrenstechnik e.V* **87**, 152–159 (2014).
60. A. Paillard, F. Hindré, C. Vignes-Colombeix, J.-P. Benoit, E. Garcion, The importance of endo-lysosomal escape with lipid nanocapsules for drug subcellular bioavailability. *Biomaterials* **31**, 7542–7554 (2010).
61. K. Gupta, S. Kshirsagar, W. Li, L. Gui, S. Ramakrishnan, P. Gupta, P. Y. Lwa, R. P. Hebbel, VEGF Prevents Apoptosis of Human Microvascular Endothelial Cells via Opposing Effects on MAPK/ERK and SAPK/JNK Signaling. *Experimental cell research* **247**, 495–504 (1999).
62. W. J. Lamoreaux, M. E. C. Fitzgerals, A. Reiner, K. A. Hasty, S. T. Charles, Vascular Endothelial Growth Factor Increases Release of Gelatinase A and Decreases Release of Tissue Inhibitor of Metalloproteinases by Microvascular Endothelial Cellsin Vitro. *Microvascular research* **55**, 29–42 (1998).
63. A. Pardee, G1 events and regulation of cell proliferation. *Science* **246**, 603–608 (1989).
64. N. Ferrara, H.-P. Gerber, J. LeCouter, The biology of VEGF and its receptors. *Nature Medicine* **9**, 669 (2003).
65. I. Arnaoutova, H. K. Kleinman, *In vitro* angiogenesis. *Nature protocols* **5**, 628 (2010).
66. M. M. A. Abdel-Mottaleb, D. Neumann, A. Lamprecht, In vitro drug release mechanism from lipid nanocapsules (LNC). *International journal of pharmaceutics* **390**, 208–213 (2010).
67. A. Béduneau, F. Hindré, A. Clavreul, J.-C. Leroux, P. Saulnier, J.-P. Benoît, Brain targeting using novel lipid nanovectors. *Journal of Controlled Release* **126**, 44–49 (2008).
68. A. Boechat, C. Oliveira, A. Tarragô, A. da Costa, A. Malheiro, S. Guterres, A. Pohlmann, Methotrexate-loaded lipid-core nanocapsules are highly effective in the control of inflammation in synovial cells and a chronic arthritis model. *International journal of nanomedicine* **10**, 6603–6614 (2015).
69. G. V. U. Gamboa, S. D. Palma, A. Lifschitz, M. Ballent, C. Lanusse, C. Passirani, J. P. Benoit, D. A. Allemandi, Ivermectin-loaded lipid nanocapsules: toward the development of a new antiparasitic delivery system for veterinary applications. *Parasitology research* **115**, 1945–1953 (2016).
70. F. Lacoeuille, F. Hindre, F. Moal, J. Roux, C. Passirani, O. Couturier, P. Cales, J. J. Le Jeune, A. Lamprecht, J. P. Benoit, In vivo evaluation of lipid nanocapsules as a promising colloidal carrier for paclitaxel. *International journal of pharmaceutics* **344**, 143–149 (2007).
71. A. Lamprecht, Y. Bouligand, J.-P. Benoit, New lipid nanocapsules exhibit sustained release properties for amiodarone. *Journal of Controlled Release* **84**, 59–68 (2002).
72. H. Potthast, J. B. Dressman, H. E. Junginger, K. K. Midha, H. Oeser, V. P. Shah, H. Vogelpoel, D. M. Barends, Biowaiver monographs for immediate release solid oral dosage forms. *Journal of pharmaceutical sciences* **94**, 2121–2131 (2005).
73. G. Bastiat, C. O. Pritz, C. Roider, F. Fouchet, E. Lignieres, A. Jesacher, R. Glueckert, M. Ritsch-Marte, A. Schrott-Fischer, P. Saulnier, J.-P. Benoit, A new tool to ensure the fluorescent dye labeling stability of nanocarriers. *Journal of controlled release : official journal of the Controlled Release Society* **170**, 334–342 (2013).
74. A. Cahouet, B. Denizot, F. Hindré, C. Passirani, B. Heurtault, M. Moreau, J.J. Le Jeune, J.P. Benoı̂t, Biodistribution of dual radiolabeled lipidic nanocapsules in the rat using scintigraphy and γ counting. *International journal of pharmaceutics* **242**, 367–371 (2002).
75. S. Hirsjärvi, S. Dufort, J. Gravier, I. Texier, Q. Yan, J. Bibette, L. Sancey, V. Josserand, C. Passirani, J.-P. Benoit, J.-L. Coll, Influence of size, surface coating and fine chemical composition on the in vitro reactivity and in vivo biodistribution of lipid nanocapsules versus lipid nanoemulsions in cancer models. *Nanomedicine : nanotechnology, biology, and medicine* **9**, 375–387 (2013).

# Chapter 3 – Supporting Information

---

# Intracellular availability of poorly soluble drugs from lipid nanocapsules

**Supplemental Figure 1**

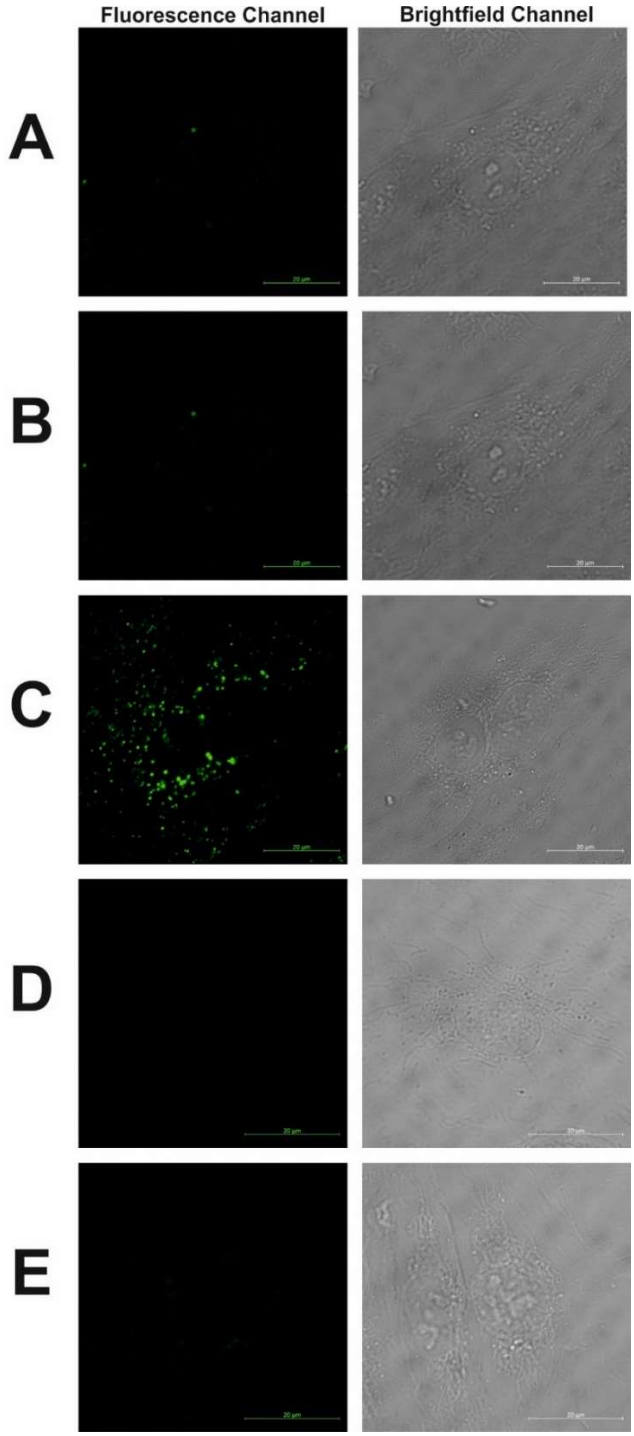


**Figure S1.** Confocal laser scanning microscope images of HDMECs after incubation for 45 min at 37°C with (A) medium (untreated control), (B) 0.6 mg/ml LNCs, (C) 0.6 mg/ml RGD-LNCs, (D) 0.6 mg/ml mPEG-LNCs and (E) 0.6 mg/ml RGD-LNCs + 500 µM free RGD (scale bar: 20 µm, left: fluorescence channel, right: brightfield channel).

Confocal laser scanning microscopy (CLSM) was used to confirm the excellent cellular uptake revealed by FACS analysis and to determine whether the LNCs were cell-surface bound or internalized.

**Supplemental Figure 2**

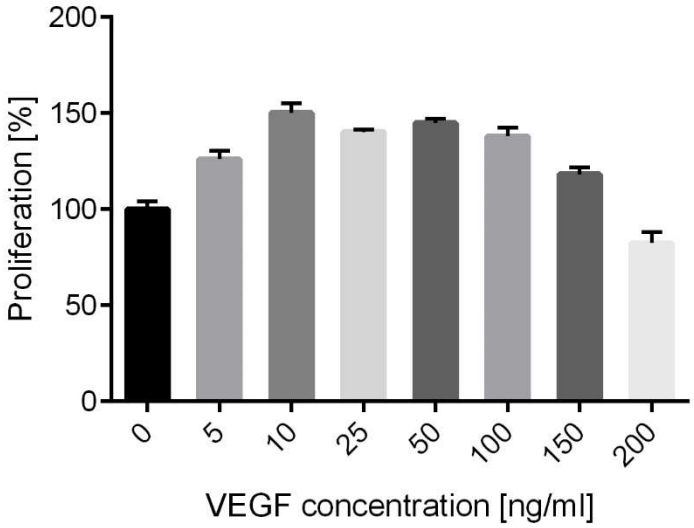


**Figure S2.** Dose dependent effect of vascular endothelial growth factor (VEGF) on the proliferation rate of human dermal microvascular endothelium cells (HDMEC). Cells were incubated for a 24 h period with different VEGF concentrations ranging from 5 – 200 ng/ml in basal medium. MTT assay showing the proliferation rate (%) normalized on cells treated with basal medium. This result defines 10 ng/ml as the most effective VEGF concentration to promote cell proliferation of HDMECs. Consequentially, this VEGF concentration was used in all *in vitro* experiments.

**Supplemental Figure 3**

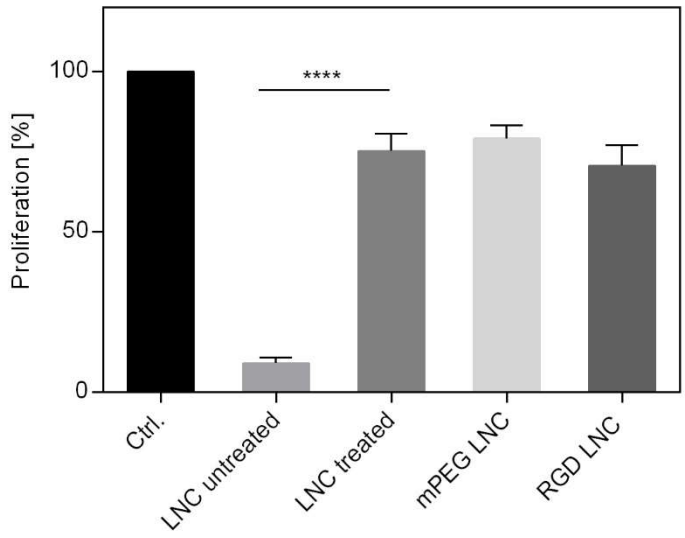


**Figure S3.** MTT assay showing the proliferation rate (%) normalized to untreated cells as control. HDMECs were incubated for a 24 h period with either 0.6 mg/ml of unpurified LNCs (LNC untreated), LNCs after dialysis and filtration by ultracentrifugation (LNC treated), mPEG-grafted LNCs and RGD-grafted LNCs, both purified as well.

This analysis revealed that interestingly, freshly prepared, drug-free, unmodified LNCs showed major toxic effects on proliferating HDMECs. This toxicity could be avoided by using the same purification processes as were used after the peptide grafting, indicating that toxicity was probably due to free components of the initial mixture, which could be removed by dialysis and centrifugation. All further experiments were conducted with purified LNCs, to preclude false-positive results.

# Chapter 4

# Design of dye and superparamagnetic iron oxide nanoparticle loaded lipid nanocapsules with dual detectability in vitro and in vivo

Published in

*International journal of pharmaceutics*

2020, 585, 119433

This chapter was published as: *M. S. Bohley, E. Birch, F. J. Baumann, A. E. Dillinger, E. R. Tamm, A. M. Goepferich, Design of dye and superparamagnetic iron oxide nanoparticle loaded lipid nanocapsules with dual detectability in vitro and in vivo. International journal of pharmaceutics 585, 119433 (2020)*

# Abstract

Lipid nanocapsules are treasured nanoparticulate systems, although they lack detectability in biological environments. To overcome this, we designed LNCs loaded simultaneously with fluorescent dye and superparamagnetic iron oxide nanoparticles (Dual LNCs). The introduction of both labels did not alter nanoparticle characteristics such as size (50 nm), size distribution (polydispersity index < 0.1) or surface modifications, including the effectiveness of targeting ligands. Furthermore, the colloidal stability, particle integrity and biocompatibility of the nanoparticles were not negatively affected by label incorporation. These Dual LNCs are concomitantly visualizable via fluorescence and transmitted light imaging after either the internalization by cells or systemic administration to mice. Importantly, they are detectable in liver sections of mice using transmission electron microscopy without additional enhancement. The iron content of 0.24% (m/m) is sufficiently high for precise quantification of nanoparticle concentrations via inductively coupled plasma optical emission spectroscopy. Dual LNCs are precious tools for the investigation of *in vitro* and *in vivo* performances of lipid nanocapsule formulations, since they allow for the use of complementary imaging methods for broad range detectability.


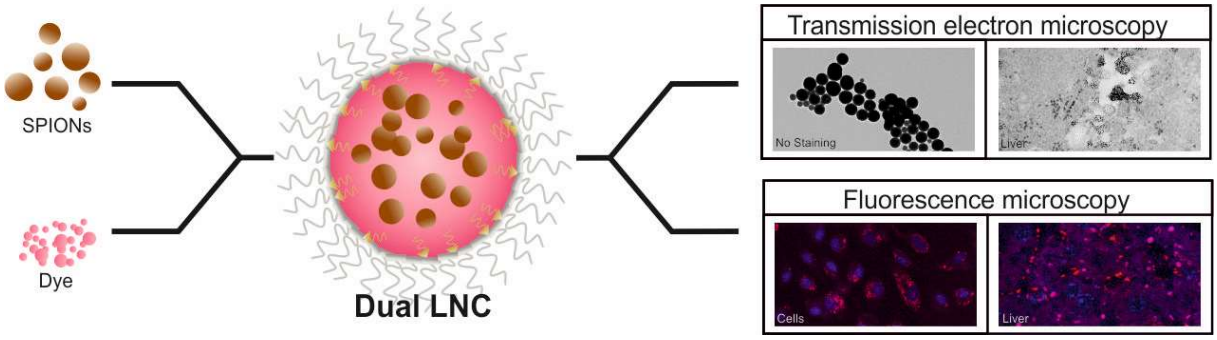

# 1 Introduction

Lipid nanocapsules (LNCs) are valuable drug delivery systems, as they offer the capacity to encapsulate a broad range of drugs and the potential to modify their surfaces with various ligands for targeting or therapeutic purposes. Furthermore, they are biocompatible, and their preparation is simple, generating narrow size distributions with achievable sizes between 25 and 100 nm (*1*). Labeling of the nanocapsules is necessary for assessment of their *in vitro* and *in vivo* performance. For this reason fluorescent tags are usually introduced to the LNC core or shell, which allow for quick and easy quantification of the particles and enable visualization, localization and tracking of LNCs after *in vivo* or *in vitro* application (*2*). Despite their advantages, fluorescent tags can show chemical instabilities or leakage of dyes and suffer from the typical limited resolution and scope of fluorescence microscopy (*2, 3*). In order to gain high resolution visualization via transmission electron microscopy (TEM), superparamagnetic iron oxide nanoparticles (SPIONs) are an ideal choice for use as labels (*4, 5*). Besides high-resolution imaging, *in vitro* or *in vivo* samples containing SPIONs could then be accurately quantified using inductively coupled plasma optical emission spectroscopy (ICP-OES) (*6*). Since it is also possible to use SPIONs for magnetic resonance imaging (MRI), this method could be further used to provide a detailed impression of the LNC biodistribution (*7*). Combining the advantages of both labels by dually labeling LNCs with fluorescent dye and SPIONs would therefore allow for complementary broad range imaging and quantification.

Since nanoparticle composition, including size, zeta potential and attached ligands, are crucial for the biological effects of LNCs, labeling should not affect any of these properties (*8*). Therefore, the aim of this study was to design dually labeled LNCs (Dual LNCs) for enhanced detectability without altering any nanoparticle characteristics. Dual LNCs were analyzed and compared with fluorescent dye labeled LNCs (Dye LNCs) and SPION loaded LNCs (SPION LNCs) regarding physicochemical properties, colloidal stability, particle integrity, biocompatibility, cellular uptake, and *in vitro* and *in vivo* detectability. For investigations of cellular uptake Dual LNCs and Dye LNCs were surface grafted with an αvβ3 integrin-specific ligand cyclo-(Arg-Gly-Asp-D-Phe-Cys) (RGD) to facilitate internalization (*9, 10*). As a special focus was on the enhancement of *in vivo* detectability, visibility of Dual LNCs in liver tissues after systemic administration was examined using both optical and transmission electron microscopy.

# 2 Materials and Methods

## 2.1 Materials

Sodium oleate was purchased from TCI Europe (Zwijindrecht, Belgium). Kolliphor® HS15 was obtained from BASF and Lipoid® S75-3 was acquired from Lipoid GmbH (Ludwigshafen, Germany). Miglyol® 812 (medium chain triglycerides (MCT)) was purchased from Caesar & Loretz GmbH (Hilden, Germany). 1,1′-Dioctadecyl-3,3,3′,3′-Tetramethylindocarbocyanine perchlorate (DiI), 3,3′-Dioctadecyloxacarbocyanine perchlorate (DiO) and 1,1′-dioctadecyl-3,3,3′,3′-tetramethylindodicarbocyanine perchlorate (DiD) were purchased from Invitrogen (Thermo Fisher Scientific, Waltham, MA, USA). 1,2-Distearoyl-sn-glycero-3-phosphoethanolamine-N[maleimide(polyethyleneglycol)-2000] (ammonium salt) (DSPE-PEG2000-maleimide) was purchased from Avanti Polar Lipids Inc. (Alabaster, AL, USA). Cyclo-(Arg-Gly-Asp-D-Phe-Cys) acetate salt (RGD) was purchased from Bachem Distribution Service GmbH (Weil a. Rhein, Germany). Dulbecco's phosphate buffered saline (DPBS) was acquired from Gibco® Life Technologies (Thermo Fisher Scientific, Waltham, MA, USA). Fetal Calf Serum (FCS) was purchased from Biowest (Nuaillé, France). 3-(4,5-Dimethyl-2-thiazolyl)-2,5-diphenyl-2H-tetrazolium bromide (MTT) and sodium dodecyl sulfate (SDS) were purchased from AppliChem (Darmstadt, Germany). Leibovitz's L-15 and Trypsin-EDTA (0.5%) were purchased from Life Technologies (Thermo Fisher Scientific, Waltham, MA, USA). All other chemicals were obtained from Merck (Darmstadt, Germany) at synthesis grade or higher. Ultrapure water was obtained using a MilliQ System from Millipore (Schwalbach, Germany).

## 2.2 Cell culture

Human Dermal Microvascular Endothelial Cells (HDMECs) were cultured in Endothelial Cell Growth Medium MV (GM) and Endothelial Cell Basal Medium MV (BM), all purchased from PromoCell GmbH (Heidelberg, Germany). HDMECs were used in low passage numbers ranging from 4 to 7. Mouse fibroblast L-929 cells were cultured in Eagle's Minimal Essential Medium (EMEM) with 10% FCS.

## 2.3 SPION synthesis

Iron oleate was freshly prepared before SPION synthesis, according to a previously described protocol (*11*). In short: 40 mL ethanol, 30 mL ultrapure water and 70 mL hexane were mixed, then 20 mmol of iron(III)chloride hexahydrate and 60 mmol sodium oleate were added. This mixture was heated to 70°C for 4 h before cooling to room temperature. The upper organic layer containing the iron oleate complex was separated and washed 3 times with ultrapure water.

The hexane was evaporated, and the remaining oily-brown mixture was dried for 12 h under vacuum at 30°C. For encapsulation into LNCs, the synthesized SPIONs must be hydrophobic, uniform and extremely small and so a previously described protocol was followed (*7*). In short: 2 mmol of iron-oleate complex and 12 mmol oleyl alcohol were mixed into 59 mmol of diphenyl ether. This mixture was degassed under vacuum at 90°C for 2 h, then heated to 200°C at a rate of roughly 10°C/min and kept at 200°C for 30 mins in an argon atmosphere. Afterwards, the solution was rapidly cooled to room temperature. Acetone was added to precipitate the nanoparticles by ultracentrifugation (5 min, 1000 g) in a ratio of 1 to 2.5 nanoparticle solution:acetone. The remaining SPIONs were with a vortex dispersed in MCT for use as required.

### 2.4 LNC preparation

LNCs were made in accordance with a protocol previously described (*12*). To incorporate the SPIONs, MCT with dispersed SPIONs from the synthesis described above were used. For the preparation of 50 nm LNCs 887.5 mg Kolliphor® HS15 40% (w/w), 30 mg Lipoid® S75-3, 415 mg MCT (with SPIONs if required), 12 mg NaCl, 655.8 µL water and fluorescent dyes (DiD, DiI and/or DiO 1.5% (w/w)) were heated in a phase inversion process of 3 cycles between 90°C and 60°C. In the third cycle, water was added at the phase inversion temperature leading to stable LNC formation (*13*). 25 nm LNCs were synthesized following the same method as above but with different volumes of the reagents: 1414 mg Kolliphor® HS15 40% (w/w), 30 mg Lipoid® S75-3, 204 mg MCT (with SPIONs if required), 12 mg NaCl and 315 µL water. The final dispersions were filtered through a 0.22 µm regenerated cellulose (RC) membrane for sterilization and stored at room temperature in the dark.

### 2.5 Physicochemical characterization

Spectral properties of LNCs were analyzed on a Cary Eclipse fluorescence spectrophotometer (Agilent, Santa Clara, USA). Size and morphology of Dual LNCs were evaluated on a Zeiss Libra 120 electron microscope (Zeiss, Oberkochen, Germany) without additional contrasting or enhancement. For this, LNCs were mounted on plasma cleaned, carbon-coated nickel grids (300 mesh; Plano, Wetzler, Germany) and incubated for 1 min. Sample grids were dried before use. Dynamic light scattering (DLS) was used to determine the Z-average particle diameter, the polydispersity index (PDI) and the zeta potential of SPIONs and LNCs using a Zetasizer Nano ZEN 3600 (Malvern Instruments, Worcestershire, UK). Batches were diluted in MCT or 10% DPBS, respectively, and were analyzed at 25°C in triplicate. Data were collected and analyzed using the Malvern Zetasizer software.

### 2.6 Iron content quantification

Inductively coupled plasma optical emission spectroscopy (ICP-OES) was used to quantify the iron content of Dual LNCs. 120 µL of the LNC suspension was added to aqua regia and heated to 100°C for one hour. After heating, 1 M nitric acid was added to adjust the aqua regia concentration to 32%. The iron content of the samples (n = 3) was then determined using a SpectroBlue TI/EOP (Analytical Instruments GmbH, Kleve, Germany). Data was calculated using a calibration of iron(III)chloride in 32% aqua regia 0 - 250 µM.

### 2.7 Biocompatibility

Cytotoxicity of the labeled LNCs was determined using the MTT reduction assay according to the ISO guideline (10993-5:2009) for *in vitro* cytotoxicity testing (*14*). In short, either 10 000 cells/well of L-929 or HDME cells were seeded in 96-well plates and incubated for 36 h to allow the cells to adhere. Then, the medium was replaced with dilutions of DiO LNCs or Dual LNCs in a concentration range of 0.001 - 5 mg/mL in EMEM or BM supplemented with 4% FCS. SDS (0.1%) and pure medium served as controls (n = 6). The cells were incubated at 37°C for 24 h, then the particles were removed, and the cells washed with DPBS. 0.63 mg/mL MTT solution was added to each well and the plates were further incubated for 4 h. Afterwards, the MTT solution was aspirated and 10% SDS solution was added. The cells were incubated overnight in the dark at room temperature. The absorbance was measured at 570 and 690 nm using a FluoStar Omega Microplate Reader (BMG LABTECH GmbH, Ortenberg, Germany). Absorbance values were used to calculate the viability of cells. Results were normalized to the control (untreated cells). To determine the morphology of cells, microscope images were recorded with a Nikon SD-U1 camera (Nikon, Düsseldorf, Germany) connected to a Leica DM IRB microscope (Leica, Wetzlar, Germany).

### 2.8 Colloidal stability

To determine if incorporation of SPIONs had any effect on the colloidal stability of LNCs, stability tests were conducted for the 50 nm LNCs over a 7-day time period. To this end n = 3 samples of SPION LNCs, Dual LNCs and Dye LNCs were incubated at either 20°C or 37°C. Size and PDI were determined at defined intervals using DLS.

### 2.9 LNC integrity

A fluorescence resonance energy transfer (FRET) experiment was performed to evaluate the integrity of LNCs. Therefore, LNCs and SPION LNCs with encapsulated DiO and DiI were made. DiO and DiI labelled LNCs were diluted with either DPBS or 10% FCS to a final concentration of 10 mg/mL.

Samples (n = 3) were incubated at 37°C or 20°C respectively. DiO fluorescence was excited at 460 nm and fluorescence emission spectra were recorded between 485 and 710 nm at defined time points (0 h - 7 d) on a Cary Eclipse fluorescence spectrophotometer (Agilent, Santa Clara, USA). FRET ratios were calculated as previously described (*15*).

### 2.10 RGD peptide grafting

For uptake experiments, the RGD peptide was grafted onto LNCs. Initially, RGD peptides were coupled to DSPE-PEG2000-maleimide using conjugation between the thiol of the peptide and the maleimide (*16*). Then, using the post-insertion method, this was inserted into the shell of the LNCs (*17*). Modified LNCs were dialyzed against DPBS overnight using Spectra/Por® Float-A-Lyzer® G2 MWCO 300 kDa (Sigma-Aldrich, Germany) and subsequently centrifuged twice (15 min, 4000 g) using an Amicon® Ultra-4 MWCO 100 kDa centrifugal filter (Merck, Germany) for further purification.

### *2.11 In vitro* imaging

300 000 HDMECs cells/well were seeded on coverslips in a 6-well plate and incubated for 36 h to allow the cells to adhere. Then, the medium was aspirated, cells were washed with DPBS and dilutions of the RGD-grafted DiO LNCs and RGD-grafted Dual LNCs at a concentration of 0.1 mg/mL in Leibovitz's solution were added and incubated for 45 min at 37°C. Then, samples were removed, cells were washed with DPBS, fixated with 4% PFA solution and washed again. The coverslips were then extracted from the plate and embedded using Mowiol® with DAPI stain onto microscope slides. The slides were examined using a Zeiss Axio Imager fluorescence microscope (Carl Zeiss AG, Göttingen, Germany) and a 40× Plan-Neofluar (NA 1.3) (Zeiss) objective. Particle uptake was evaluated by recording the fluorescence image for detection of the incorporated DiO and of the additionally applied DAPI staining, to localize cell nuclei. DiO and DAPI fluorescence was excited with a LED-module at 475 and 360 nm and emission was recorded using an 450 - 488 and 410 - 440 nm emission filter. Complementary transmitted light images were recorded to detect SPIONs.

### *2.12 In vivo* imaging

Female, 4-week-old 129SV mice were used as animal models. Mice were bred in-house at the animal laboratories of the University of Regensburg and housed under standardized conditions 62% air humidity and 21°C room temperature. Before the experiments, mice were anesthetized by isoflurane inhalation and then 100 µL of Dual RGD-LNC solution with a concentration of 10 mg/mL was injected systemically (n = 3). After 1 h of circulation, mice were anesthetized with a mixture of ketamine and xylazine, perfused with 4% (w/v) paraformaldehyde (PFA) solution and livers were removed.

All animal experiments were carried out according to the national and institutional guidelines and were approved by the local authority (Regierung der Oberpfalz, Bavaria, Germany, reference no. 55.2-2532-2-363).

Immediately after removal, one part of the liver was fixed in a solution of 4% PFA for 12 h at 4°C for the preparation of cryosections. The livers were then exposed to a sucrose gradient (10%, 20% and 30%) for 12 h each, washed with DPBS, embedded in Tissue Tek O.C.T. Compound (Sakura Finetek) and finally frozen in the gas phase of liquid nitrogen. Thereafter, specimens were cut into 12 µm sections using an HM 500 OM microtome (Microm International), transferred onto microscope slides and mounted with Mowiol® supplemented with DAPI, to counterstain nuclear DNA. For the preparation of semi-thin and ultra-thin sections, livers were placed for 24 h in Karnovsky fixative, and embedded either in Epon or London Resin white (L.R. white) (Serva, Garden City Park, NY) as described elsewhere (*18, 19*). Semi-thin sections (1.0 µm thick) were cut and examined using a Zeiss Axio Imager fluorescence microscope (Carl Zeiss AG, Göttingen, Germany). The objective used was a 40× Plan-Neofluar (NA 1.3) (Carl Zeiss). DiI and DAPI fluorescence was excited with a LED-module at 555 and 360 nm and emission was recorded using a 579 - 604 and 410 - 440 nm emission filter. Additionally, Epon or L.R. white ultra-thin sections (70 - 80 nm thick) were processed according to protocols published previously (*20, 21*). Epon sections were contrasted with uranyl acetate and lead citrate. All sections were analyzed using a Zeiss Libra 120 electron microscope (Zeiss, Oberkochen, Germany).

### 2.13 Statistical analysis

All data are indicated as means ± SD of at least three independent experiments. Statistical analysis was performed using GraphPad Prism 6 with one-way ANOVA and significant differences were indicated as: *($P < 0.05$), **($P < 0.01$), ***($P < 0.001$) and ****($P < 0.0001$) related to the control (unless otherwise stated).

# 3 Results and Discussion

## 3.1 Synthesis, Characterization and Biocompatibility of Dual LNCs

For the manufacturing of Dual LNCs, SPIONs were prepared with a simple one-pot reaction and dispersed in the oily core component of the LNCs (*7*). DLS measurements of freshly prepared SPIONs revealed a hydrodynamic diameter of approximately 6 - 8 nm (Supporting Information Figure S1). TEM images showed aggregates, as well as single SPIONs of different sizes, whereby the larger SPIONs were in a size range of 4 - 8 nm, in accordance with the results gained from DLS measurements. In the second step, Dual LNCs with incorporated SPIONs and lipophilic fluorescent dye were manufactured, using our usual LNC manufacturing protocol (*12*).

To determine whether SPIONs were actually located in the core of LNCs and whether the structure of the LNCs was affected by this, TEM imaging was performed (Figure 1A). TEM images revealed that SPIONs were successfully incorporated, resulting intact, spherical and electron dense Dual LNCs.

Since it is known that size, PDI and surface characteristics of nanoparticles are of paramount importance for the interaction of a nanomaterial with its biological environment, the introduction of labels must not result in alterations to those properties (*8*). It has already been shown that the introduction of fluorescent dyes into the LNC core had not lead to any changes (*22*). To determine whether this also applies for the incorporation of SPIONs, 50 nm LNCs with either SPIONs alone (SPION LNCs) or dye and SPIONs (Dual LNCs) were prepared and analyzed regarding particle size, PDI and zeta potential and compared to Dye LNCs. Figure 1B revealed that neither the incorporation of SPIONs, nor the incorporation of dye and SPIONs together had any significant effect on the hydrodynamic diameter or the PDI of the LNCs. Additionally, the zeta potential of Dye LNCs did not significantly differ due to the incorporation on SPIONs (data not shown).

It was also possible to synthesize very small Dual LNCs with a hydrodynamic diameter of below 25 nm, again with no alterations in the particle size or PDI compared to Dye LNCs (Supporting Information S2). This showed that it is possible to synthesize Dual LNCs with different diameters for use in alternative biomedical applications, simply by varying initial quantities of reagents used for the synthesis (*13*).

With the evidence of detectability of Dual LNCs via TEM, the fluorescence detectability was investigated. To this end, 50 nm Dye LNCs and Dual LNCs with different fluorescence dyes were prepared and emission spectra were recorded (Fig. 1B - 1D).

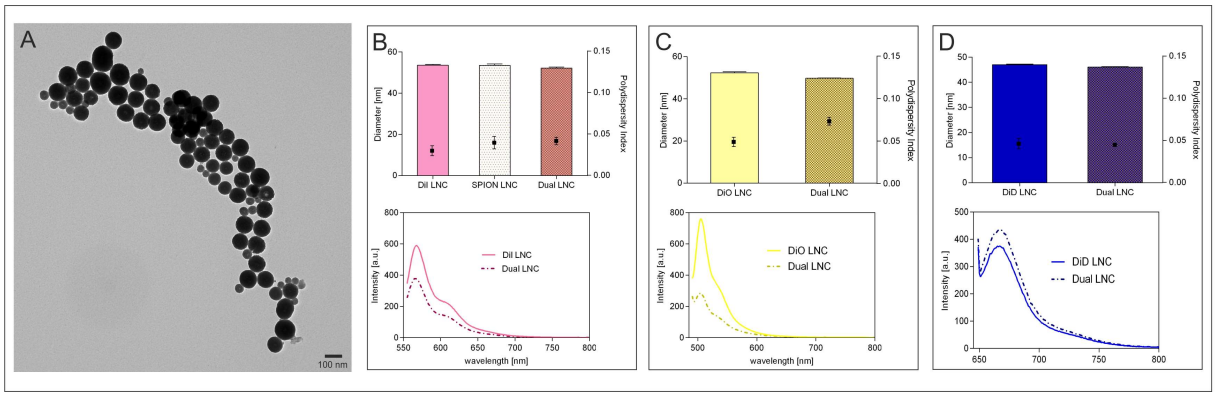


**Figure 1.** Dual LNC characteristics. (A) TEM image of Dual LNCs revealing intact, spherical and electron dense nanoparticles. (B-D) Characterization of different Dye LNCs (B: DiI, C: DiO, D: DiD) in comparison with SPION LNCs and Dual LNCs regarding hydrodynamic diameter (bars), PDI (squares) and fluorescence properties (spectra).

Although the fluorescence spectra of Dual LNCs did not correspond exactly to the spectra of Dye LNCs, all emission maxima at the defined wavelengths were present, indicating detectability and quantifiability of all Dual LNCs formulations. These results revealed that a wide range of lipophilic fluorescent dyes could be used, as required to avoid disturbance of other stains for simultaneous fluorescence imaging, for example in the case of antibody staining.

Since the iron content can be used alongside the fluorescent properties for quantitative purposes, ICP-OES was used to determine the absolute iron content of Dual LNCs. For the 50 nm Dual LNCs, the iron content was 0.24% (m/m), corresponding to approximately 1200 iron complexes per particle. As this easy and accurate method allows for a quick and simple iron quantification, ICP-OES can prospectively be used to determine Dual LNC concentrations in cells or tissues after *in vivo* application (*23*).

For cell and *in vivo* experiments, the biocompatibility of Dual LNCs compared to Dye LNCs was investigated. Although LNCs are made out of fully biocompatible excipients and are not known to cause any cytotoxic effects, the incorporation of SPIONs could potentially alter the biocompatibility, given that the biocompatibility of SPIONs mainly depends on their surface composition and the used cell type (*24–27*). The assessment of cytotoxicity of Dual LNCs compared to Dye LNCs revealed no notable differences between them (Supporting Information S3A and S3B).

### 3.2 Stability of Dual LNCs

Colloidal stability was assessed via DLS measurements of hydrodynamic diameter and PDI as a function of incubation time (0 h - 7 d) at 37°C in DPBS (Supporting Information S5). This assessment demonstrated that all three LNC formulations displayed satisfactory colloidal stability, with none showing any changes in size or PDI up to one week at 37°C (Fig. 2A and 2B). In addition to this, no significant changes in size or PDI were detected when incubated in the dark at room temperature (Supporting Information S4A and S4B) for a 28-day time period.

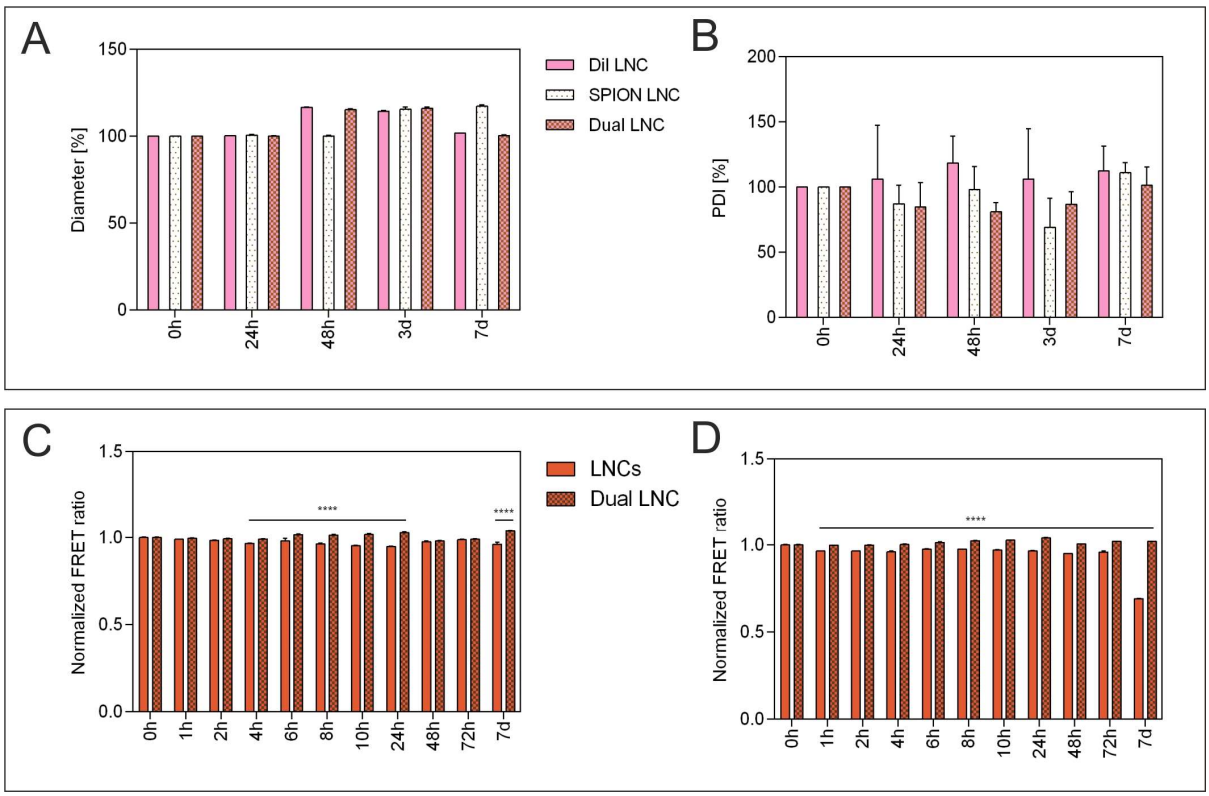


**Figure 2.** Dual LNC stability and integrity. Assessment of percentage (A) diameter and (B) PDI change over 7 days at 37°C in DPBS revealing no significant changes in diameter or PDI of all LNC formulations. Determination of Dual LNC integrity by FRET measurements over a 7-day time period in (C) DPBS and (D) 10% FCS at 37°C displayed an enhancement of nanoparticle integrity by SPION incorporation, particularly in the presence of 10% FCS. Data was normalized to t = 0 h.

To investigate whether the incorporation of SPIONs into the core of LNCs had an impact on the nanoparticle integrity, FRET experiments were carried out. To this end, a lipophilic FRET pair (DiI and DiO) was loaded into the core of LNCs either with or without the addition of SPIONs.

The release of one FRET partner due to leakage or disruption of the LNC is indicated by a decline in the FRET efficacy (*28, 29*). The normalized FRET ratios were determined as a function of time over a 7-day period. Nanoparticle integrity was determined under *in vitro* and *in vivo* mimicking conditions, by incubating Dye LNCs and Dual LNCs in either DPBS or 10% FCS at 37°C (Fig. 2C and 2D). As shown in Figure 2C, Dual LNCs revealed reasonable stability with regards to the nanoparticle integrity in DPBS at 37°C for one week, with a slight but significant advantage over Dye LNCs. These results are in accordance with the results generated at room temperature, where Dual LNCs and Dye LNCs showed almost no changes in the FRET ratio over the entire time period (Supporting Information S4C). Similar results were obtained with under *in vivo* mimicking conditions (Fig. 2D), whereby the supportive effect of incorporated SPIONs on the Dual LNC integrity was more pronounced. This positive effect could be due to physicochemical interactions of the SPION-oleate-chains with the MCT in the lipophilic core of the LNCs. This is very beneficial, as the presence of serum normally leads to the formation of a protein corona around the particles and this corona has been reported to favor particle disruption and cargo leakage (*15, 30*).

In summary, the FRET experiments revealed no negative effects on colloidal stability or nanoparticle integrity by the incorporation of SPIONs into LNCs. In fact, Dual LNCs seemed to have a slight advantage over Dye LNCs with regards to nanoparticle integrity, especially under *in vitro* and *in vivo* mimicking conditions.

### *3.3 In vitro* imaging

To evaluate the detectability of Dual LNCs in cell culture the *in vitro* detectability with optical microscopy was investigated. To that end, Dual LNCs and Dye LNCs were grafted with an αvβ3 integrin-specific ligand, RGD, to facilitate cellular uptake by HDME cells (*10*). Cells incubated with either Dual RGD-LNCs or DiO RGD-LNCs displayed excellent cellular uptake of both RGD-LNC types (Fig. 3). As the coupled RGD-ligand favors receptor mediated endocytosis, both RGD-LNC types could be localized in endosomes, without showing any unspecific adhesion to the cellular membrane. This additionally indicated that the targeting ligand on the surface of the Dual RGD-LNCs is still intact and is able to serve its purpose, without showing any deviations due to SPION incorporation. Despite a reduction of fluorescence intensity in the case of Dual RGD-LNCs due to quenching of DiO by SPIONs (Fig. 1C), it was possible to satisfactorily image the internalized Dual RGD-LNCs. To quantitatively assess the cellular uptake of RGD-grafted LNCs, fluorescent activated cell sorting could further be used.

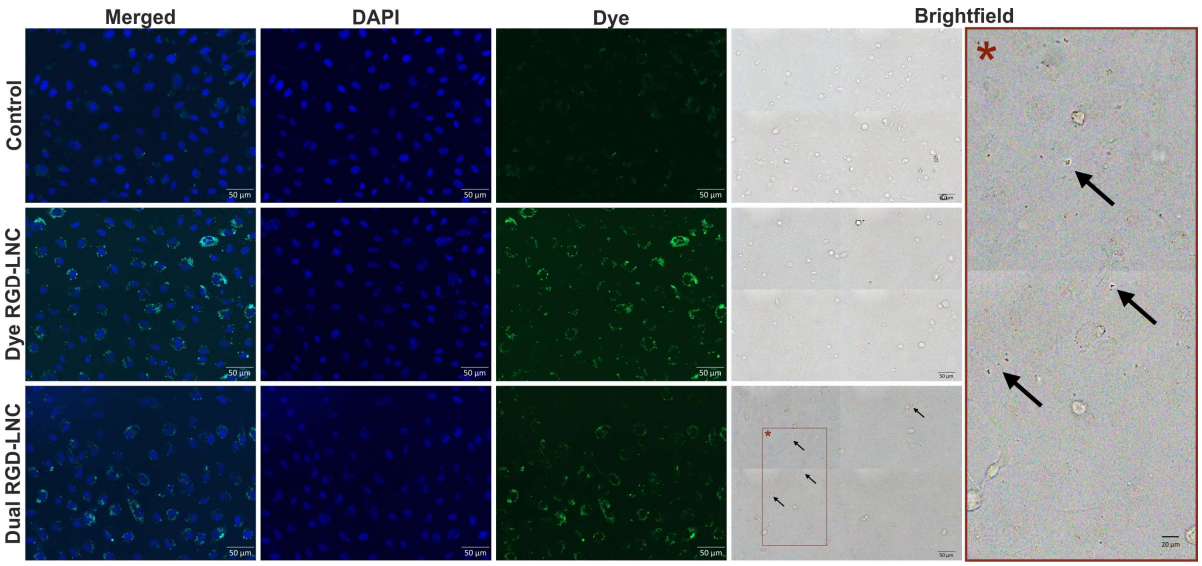


**Figure 3.** *In vitro* imaging. Fluorescence microscope images of untreated HDMECs (control) and HDMECs treated with either Dye RGD-LNCs or Dual RGD-LNCs. Fluorescence was used to detect DAPI (staining of cell nuclei, blue) as well as the incorporated DiO (green), whereas transmitted light was used to visualize SPIONs. Red rectangle: magnified image of the brightfield channel of Dual LNCs, with arrows marking clusters of SPIONs.

Additionally, the transmitted light images of cells incubated with Dual RGD-LNCs showed dark brown spots colocalized with the fluorescence signal, indicating that they stem from the encapsulated SPIONs in the Dual RGD-LNCs, further supported by the fact that these spots are not visible in the brightfield images of DiO RGD-LNC treated cells or the control cells. Since these dark spots seem to be organized in small groups, this could be groups of Dual RGD-LNCs gathered together in intracellular vesicles after being taken up via receptor-mediated endocytosis (*31*).

This uptake experiment demonstrated the improved *in vitro* detectability of Dual LNCs, as they were visualized with fluorescence imaging and/or transmitted light imaging. Furthermore, the functionality of attached targeting ligands was not affected by loading of LNCs with SPIONs.

### *3.4 In vivo* imaging

The *in vivo* detectability was assessed after the systemic administration of Dual RGD-LNCs to mice. Since the majority of every systemically applicated LNC ends up in the liver, the liver was chosen as model tissue (*32*). To investigate the biodistribution and localization of the nanoparticles after circulation in the blood, one option is the preparation of liver cryosections and the subsequent fluorescence microscopy. Since cryosections are relatively quick to make and allow

for additional antibody staining, they are often the primary choice (*19*). Here, fluorescence imaging of liver cryosections gave a clear indication of the presence of Dual LNCs (Fig. 4A).
To further investigate whether a combination of fluorescence imaging and transmitted light imaging could be used to detect not only the dye but also the SPIONs, semi-thin sections were prepared. Due to the reduced tissue sample thickness, semi-thin sections enabled the use of both transmitted light and fluorescence imaging. Figure 4B demonstrates Dual LNCs are simultaneously detectable via fluorescence and transmitted light (brightfield) imaging.

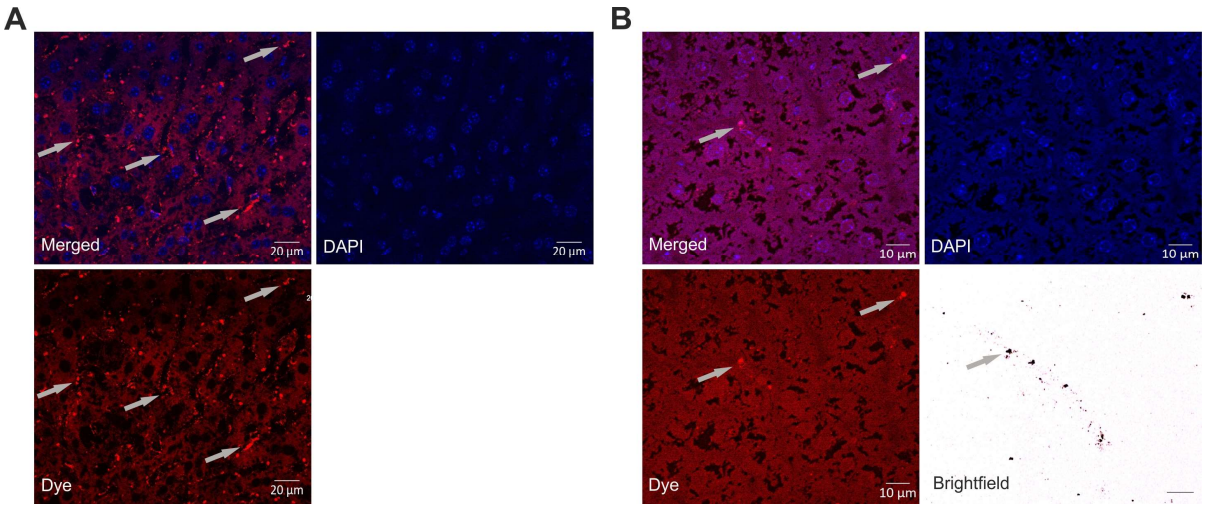


**Figure 4.** Optical microscopy. Liver sections after the systemic application of Dual LNCs loaded with DiI (red) and SPIONs to mice and 1 h blood circulation time, additionally stained with DAPI (blue). A: Images of liver cryosections reveal an appropriate detectability of Dual LNCs via fluorescence. B: Images of liver semi-thin sections reveal simultaneous detectability of Dual LNCs via fluorescence and transmitted light (brightfield). Arrows marking clusters of Dual LNCs.

Overall, *in vivo* experiments revealed the benefits of Dual LNCs compared to Dye LNCs, with regards to optical microscopy, since fluorescence and transmitted light can be used simultaneously. This allows rapid detection and rough localization of LNCs in different tissue samples. As TEM imaging provides higher resolution imaging and allows precise and exact localization of nanomaterials, visualization of LNCs with TEM in *in vivo* samples would be highly desirable. To investigate whether Dual LNCs are detectable using TEM after *in vivo* application, ultra-thin liver sections were made, and TEM images were taken. Figure 5 shows that the electron dense Dual LNCs were easily recognizable in Epon sections at first sight, due to their excellent contrast, without requiring any additional enhancement. They appeared as dark round structures located in a liver cell, differentiating from ribosomes and glycogen due to their contrast and their

composition (Fig. 5A and 5B). Higher magnification revealed the inner structure of the Dual LNCs by showing even the single SPIONs that are located in the core of the Dual LNCs (Fig. 5C). Moreover, the electron dense Dual LNCs were detectable in L.R. white sections, without using uranyl acetate or lead citrate contrasting (Supporting Information S6).

The ability to visualize Dual LNCs using TEM allows us to not only track their cellular journey from endocytosis to exocytosis, but also allows us to fully investigate the biodistribution of LNCs after systemic administration. Additionally, MRI measurements and ICP-OES measurements could be used to visualize the fate of the particles after systemic administration and quantitatively investigate the LNC biodistribution.

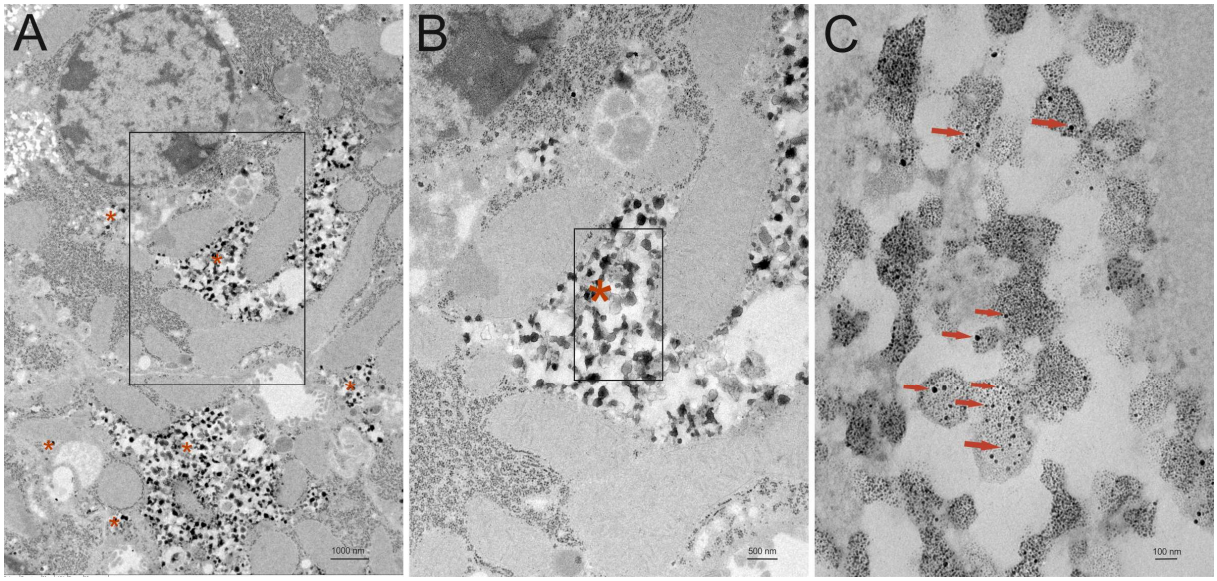


**Figure 5.** *In vivo* TEM imaging. Images of liver sections after the systemic application of Dual LNCs, with the right-hand image in each case being a magnified version of the square indicated to the left. Asterisks indicate areas with a multitude of particles where Dual LNCs can be visualized as dark, electron-dense spots in a liver cell. High magnification images revealing even single SPIONs inside the Dual LNCs, indicated by arrows.

# 4 Conclusion

We designed dually labeled LNCs, which are loaded simultaneously with fluorescent dye and electron dense SPIONs. The introduction of labels did not alter nanoparticle characteristics including size, PDI and zeta potential. Furthermore, colloidal stability, particle integrity and biocompatibility of LNCs were not negatively affected by SPION incorporation. After uptake into HDME cells or systemic application and accumulation in the liver of mice, Dual LNCs revealed excellent detectability using optical microscopy. In addition to optical microscopy, it is now possible to use TEM imaging to determine the very exact localization of LNCs in tissue samples and accurately quantify Dual LNCs using ICP-OES. Therefore, Dual LNCs are a valuable tool for the investigation of *in vitro* and *in vivo* performances of LNC formulations.

# References


1. N. T. Huynh, C. Passirani, P. Saulnier, J. P. Benoit, Lipid nanocapsules: a new platform for nanomedicine. *International journal of pharmaceutics* **379**, 201–209 (2009).
2. G. Bastiat, C. O. Pritz, C. Roider, F. Fouchet, E. Lignieres, A. Jesacher, R. Glueckert, M. Ritsch-Marte, A. Schrott-Fischer, P. Saulnier, J.-P. Benoit, A new tool to ensure the fluorescent dye labeling stability of nanocarriers. *Journal of controlled release: official journal of the Controlled Release Society* **170**, 334–342 (2013).
3. Y. Liu, Y.-c. Tseng, L. Huang, Biodistribution Studies of Nanoparticles Using Fluorescence Imaging. *Pharmaceutical Research* **29**, 3273–3277 (2012).
4. J. Park, J. Joo, S. G. Kwon, Y. Jang, T. Hyeon, Synthesis of monodisperse spherical nanocrystals. *Angewandte Chemie (International ed. in English)* **46**, 4630–4660 (2007).
5. E. Luque-Michel, V. Sebastian, A. Larread, C. Marquina, M. J. Blanco-Priet, Co-encapsulation of superparamagnetic nanoparticles and doxorubicin in PLGA nanocarriers. *European Journal of Pharmaceutics and Biopharmaceutics* **145**, 65–75 (2019).
6. X. Ma, A. Gong, B. Chen, J. Zheng, T. Chen, Z. Shen, A. Wu, Exploring a new SPION-based MRI contrast agent with excellent water-dispersibility, high specificity to cancer cells and strong MR imaging efficacy. *Colloids and Surfaces B: Biointerfaces*, 44–49 (2015).
7. B. H. Kim, N. Lee, H. Kim, K. An, Y. I. Park, Y. Choi, K. Shin, Y. Lee, S. G. Kwon, H. B. Na, J.-G. Park, T.-Y. Ahn, Y.-W. Kim, W. K. Moon, S. H. Choi, T. Hyeon, Large-scale synthesis of uniform and extremely small-sized iron oxide nanoparticles for high-resolution T1 magnetic resonance imaging contrast agents. *Journal of the American Chemical Society* **133**, 12624–12631 (2011).
8. S. E. A. Gratton, P. A. Ropp, P. D. Pohlhaus, J. C.r. Luft, V. J. Madden, M. E. Napier, J. M. DeSimone, The effect of particle design on cellular internalization pathways. *Proceedings of the National Academy of Sciences of the United States of America* **105**, 11613–11618 (2008).
9. E. F. Plow, T. A. Haas, L. Zhang, J. Loftus, J. W. Smith, Ligand binding to integrins. *J. Biol. Chem.* **275**, 21785–21788 (2000).
10. X. Liu, W. Cui, B. Li, Z. Hong, Targeted therapy for glioma using cyclic RGD-entrapped polyionic complex nanomicelles. *International journal of nanomedicine* **7**, 2853–2862 (2012).
11. J. Park, K. An, Y. Hwang, J.-G. Park, H.-J. Noh, J.-Y. Kim, J.-H. Park, N.-M. Hwang, T. Hyeon, Ultra-large-scale syntheses of monodisperse nanocrystals. *Nature Mater* **3**, 891–895 (2004).
12. M. Bohley, A. Haunberger, A. Goepferich, Intracellular availability of poorly soluble drugs from lipid nanocapsules. *European Journal of Pharmaceutics and Biopharmaceutics* **139**, 23–32 (2019).
13. B. Heurtault, P. Saulnier, B. Pech, A Novel Phase Inversion-Based Process for the Preparation of Lipid Nanocarriers. *Pharmaceutical Research*, 875–880 (2002).
14. *ISO 10993-5: Biological evaluation of medical devices. In Part 5: Tests for in vitro cytotoxicity* (2009).
15. K. Abstiens, S. M. Figueroa, M. Gregoritza, A. M. Goepferich, Interaction of functionalized nanoparticles with serum proteins and its impact on colloidal stability and cargo leaching. *Soft Matter* **15**, 709–720 (2019).
16. M. Brinkley, A brief survey of methods for preparing protein conjugates with dyes, haptens and crosslinking reagents. *Bioconjugate chemistry* **3**, 2–13 (2002).
17. T. Perrier, P. Saulnier, F. Fouchet, N. Lautram, J.-P. Benoît, Post-insertion into Lipid NanoCapsules (LNCs): From experimental aspects to mechanisms. *International journal of pharmaceutics* **396**, 204–209 (2010).

18. M. KARNOVSKY, A formaldehyde-glutaraldehyde fixative of high osmolality for use in electron microscopy. *J. Cell Biol.* **27**, 137A-138A (1965).
19. P. Bergese, K. Hamad-Schifferli, Eds., *Nanomaterial Interfaces in Biology*, *Methods and Protocols* (Humana Press, Totowa, NJ, 2013).
20. K. C. RICHARDSON, L. JARETT, E. H. FINKE, Embedding in epoxy resins for ultrathin sectioning in electron microscopy. *Stain technology* **35**, 313–323 (1960).
21. B. M. Braunger, A. Ohlmann, M. Koch, N. Tanimoto, C. Volz, Y. Yang, M. R. Bösl, A. Cvekl, H. Jägle, M. W. Seeliger, E. R. Tamm, Constitutive overexpression of Norrin activates Wnt/β-catenin and endothelin-2 signaling to protect photoreceptors from light damage. *Neurobiology of Disease* **50**, 1–12 (2013).
22. A. Barras, A. Mezzetti, A. Richard, S. Lazzaroni, S. Roux, P. Melnyk, D. Betbeder, N. Monfilliette-Dupont, Formulation and characterization of polyphenol-loaded lipid nanocapsules. *International journal of pharmaceutics* **379**, 270–277 (2009).
23. L. Maurizi, U. Sakulkhu, A. Gramoun, J.-P. Vallee, H. Hofmann, A fast and reproducible method to quantify magnetic nanoparticle biodistribution. *Analyst* **139**, 1184–1191 (2014).
24. D. Piché, I. Tavernaro, J. Fleddermann, J. G. Lozano, A. Varambhia, M. L. Maguire, M. Koch, T. Ukai, Armando J. Hernández Rodríguez, L. Jones, F. Dillon, I. R. Molina, M. Mitzutani, Evelio R. González Dalmau, T. Maekawa, P. D. Nellist, A. Kraegeloh, N. Grobert, Targeted T1 Magnetic Resonance Imaging Contrast Enhancement with Extraordinarily Small CoFe2O4 Nanoparticles. *ACS applied materials & interfaces*, 6724–6740 (2019).
25. M. Mahmoudi, S. Sant, B. Wang, S. Laurente, T. Sen, Superparamagnetic iron oxide nanoparticles (SPIONs). *Advanced drug delivery reviews* **63**, 24–46 (2011).
26. A. K. Gupta, M. Gupta, Cytotoxicity suppression and cellular uptake enhancement of surface modified magnetic nanoparticles. *Biomaterials* **26**, 1565–1573 (2005).
27. A. Lamprecht, J.-L. Saumet, J. Roux, J.-P. Benoit, Lipid nanocarriers as drug delivery system for ibuprofen in pain treatment. *International journal of pharmaceutics* **278**, 407–414 (2004).
28. H. Chen, S. Kim, W. He, H. Wang, P. S. Low, K. Park, J.-X. Cheng, Fast release of lipophilic agents from circulating PEG-PDLLA micelles revealed by in vivo forster resonance energy transfer imaging. *Langmuir : the ACS journal of surfaces and colloids* **24**, 5213–5217 (2008).
29. P. Zou, H. Chen, H. J. Paholak, D. Sun, Noninvasive fluorescence resonance energy transfer imaging of in vivo premature drug release from polymeric nanoparticles. *Molecular pharmaceutics* **10**, 4185–4194 (2013).
30. X. Jiang, Hydrophobic-lipophilic interactions. Aggregation and self-coiling of organic molecules. *Accounts of chemical research* **21**, 362–367 (1988).
31. S. Cressman, I. Dobson, J. B. Lee, Y. Y. C. Tam, P. R. Cullis, Synthesis of a labeled RGD-lipid, its incorporation into liposomal nanoparticles, and their trafficking in cultured endothelial cells. *Bioconjugate chemistry* **20**, 1404–1411 (2009).
32. S. Hirsjärvi, S. Dufort, J. Gravier, I. Texier, Q. Yan, J. Bibette, L. Sancey, V. Josserand, C. Passirani, J.-P. Benoit, J.-L. Coll, Influence of size, surface coating and fine chemical composition on the in vitro reactivity and in vivo biodistribution of lipid nanocapsules versus lipid nanoemulsions in cancer models. *Nanomedicine: nanotechnology, biology, and medicine* **9**, 375–387 (2013).

# Chapter 4 – Supporting Information

---

# Design of dye and superparamagnetic iron oxide nanoparticle loaded lipid nanocapsules with dual detectability in vitro and in vivo

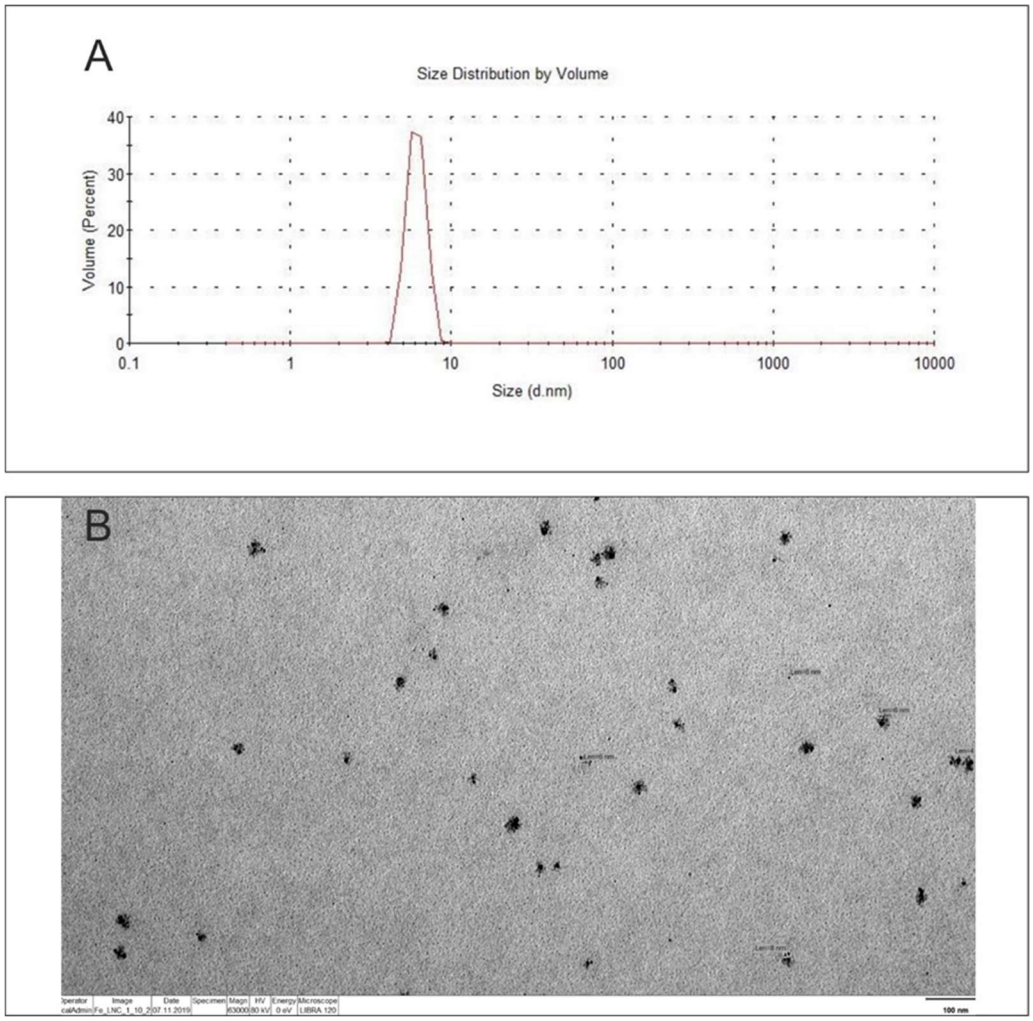


**Figure S1**. Characterization of SPIONs via (A) DLS volume-weighted size distribution with a peak mean size of 6.18 nm and (B) TEM imaging. Both methods reveal a diameter of SPIONs dispersed in MCT of 4 - 8 nm.

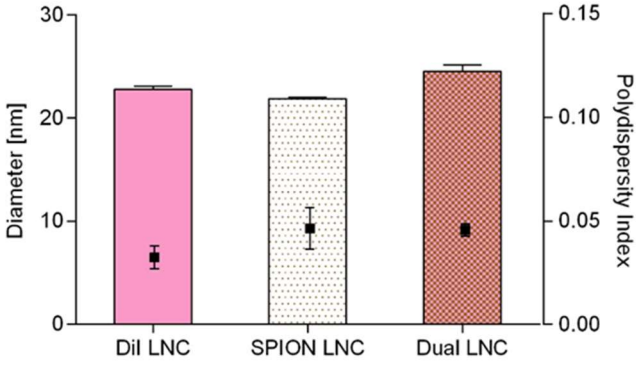


**Figure S2**. Comparison of different 25 nm LNCs regarding hydrodynamic diameter (bars) and PDI (squares), with no detectable differences in either size or PDI values due to the encapsulation of SPIONs or SPIONs alongside with dye.

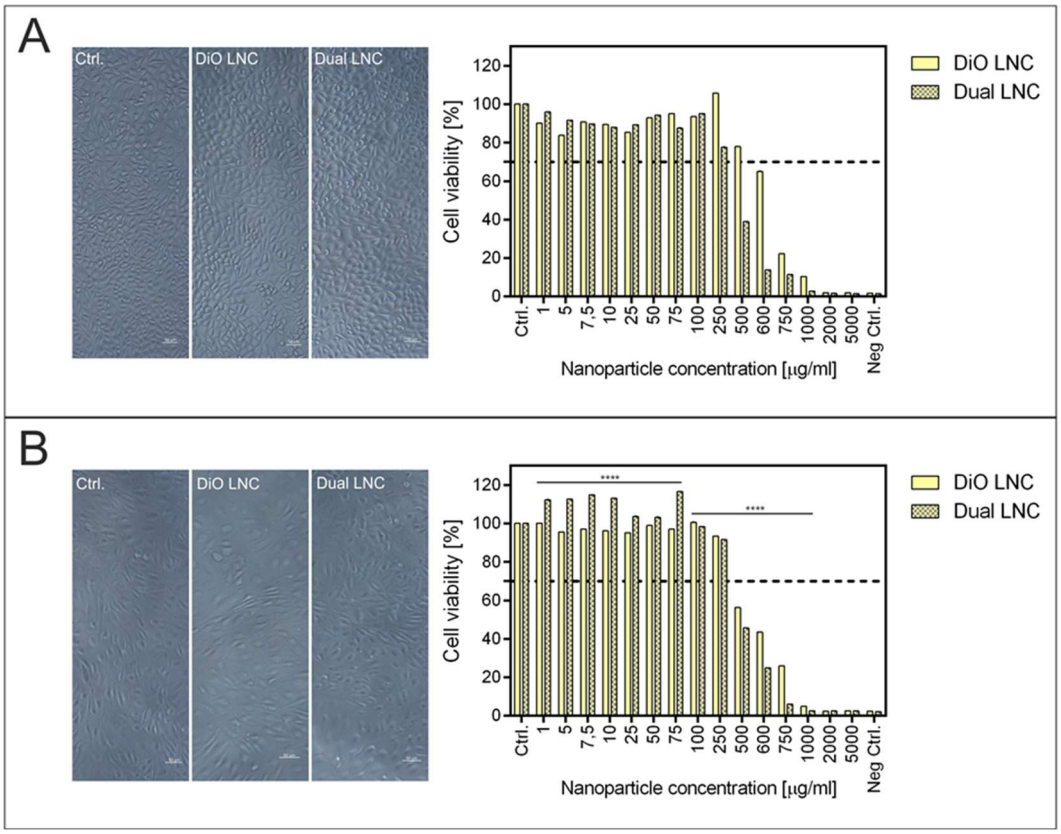


**Figure S3**. Effects on cell viability and cell morphology of Dye and Dual LNCs on (A) L-929 and (B) HDME cells. No changes in the morphology of cells could be detected in the presence of Dye LNCs or Dual LNCs in (A) L-929 cells and (B) HDME cells. The cell viability after treatment with different LNC concentrations (1 to 5000 µg/mL) was determined by using an MTT assay. Biocompatibility (cell viability over 70%) was given in a concentration range of 0 to 250 µg/mL for both Dual LNCs and Dye LNCs.

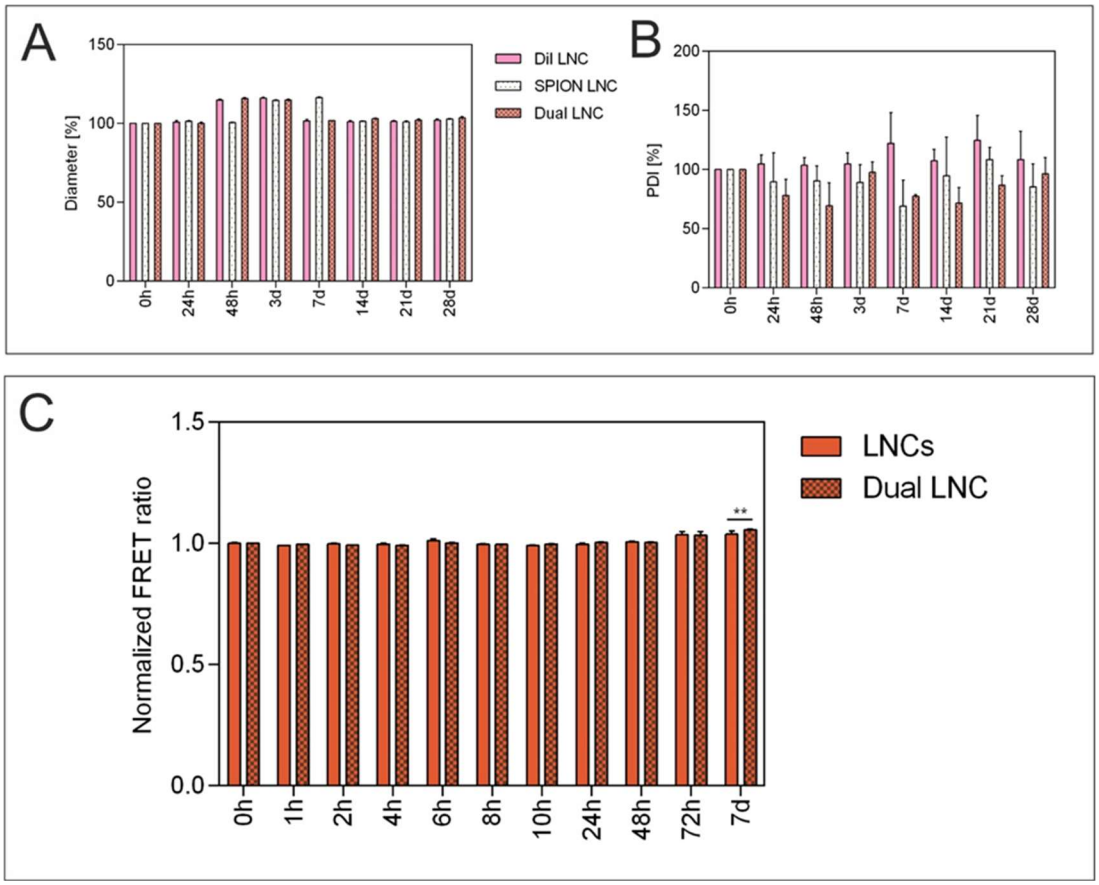


**Figure S4**. Dual LNC stability and nanoparticle integrity. Assessment of (A) Percentage diameter and (B) PDI over 28 d at room temperature in DPBS revealed excellent colloidal stability of all LNC formulations for the whole time period. Determination of Dual LNC particle integrity by FRET measurements over a 7-d time period in (C) DPBS at room temperature displayed consistently good FRET values over the whole week with a slight advantage of the Dual LNCs, becoming significant at an incubation time of 7 d. Data was normalized to t = 0 h.

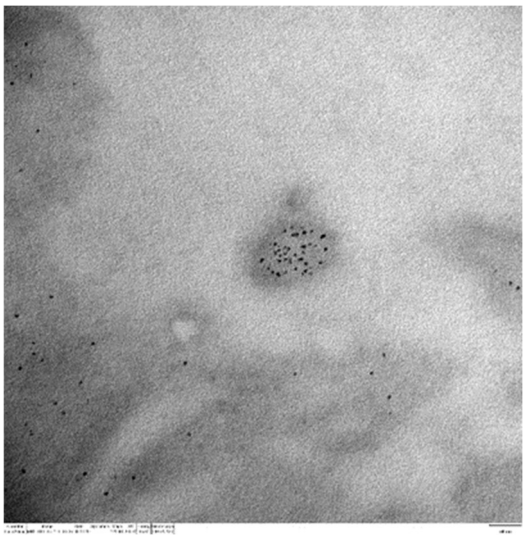

**Figure S5.** TEM imaging. Images of L.R. white liver sections after the systemic application of Dual LNCs. Dual LNCs can be visualized as dark, electron-dense spots without any additional staining or enhancement of the particles.

# Chapter 5

# Targeted Lipid Nanoparticles for the Treatment of Neovascular Ocular Diseases

# Abstract

Every year diabetic retinopathy, wet age-related macular degeneration, and retinopathy of prematurity cause millions of cases of blindness and vision impairment. Their pathogenesis shares a complex triad of neovascularization, inflammation and immune system activation that is fueled by growth factors, cytokines, local complement and complement regulatory factors originating from the retinal pigment epithelium (RPE). However, despite the cell monolayer ‘s pivotal role there is no therapeutic tool to specifically deliver drugs to the RPE. Here, we show that lipid nanoparticles can be designed to transport drugs to the RPE following intravenous injection and address all three pathomechanisms. A single injection of Cyclosporin A loaded nanoparticles cured retinopathy of prematurity in a mouse model. By counteracting neovascularization, dampening inflammation and normalizing levels of growth factors, growth factor receptors and cytokines, our nanotherapeutic thus paves the way for the causal treatment of all neovascular ocular diseases.

# 1 Introduction

Retinopathy of prematurity (ROP), diabetic retinopathy (DR), and wet age-related macular degeneration (wet AMD) are all among the leading causes of blindness *(1, 2)*. While uncontrolled neovascularization is a late and apparent characteristic giving rise to their subsumption under neovascular ocular diseases, ample research efforts revealed that inflammation and immune response contribute substantially to the pathology of disease development *(3–5)*. As main producer of angiogenic growth factors such as the vascular endothelial growth factor (VEGF), pro-inflammatory cytokines such as interleukin-1β (Il-1ß), local complement and complement regulatory proteins, the retinal pigment epithelium (RPE) plays a central role in the overall ocular homeostasis and drives the pathogenesis of all three diseases when deranged *(6, 7)*.

However, even though the pivotal pathophysiological role of the RPE has been described in abundance *(6, 8, 9)*, the tissue escapes drug therapy (*10*). Simple means of systemic drug administration fail since dosing regimens that would build up relevant RPE levels would trigger severe side effects due to the unfavorable drug distribution in the organism. The alternative, local intraocular drug therapy, also suffers from a number of shortcomings (*10–13*), the most prominent being the lack of RPE specificity. This is also the case with today's standard clinical drug therapy for ROP *(14–17)*, DR *(18)*, and wet AMD *(19, 20)* that exclusively relies on suppressing neovascularization using anti-VEGF antibodies, aptamers and other biologics *(21)*. Their high molecular weight endows them with intraocular half-lives in the order of several days *(22)* giving rise to their ability to neutralize VEGF for weeks *(23–25)*. While the therapy is the best we have at the moment as it allows to efficiently dampen neovascularization *(26, 27)*, constantly depriving the retina of VEGF comes at the price of side effects such as retinal degeneration caused by the progressive death of retinal cells *(28, 29)*. While the clinical relevance of this is still a matter of debate *(30)*, the treatment fails to reach out to the RPE to address the source of neovascularization, inflammation, and immune system activation. This makes it quite unsuited to serve as a preventive therapy, to hinder early disease development and protect millions of patients from visual impairment.

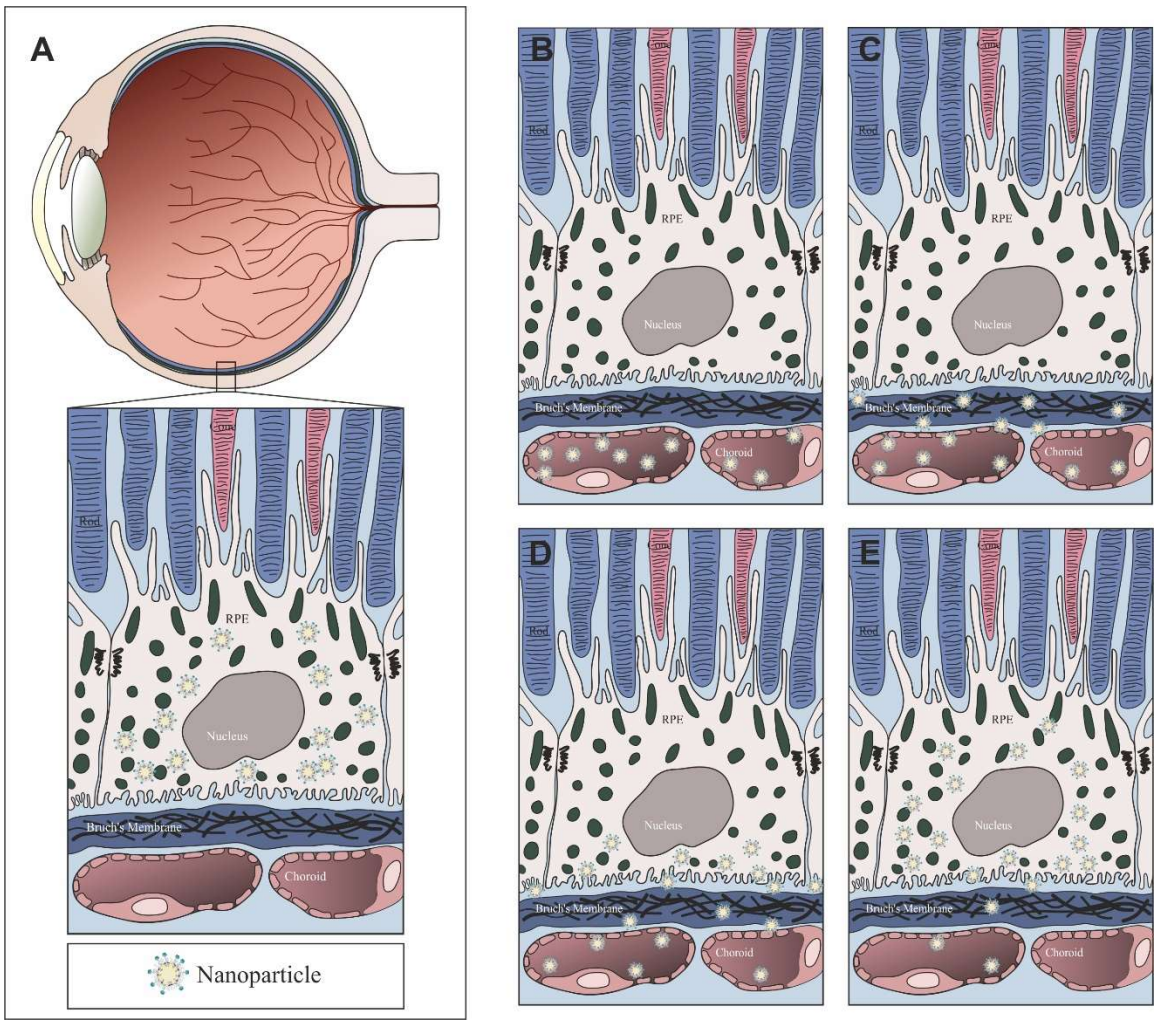


***Figure 1. Illustration of a nanotherapeutic targeting the RPE following systemic i.v. injection.***

*(**A**) Schematic drawing that shows the localization of the finally intended nanoparticle accumulation in the RPE cell monolayer. (**B-E**) Individual steps of nanoparticle transport into the RPE along the route that natural lipoprotein particles (LDL and VLDL) take. (**B**) Nanoparticles immediately after injection interacting with endothelial cells of the choroid. (**C**) Nanoparticles extravasate form the blood and cross Bruch's Membrane. (**D**) Nanoparticles are taken up by RPE cells. (**E**) Nanoparticles accumulate inside RPE cells and form a depot.*

To overcome this constraint, we explored if it was possible to design nanoparticles that enter the retina via the choroid and form a drug depot in the RPE (Fig. 1A). However, addressing nanoparticles from the central circulation to the posterior eye is challenging, since a drug transporter would need to permeate through the endothelial cell layer and the Bruch's Membrane on its way from the choroid to the RPE (Fig. 1B to E) *(10, 31)*.

To meet this challenge, we designed lipid nanocapsules (LNCs) that mimic 25 nm low-density lipoprotein (LDL) and 60 nm very low-density lipoprotein (VLDL) particles respectively. Both have the ability to cross the corresponding biological barriers and supply RPE cells with lipids *(12, 32, 33)*. Like their natural counterparts our 50-60 nm LNCs consist of a triglyceride core and a phospholipid shell that binds to lipoprotein receptors like the scavenger receptor CD36 on RPE cells and triggers particle uptake (Fig. 2A) *(34, 35)*. To further increase RPE cell avidity, LNCs were outfitted with cyclo(-Arg-Gly-Asp-D-Phe-Cys) (cRGD) that was tethered to the particle corona via PEG chains (Fig. 2A and Fig. S1A and B). As a ligand with nanomolar affinity *(36)* for $\alpha_v\beta_3$ and $\alpha_v\beta_5$ integrins expressed by RPE cells *(37)*, cRGD was intended to allow together with phospholipids for hetero-multivalent binding *(38)* to increase the specificity and avidity of particles for the target cells *(39)*.

While it was our primary goal to see if these nanoparticles would reach the RPE following intravenous (i.v.) injection in mice, we were also keen to explore if they would form a depot in the cell monolayer and allow a transported drug to interfere with the pathomechanisms outlined above. To this end, we loaded the particles with Cyclosporin A (CsA) (Fig. S1C and D) known for its pronounced antiangiogenic, anti-inflammatory, and immuno-modulatory potential *(40–42)*. We assessed their therapeutic potential in oxygen induced retinopathy (OIR), a mouse model of ROP. Analyzing the levels of VEGF, VEGF receptor type 2 (VEGF-R2), glial fibrillary acidic protein (GFAP) and IL-1β expression in the sensory retina and the RPE-choroid complex, we assessed if our nanotherapeutic truly addressed the pathological triad of neovascular ocular diseases. Overall, we wanted to find out if such drug loaded nanoparticles would prevent disease development.

# 2 Results

## 2.1 Nanoparticles address RPE and endothelial cells *in vitro*

First, we investigated the interaction of the hetero-multivalent particles with the target cells and determined their cellular internalization *in vitro*. Alongside RPE cells we used endothelial cells to study the cellular uptake of nanoparticles. While the former are the ultimate target, the latter are part of the barrier that the nanoparticles need to overcome on their way from the blood to the retina. Similar results were obtained for both cell types (Fig. 2B). While the cellular uptake of control LNCs was only moderate, cRGD-modified nanoparticles (RGD-LNCs) were taken up excessively.

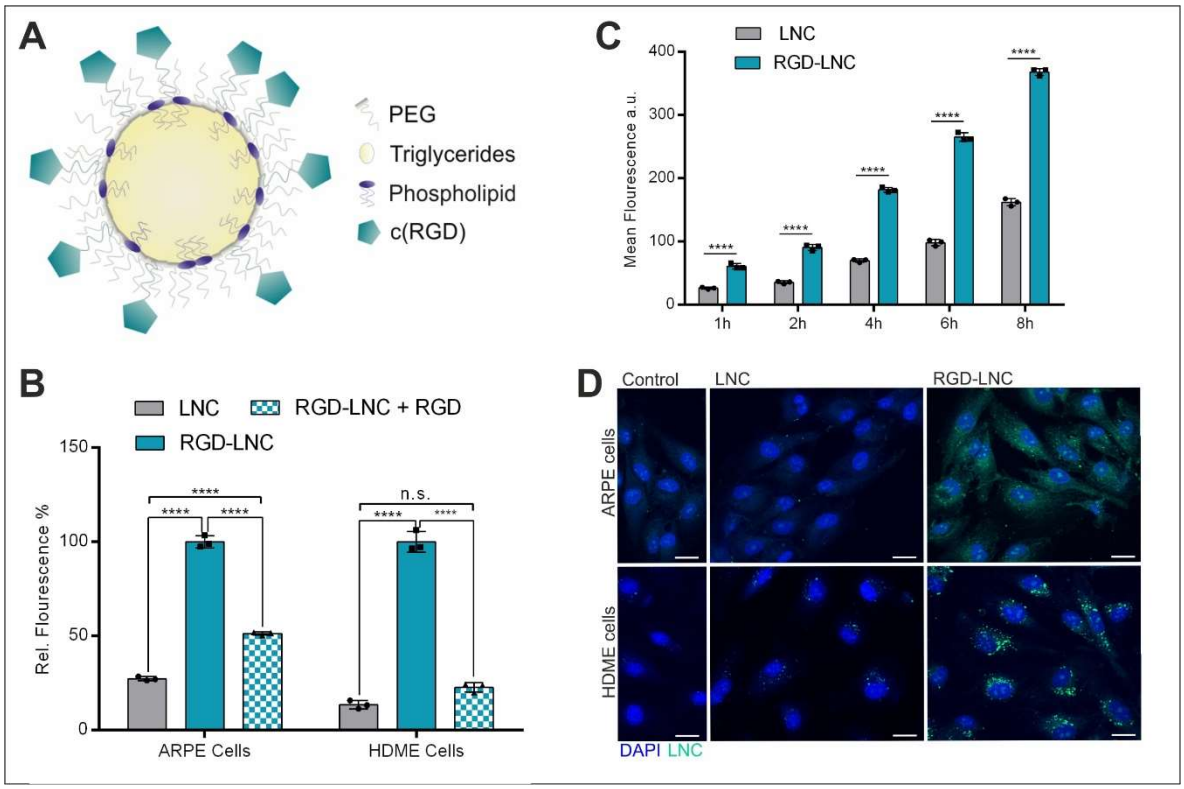


***Figure 2. LDL mimicking and integrin addressing lipid nanoparticles target RPE and endothelial cells.***

*(**A**) Schematic illustration of the LDL-mimicking nanoparticle composition and the hetero-multivalent targeting concept of RGD-LNCs. (**B**) Ligand-mediated cellular uptake of LNCs and RGD-LNCs in human retinal pigment epithelial (ARPE) cells and human dermal microvascular endothelial (HDME) cells, partially inhibited by free RGD. (**C**) Ligand-mediated uptake kinetic of LNCs and RGD-LNCs in ARPE cells. (**D**) Cellular localization of LNCs and RGD-LNCs in HDME and ARPE cells. Scale bar: 20 µm. Data are mean ± SD of n = 3 biologically independent samples per group. Levels of statistical significance are indicated as **** P ≤ 0.0001 and n.s.: non-significant. P values determined by two-way ANOVA (**B**) and one-way ANOVA (**C**).*

This confirmed the benefits of the hetero-multivalent nanoparticle design. The two targeting moieties, cRGD and the phospholipid, were of significant advantage for RPE cell recognition and internalization. The significance of the integrin ligand was demonstrated further by the sharp decrease of cellular uptake of RGD-LNCs when $\alpha_v\beta_3$ and $\alpha_v\beta_5$ integrin receptors were blocked with free cRGD (Fig. 2B). On the other hand, the cell uptake of both, RGD-LNCs and LNCs, increased continuously with time (Fig. 2C), which can be attributed to the scavenger receptor CD36 that both particle species bind to. The true internalization of the nanoparticles into cells was confirmed using fluorescence microscopy (Fig. 2D). The images show that the nanoparticles are exclusively located in the cytosolic region of both cell types and that there is no unspecific adhesion to the cell surface.

### 2.2 Nanoparticles accumulate in RPE cells *in vivo*

To investigate the fate of RGD-LNCs following i.v. injection we first assessed their whole-body distribution relative to their ocular accumulation. One hour after injection, approximately 10% of the administered dose of RGD-LNCs reached the eye per gram of tissue which is comparable to the amounts found in the liver (Fig. 3A). Furthermore, it is equal to 2.0% of the total dose of RGD-LNCs that accumulates in the retina (Fig. 3B). Given the low mass of the tissue this is an outstanding efficacy compared to other nanotherapeutics *(43)*. The data also rigorously supports the advantage of the hetero-multivalent nanoparticle design since ocular accumulation is 8 times higher for RGD-LNCs compared to LNCs (Fig. 3A and B).

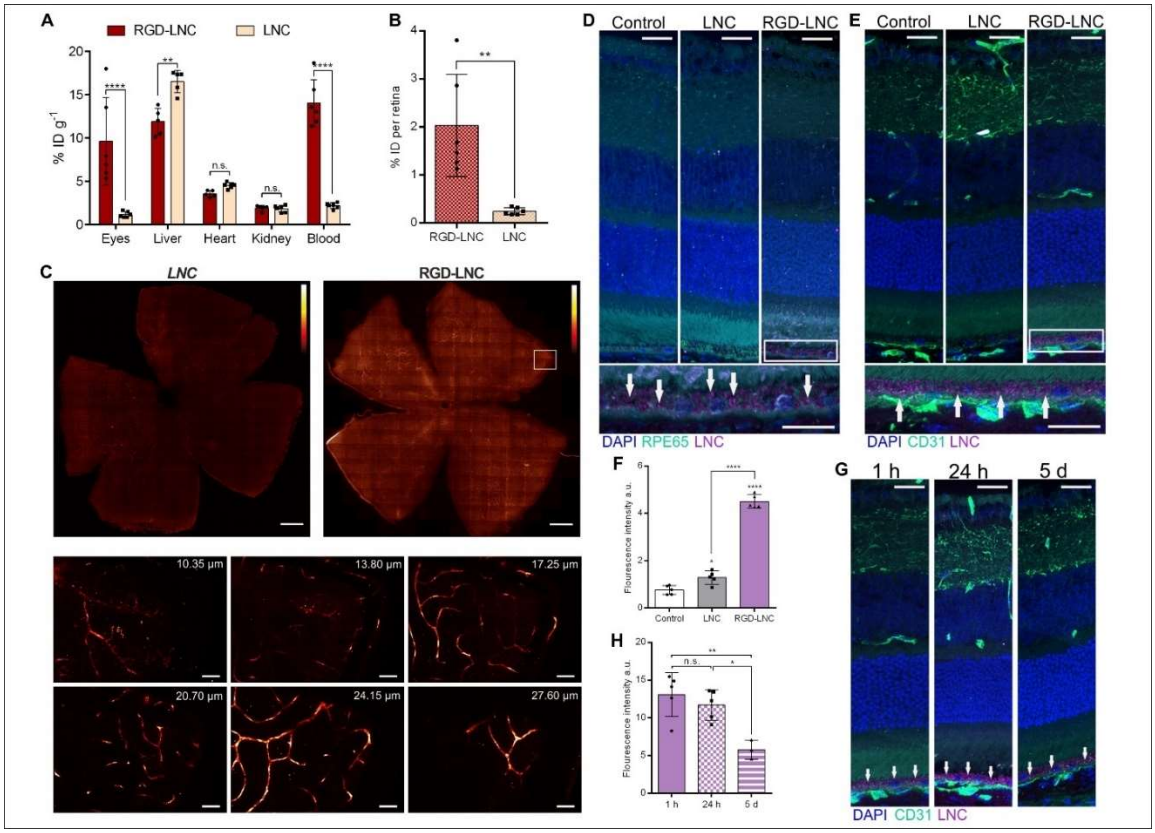


***Figure 3. Targeted and cell specific intraocular nanoparticle enrichment after i.v. injection.***

*(**A**) Tissue distribution of nanoparticles after systemic administration and 1 h of blood circulation in % initial dose (ID) per g tissue. (**B**) Absolute target tissue distribution in % ID of RGD-LNCs and LNCs in the retina. (**C**) Images of retinae of mice treated with nanoparticles 1 h after administration and detailed images (z-stacks) of RGD-LNCs in the different vascular layers. Scale bars: 100 µm (top) and 20 µm (bottom). (**D**, **E** and **G**) Cell specificity of nanoparticle accumulation in the posterior eye, (**D** and **E**) 1 h after administration, and (**G**) at different time points. Nanoparticle accumulation in the RPE indicated with white arrows. Blue: DAPI staining of cell nuclei; green: RPE65 (**D**) and CD31 (**E** and **G**); lilac: nanoparticle-associated fluorescence. Squared out regions are shown as magnification. Scale bars: 20 µm. (**F** and **H**) Quantitative analysis of nanoparticle fluorescence 1 h after administration (**F**) and at different time points (**H**). Results are presented as mean ± SD of n = 6 (**A**) and (**B**) mice per treatment group, n = 5 (**F**) or at least n = 3 (**H**). Levels of statistical significance are indicated as * P ≤ 0.05, ** P ≤ 0.01, **** P ≤ 0.0001 and n.s.: non-significant. P values determined by two-way ANOVA (**A**), unpaired t-test (**B**) and one-way ANOVA (**F** and **H**).*

As previous *in vivo* experiments have shown that monovalent cRGD-grafted quantum dots bind exclusively to choroidal and intraretinal endothelial cells but not to RPE cells *(44, 45)*, it was of utmost importance to investigate if the hetero-multivalent RGD-LNCs would overcome this limitation. As expected, retina whole mounts of mice following i.v. injection with RGD-LNCs and LNCs revealed endothelial cell binding (Fig. 3C). As previously shown for cRGD-grafted quantum dots [44], there is strong association of RGD-LNCs with the whole retinal vasculature and particles accumulate in all three layers of the retinal network: the superficial, the intermediate and the deep vascular plexus (Fig. 3C). Especially with regard to the treatment of neovascular ocular diseases with retinal neovascularization such as ROP and DR, this can be very advantageous and provide another target for counteracting neovascularization. In addition to the localization in retinal endothelial cells, TEM imaging of retinal sections revealed the presence of RGD-LNCs in choroidal endothelial cells, Bruch's Membrane and RPE cells, indicating that our particles might indeed follow the LDL/ VLDL route towards the RPE (Fig. S2A to C). Fluorescence microscope images showed excessive amounts of RGD-LNCs, but not LNCs, in the RPE one hour after i.v. injection (Fig. 3D and E). The quantification of nanoparticles in the RPE using fluorescence density measurements revealed that both LNCs and RGD-LNCs reached the RPE but only the hetero-multivalent particles led to a significant accumulation in the tissue (Fig. 3F). Moreover, neither RGD-LNCs nor LNCs were found in any other cell type in the eye, proving endothelial and mainly RPE cell specificity (Fig. 3D and E).

As a final step, the residence time of RGD-LNCs in the RPE was evaluated by taking fluorescence images of the posterior eye one hour, 24 hours and 5 days after i.v. administration. While fluorescence imaging revealed the presence of RGD-LNCs in the RPE for all three time points (Fig. 3G), the quantitative evaluation showed that the maximal accumulation was reached one hour after i.v. injection (Fig. 3H). It remained on a constant level for at least 24 hours. Surprisingly, after 5 days, substantial amounts of RGD-LNCs could still be detected in the tissue, which is highly beneficial with respect to any prospective therapy.

### 2.3 Cyclosporin A-loaded nanoparticle treatment prevents ROP

The accumulation of RGD-LNCs in RPE cells opened the door to investigate the therapeutic potential of CsA loaded RGD-LNCs (CsA RGD-LNCs) for the treatment of neovascular ocular disease. For our investigations we chose the mouse model of OIR since it is considered the standard animal model for ROP and proliferative DR *(46)*. Moreover, it most closely reflects the pathogenesis of ROP where the transient oxygen administration to preterm infants triggers abnormal blood vessel growth *(3)*. To induce the disease, we subjected newborn mice to oxygen treatment on postnatal day 7 (P7) which causes an initial loss of retinal vessels due to suppressed VEGF levels (Fig. 4A). Termination of oxygen treatment on P12 induces massive VEGF overexpression accompanied by inflammatory *(47)* and immune responses *(48, 49)* that both spur neovascularization. Considering this mechanism, we treated the animals on P12 with a single i.v. nanoparticle injection, right before neovascularization started (Fig. 4A). To assess the potential of the drug loaded nanoparticles comprehensively, the effects of CsA RGD-LNCs were compared to those obtained for a matching dose of intravenously applied CsA solution (free CsA) and the PBS control.

First, we analyzed the inhibitory effect of CsA loaded nanoparticles on neovascularization as the most relevant metric for the therapeutic success *(50)*. Fig. 4B shows the pathological changes in the retinal vasculature caused by OIR that contains large areas of newly formed, leaky vessels and neovascular tufts (Control OIR). In contrast, the retinae of CsA RGD-LNC treated mice show a dramatic decrease of neovascular zones, leaky vessels and neovascular tufts (Fig. 4B, CsA RGD-LNC).

To assess the efficacy of CsA RGD-LNCs quantitatively, the areas of leakage, tufts and proliferating vessels were measured and normalized to the overall retinal area as extent of neovascularization. CsA RGD-LNCs were able to suppress neovascularization substantially by a factor of 6 while an identical dose of CsA injected as aqueous solution had no effect (Fig. 4C). Apparently, a single injection of CsA RGD-LNCs administered directly after the oxygen treatment delivers enough CsA to the RPE to effectively prevent ROP from developing. That the targeted delivery system is mandatory to deliver the drug was strongly supported by the drug content we found in the posterior eye on P17 (Fig. 4D). Five days after injection, CsA was still detectable in the retinae of mice suffering from OIR that received the nanoparticle formulation but not in animals that were treated with the drug solution. Overall, the results demonstrate that RGD-LNCs are a highly precious tool for transporting drugs to the RPE and make them available for several days.

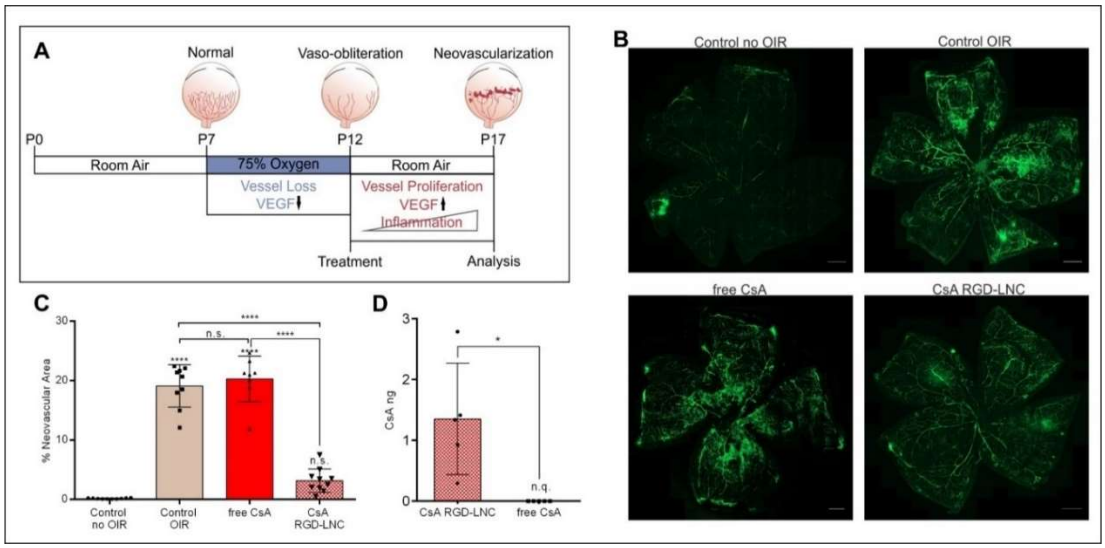


***Figure 4. CsA loaded nanoparticle effectiveness on the progression of ROP.***
***(A)*** *Scheme depicting the pathogenesis and intervention regime in the mouse model of OIR.* ***(B)*** *Representative images of retina whole mounts showing the retinal vasculature at P17. Untreated control (without and OIR; Control no OIR and Control OIR) compared to free CsA and CsA RGD-LNCs treated mice. Green: FITC-Dextran. Scale bars: 500 µm.* ***(C)*** *Quantification of the relative neovascular area.* ***(D)*** *Absolute CsA content in the posterior eye of mice with OIR at P17 after injection of CsA RGD-LNCs or free CsA. n.q.: not quantifiable. Results are presented as mean ± SD of at least n = 8 (**C**) and n = 5 (**D**) mice per treatment group. Levels of statistical significance are indicated as * P ≤ 0.05, **** P ≤ 0.0001 and n.s.: non-significant. P values determined by one-way ANOVA (**C**) and unpaired t-test (**D**).*

## 2.4 Cyclosporin A-loaded nanoparticles fight the pathophysiological triad

Since our CsA loaded particles had tremendous effects on the inhibition of neovascularization we were intrigued to have a closer look at the underlying mechanisms. CsA exhibits its antiangiogenic potential by the inhibition of VEGF-R2 glycosylation and intracellular trafficking. It further interferences with the VEGF signaling pathway at various intracellular sites and counteracts TGFβ-related VEGF production in RPE cells *(42, 51, 52)*. To this end, changes in VEGF-R2 and VEGF levels were quantitatively assessed. Immunohistochemical analysis revealed that the treatment with CsA RGD-LNCs decreased elevated VEGF-R2 levels in OIR mice down to the physiological values measured in healthy control animals (Fig. 5A). For VEGF, similar results were obtained with a reduction to physiological values in both the RPE-choroid complex (Fig. 5B) and the retina (Fig. 5C) upon CsA RGD-LNCs treatment, indicating the inhibition VEGF production in the RPE and the significant reduction of VEGF availability in the retina. Therefore, the results impressively demonstrate that CsA RGD-LNCs counteract the VEGF-driven neovascularization by restoring rather than suppressing physiological VEGF and VEGF-R2 levels.

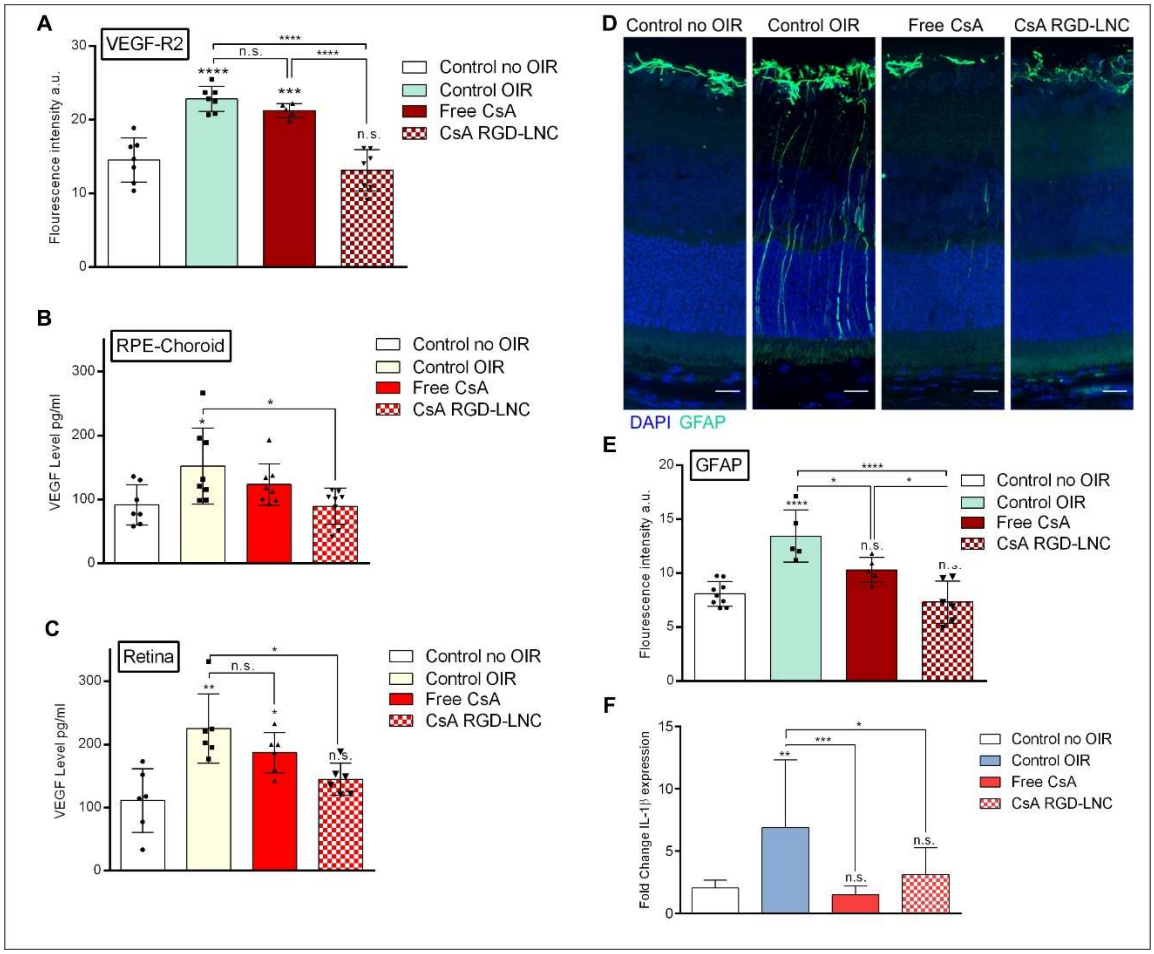


***Figure 5. Molecular angiogenic and inflammatory responses to nanoparticle therapy.***

*(**A**) Quantitative analysis of VEGF-R2 fluorescence density from cryosections immunohistochemically stained with VEGF-R2 antibody. (**B** and **C**) Assessment of VEGF protein levels in the RPE-choroid complex (**B**) or the retina (**C**) via ELISA. (**D**) Imaging of GFAP expression in the posterior eye. Blue: DAPI staining of cell nuclei; green: GFAP. (**E**) Quantitative analysis of GFAP fluorescence from sections shown in (**D**). (**F**) Representation of interleukin-1β (IL-1β) mRNA expression levels in RPE-choroid complex. Scale bars: 20 µm. Results are presented as mean ± SD of at least n = 5 (**A**, **D**, **E**, and **F**) and n = 6 (**B** and **C**) mice per treatment group. Levels of statistical significance are indicated as * P ≤ 0.05, ** P ≤ 0.01, *** P ≤ 0.001, **** P ≤ 0.0001 and n.s.: non-significant. P values determined by one-way ANOVA (**A** to **F**).*

Since CsA additionally exhibits strong influence on immune responses and a high anti-inflammatory potential by decreasing proinflammatory IL-1β levels, we next investigated the effects of CsA RGD-LNC therapy on inflammatory and immune response *(53)*. While the former is considered a 'key contributor' to ROP *(47)* the latter is considered to spur inflammatory processes of neovascular ocular diseases *(7, 54)*. Therefore, we first determined the levels of GFAP, because elevated GFAP levels indicate retinal inflammation and immune system activation *(54, 55)*. Fig. 5D displays the excessive expression of GFAP by reactive Müller cells which reflects inflammation and exuberant immune response caused by OIR. The treatment with CsA RGD-LNCs leads to a significant decrease of the marker down to normal values (Fig. 5E). Together with significantly lower production of proinflammatory IL-1β mRNA in RPE cells (Fig. 5F) it proves the substantial anti-inflammatory efficacy of CsA RGD-LNCs. Overall, the investigation of the mechanisms of CsA RGD-LNC treatment revealed bright prospects for the comprehensive therapy of ROP and other neovascular ocular diseases. CsA RGD-LNCs normalize vascularization by restoring natural VEGF and VEGF-R2 expression levels and substantially reduce inflammation, most likely in combination with dampening adverse immune responses.

### 2.5 Cyclosporin A-loaded nanoparticles as a prophylaxis for ROP

Our investigations revealed that a single dose of CsA loaded nanoparticles suffices to bring the pathogenesis of ROP to a complete halt. This opens the door to use CsA RGD-LNCs for a preemptive treatment of preterm infants at risk of developing ROP after oxygen treatment. Therefore, we determined if there would be negative effects on the eyes of healthy mice that were injected with CsA RGD-LNCs (Fig. 6A). Investigation of the vessel status revealed no alteration and no disturbance of normal vessel development as a result of the treatment (Fig. 6B and C, and Fig. S4A and B). Furthermore, the prophylactic intervention caused no significant changes in the VEGF and VEGF-R2 expression of heathy animals (Fig. 6D, F and H, and Fig. S3C to F). This reassured us that VEGF signaling, which is essential for physiological vessel development and overall ocular homeostasis and integrity, remained unaffected in healthy animals. Similar results were obtained for GFAP protein and IL-1β mRNA levels, that were unaffected as well (Fig. 6E, G and I, and Fig. S3G).

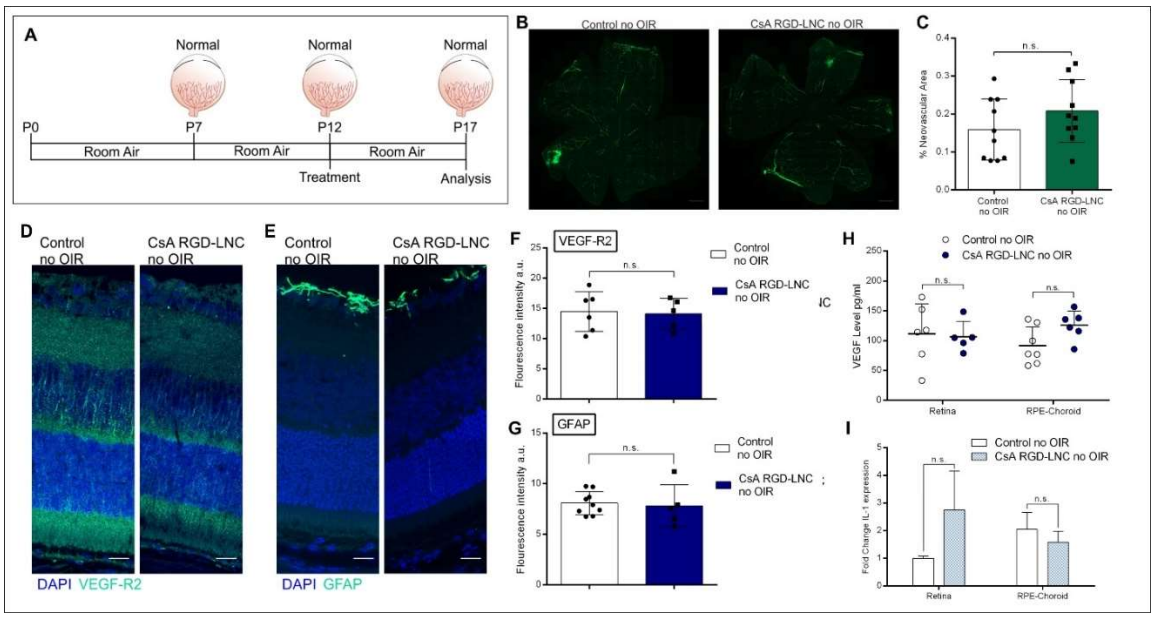


***Figure 6. Clinical and molecular effects of nanoparticle therapy on healthy mice.***

*(**A**) Scheme depicting the intervention regime for mice without OIR. (**B**) Representative images of retina whole mounts showing the retinal vasculature. Green: FITC-Dextran. Scale bars: 500 µm. (**C**) Quantification of the relative neovascular area. (**D**) Imaging of VEGF-R2 expression in the eye. Blue: DAPI staining of cell nuclei; green: VEGF-R2. (**E**) Imaging of GFAP expression in the eye. Blue: DAPI staining of cell nuclei; green: GFAP. (**F**) Quantitative analysis of VEGF-R2 fluorescence from sections shown in (**D**). (**G**) Quantitative analysis of GFAP fluorescence from sections shown in (**E**). (**H**) Assessment of VEGF protein levels in the sensory retina or RPE-choroid complex. (**I**) Representation of IL-1β mRNA level fold change in either the sensory retina or RPE-choroid complex compared to control. Scale bars: 20 µm. Results are presented as mean ± SD of at least n = 5 (**D**, **E**, and **I**), n = 6 (**H**) and n = 10 (**C**) mice per treatment group. Levels of statistical significance are indicated as * P ≤ 0.05, ** P ≤ 0.01, *** P ≤ 0.001, **** P ≤ 0.0001 and n.s.: non-significant. P values determined by unpaired t-test (**C**, **F**, and **G**), multiple t-test (**I**) and two-way ANOVA (**H**).*

# 3 Discussion

RGD-LNCs successfully mimicked LDL and VLDL particles and were able to accumulate in RPE cells following i.v. injection. As expected, they were not exclusively distributed to the posterior eye but, like other nanoparticles, in the whole organism (Fig. 3A). However, three aspects were highly remarkable. Only LNCs that carried cRGD as $a_v\beta_3$ - and $a_v\beta_5$-integrin ligand accumulated efficiently in the RPE, proving that hetero-multivalent targeting of RPE cells was essential (Fig. 3F). Furthermore, their ability to recognize target cells was highly efficient since RGD-LNCs accumulated massively in the RPE when compared with the liver tissue which is a part of the mononuclear phagocytic system and able to actively remove particles from the central circulation (Fig. 3A and B). Given the fact, that inside the eye, particles were found exclusively in retinal vessels and the RPE (Fig. 3D and E) will allow for cell specific drug delivery. Finally, the RGD-modified particles had, compared to the control particles, elevated blood levels which could result from an interaction with circulating cells *(56)*. This is highly beneficial since it shows that the availability of particles for distribution into the eye is unbroken after 1h and further supports the feasibility of lowering injected doses in future experiments. The targeted nanoparticles had a stunning residence time in the RPE with substantial particle amounts being present for 5 days after the injection (Fig. 3H). This nanoparticle depot formation in the RPE is a tremendous advantage for the delivery of drugs since their rapid tissue clearance would be counterbalanced by long-term drug release.

A major goal was to explore if such a particle system would truly allow to address all three pathomechanisms that underly neovascular ocular diseases and if it would be of therapeutic value. To this end we decided to test drug loaded nanoparticles in a mouse model of ROP, since it is well established, robust and unanimously reflects the three relevant pathomechanisms in question *(57)*. As the model drug we decided on CsA since it addresses all relevant arms of disease development. We found that the respective CsA loaded nanoparticles were remarkably successful *in vivo*. A single i.v. dose of CsA RGD-LNCs completely prevented disease development in terms of neovascularization. (Fig. 4C) This was perfectly in line with the downregulation of VEGF and VEGF-R2 levels. (Fig. 5A to C). In contrast to the contemporary clinical practice of anti-VEGF therapy that reduces VEGF levels to zero *(30, 58)*, our nanotherapeutic rather normalized VEGF and VEGF-R2 expression to physiological levels. This is highly beneficial since physiological VEGF levels have been shown to be vital for the survival of a vast number of retinal cells including Müller cells, RPE cells, astrocytes, and ganglion cells *(59–61)*. Further valuable information was obtained from two control experiments. When mice were treated with the dose of CsA in form of a simple aqueous injection, we did not observe any therapeutic effect (Fig. 4C). Furthermore, challenging healthy mice with the therapeutic nanoparticles did not elicit any negative effect on retinal vascular development (Fig. 6 B and C). Both experiments showed that the use of targeted nanoparticles

for delivering CsA is mandatory to obtain a therapeutic effect and that our nanotherapeutic could be used as prophylactic measure that would not interfere with 'normal' retinal blood vessel development. Besides showing the highly beneficial therapeutic effect of 'normalizing' vessel growth, our results shed light on the anti-inflammatory and immune modulating potential of CsA RGD-LNCs. Retinal GFAP levels that correlate with the degree of retinal damage and inflammatory processes were found to be significantly lowered. The anti-inflammatory efficacy of our nanotherapeutic was further supported by the significant decrease of proinflammatory IL-1β mRNA expression. However, further research using appropriate disease models for DR and AMD is needed to fully understand the impact of counteracting inflammation and immune responses on the progression of neovascular diseases and its therapeutic potential. Therefore, we deem our nanoparticles the perfect tool to explore the effect of treating a pathophysiological deranged RPE in more depth in the future using AMD and DR models.

Moreover, our findings pave the way for a highly innovative treatment of neovascular ocular diseases since we have proven that rebalancing RPE function and homeostasis is a feasible and very efficient way to counteract the underlying triad of pathophysiological events. Its concrete therapeutic rational, the simplicity of i.v. injection and the need for only a single application would make our nanotherapeutic a precious tool to fight ROP more efficiently, prophylactically, safer and at lower cost. This would be of paramount value particularly for middle- and low-income countries, where the prevalence of ROP is high and the diagnostic and therapeutic possibilities are low *(62, 63)*. Even though, further research regarding nanoparticle toxicity, dosing, and long-term effects is needed to successfully translate the nanotherapeutic into clinics, we strongly believe this could represent a paradigm shift in neonatal care to a future in which a single i.v. injection of nanoparticles is a standard treatment for the millions of infants at risk for ROP.

# 4 Materials and Methods

## 4.1 Materials

Kolliphor® HS15 was obtained from BASF and Lipoid® S75-3 was acquired from Lipoid GmbH (Ludwigshafen, Germany). Miglyol® 812 (medium chain triglycerides (MCT)) was purchased from Caesar & Loretz GmbH (Hilden, Germany). 1,1′-Dioctadecyl-3,3,3′,3′-tetramethylindocarbocyanine perchlorate (DiI), 3,3′-Dioctadecyloxacarbocyanine perchlorate (DiO) and 1,1′-Dioctadecyl-3,3,3′,3′-tetramethylindodicarbocyanine perchlorate (DiD) were purchased from Invitrogen (Waltham, USA). Sodium oleate was purchased from TCI Europe (Zwijindrecht, Belgium). Cyclosporin A (CsA) was obtained from Pharma Stulln GmbH (Stulln, Germany).

1,2-Distearoyl-sn-glycero-3-phosphoethanolamine-N[maleimide(polyethyleneglycol)-2000] (ammonium salt) (DSPE-PEG2000-maleimide) was purchased from Avanti Polar Lipids Inc. (Alabaster, USA). Cyclo-(Arg-Gly-Asp-D-Phe-Cys) acetate salt (RGD) was purchased from Bachem Distribution Service GmbH (Weil a. Rhein, Germany). Dulbecco's phosphate buffered saline (DPBS) was acquired from Gibco® Life Technologies (Waltham, USA). Purified water was obtained from a MilliQ System from Millipore (Schwalbach, Germany). All other materials and reagents in analytical grade were obtained from Merck (Taufkirchen, Germany).

## 4.2 Lipid Nanoparticle Preparation & Characterization

LNC were prepared after Heurtault et. al *(64)* with slight modifications as previously described *(65)*. In short, 887.5 mg Kolliphor® HS15 40% (w/w), 30 mg Lipoid® S75-3, 415 mg MCT, 12 mg NaCl and 655.8 mg water were heated in a phase inversion process of 3 cycles between 90°C and 60°C. In the third cycle, water was added at the phase inversion temperature leading to stable LNC formation. The final dispersion was filtered through a 0.22 µm regenerated cellulose (RC) membrane for sterilization and stored at room temperature in the dark. For particle detection, fluorescent dyes (DiO, DiI, DiD 1.5% (w/w)) and/or SPION 0.24% iron (w/w) were added to the initial mixture *(66)*. For the preparation of CsA loaded LNC, MCT was replaced by 8.5% (w/w) CsA-MCT solution and particles were prepared as described above. For RGD peptide grafting, RGD was first coupled to DSPE-PEG2000-maleimide (2 h, RT, 500 rpm). Next, the conjugates were inserted in the shell of the LNC by using the post-insertion method as previously described (3 h, 37°C, 500 rpm) *(67)*. For purification and concentration, the modified LNC were dialyzed against DPBS overnight using Spectra/Por® Float-A-Lyzer® G2 MWCO 300 kDa and subsequently centrifuged twice (15 min, RT, 4000 g) using a 100 kDa molecular weight cutoff Amicon® Ultra-4 centrifugal device.

Size and ξ-potential of the resulting particles were measured in 10% DPBS (v/v) at a constant temperature of 25 °C using 2 mg/ml concentrations with a ZetaSizer Nano ZS (Malvern Instruments). To assess the CsA content and the encapsulation efficacy, CsA LNC were diluted with methanol and ultrasonicated (30 min) to disrupt the particles. Afterwards CsA was quantified by ultra-high-performance liquid chromatography in combination with mass spectrometry (UHPLC-MS), as previously described *(65, 68)*.

### 4.3 Cell Culture

Human dermal microvascular endothelial (HDME) cells were cultured in endothelial cell growth medium MV (GM) and endothelial cell basal medium MV (BM), all purchased from PromoCell GmbH (Heidelberg, Germany). HDME cells were used exclusively in low passage numbers ranging from 4 to 7. Human retina pigment epithelial cells (ARPE-19), kindly gifted by Dr. Ulrike Friedrich (Institute of Human Genetics, University of Regensburg), were cultured in DMEM-F12 (1:1) medium supplemented with 10% FBS obtained from Biowest (Nuaillé, France).

### 4.4 Cellular Targeting

Particle uptake through flow cytometry was performed as previously described *(65)*. In short, either HDME or ARPE-19 cells were seeded in 24-well plates at a density of 50 000 cells per well and incubated in BM and DMEM-F12 (1:1), respectively, for 24 h (37°C). Pre-warmed particle solutions (0.6 mg/ml in Leibovitz medium supplemented with 0.1% bovine serum albumin (BSA)) were added to the cells, after washing them with DPBS, and incubated for 1 h. To confirm the ligand specificity, cells were incubated with 1 mg/ml of RGD solution prior to particle addition. Afterwards, particle solutions were discarded, and the cells washed thoroughly with DPBS, trypsinated and centrifuged (200 × g, 5 min, 4°C). Nanoparticle associated cell fluorescence was analyzed in DPBS using a FACS Canto II cytometer (Becton Dickinson). Fluorescence was excited at 488 nm and recorded using a 530/30 nm bandpass filter. The population of viable cells was gated using Flowing software 2.5.1. (Turku Centre for Biotechnology) and the geometric mean of the nanoparticle associated fluorescence was analyzed.

For the assessment of particle uptake kinetics, ARPE-19 cells were seeded in 24-well plates at a density of 50 000 cells per well and incubated in DMEM-F12 (1:1) for 24 h (37°C). After washing the cells with DPBS, pre-warmed particle solutions (0.6 mg/ml in Leibovitz medium supplemented with 0.1% BSA) were added to the cells and incubated for 1 h, 2 h, 4 h, 6 h and 8 h. Subsequent to every incubation period cells were processed and analyzed as described above. To determine the cellular distribution of the different particle formulations HDME and ARPE-19 cells were seeded in coverslip containing 6-well plates at a density of 300 000 cells

per well and incubated over 24 h. Then, cells were washed with DPBS and incubated with pre-warmed particles solutions (0.6 mg/ml in Leibovitz medium supplemented with 0.1% BSA) for 1 h. Afterward, the solutions were discarded, and prior to the fixation with 4% paraformaldehyde (PFA), cells were washed thoroughly with DPBS. The coverslips were then transferred onto Superfrost plus glass slides and cell nuclei were stained with DAPI (0.15 µg/ml) prior to imaging using an Axio Imager fluorescence microscope with a Plan-Neofluar 40x/1.30 Oil M27 objective (Carl Zeiss AG) and the Zen Software (Carl Zeiss Microscopy).

### *4.5 In vivo* Distribution and Targeting

The *in vivo* distribution experiments were carried out according to the national and institutional guidelines and were approved by the local authority (Regierung von Unterfranken, reference number: 55.2-2532-2-329). As animal models, 10-week-old female 129SV-mice (Charles River Laboratories, Sulzfeld, Germany) were used. The different nanoparticle solutions (10 mg/ml LNC or RGD-LNC in DPBS) were injected (100 µl) via the vena jugularis after anesthesia with isoflurane inhalation and buprenorphine (0.1 mg/kg). After 1 h of particle circulation mice were anaesthetized with ketamine (125 mg per kg bodyweight) and xylazine (80 mg per kg bodyweight), the blood sample was collected, and they were killed through perfusion with DPBS. Subsequently, eyes, liver, heart, and kidneys were harvested and the posterior part of one eye or 100 mg of each organ, respectively were homogenized in RIPA buffer using an Ultra-Turrax tissue homogenizer (IKA). Then, samples were centrifuged (4 min, 4°C, 2000 g), the supernatant was collected, and the nanoparticle concentration was determined using a FLUOstar Omega microplate reader (DiD; 640/20 nm excitation and 680/20 nm emission bandpass filters) and calculated using GraphPad Prism 6.0. The second eye was placed in 4% PFA for 1 h directly after the perfusion with DBPS and then retina whole mounts were prepared. Finally, the retinae were transferred on microscope slides, and mounted with Mowiol 4-88 (Carl Roth, Karlsruhe, Germany). Images of the whole retina and detailed images of the retinal vessels were acquired using an Axio Imager fluorescence microscope with a Plan-Apochromat 20x/0.8 M27 objective and the Zen Software (Carl Zeiss Microscopy). For better visualization, the lookup table “Sun” was applied to the particle-associated fluorescence. To investigate the intraocular distribution, mice were treated with LNC and RGD-LNC loaded simultaneously with fluorescent dye and superparamagnetic iron oxide nanoparticles (Dual LNC) as described above [66]. After either 1 h, 24 h or 5 d of particle circulation, mice were anaesthetized with ketamine (125 mg per kg bodyweight) and xylazine (80 mg per kg bodyweight), killed through perfusion with 4% PFA and eyes were enucleated.

Afterward, one eye was cryoprotected by incubation in phosphate buffer (0.1 m pH 7.4) supplemented with increasing sucrose concentrations (10%, 20% and 30%) for 12 h each. Then, cryoprotected eyes were embedded in Tissue Tek O.C.T. Compound (Sakura Finetek) and subsequently frozen in liquid nitrogen. Finally, they were cut into 12 µm sections using an HM 500 OM microtome (Microm International) and transferred onto Superfrost plus glass slides. For determining the colocalization of the nanoparticles with the RPE cells, cryosections were washed with phosphate buffer (0.1 m pH 7.4) prior to the 1 h-blockage with 2% BSA. Sections were then washed with phosphate buffer (3 x, 5 min each) and incubated overnight with the primary monoclonal mouse anti-RPE-65 antibody (Abcam, Cambridge, UK) (1:100 in 1:10 blockage buffer) at 4 °C. Then, they were washed again with phosphate buffer (3 x 5 min each) and incubated for 1 h with the Alexa 488 anti-mouse secondary antibody (1:1000 in 1:10 blockage buffer) (Invitrogen, Thermo Fisher Scientific, Waltham, USA). Finally, the sections were washed again and rinsed with ultrapure water prior to mounting with Mowiol 4-88 supplemented with DAPI (0.15 µg/ml). To further assess the colocalization of the nanoparticles with vessels, cryosections were washed with phosphate buffer (0.1 m pH 7.4) prior to 1 h-blockage with 2% BSA supplemented with 0.2% cold water fish gelatin (CWFG) and 0.1% Triton. Sections were then washed with phosphate buffer (3 x, 5 min each) and incubated overnight with the primary polyclonal goat anti-CD31 antibody (R&D systems, Minneapolis, USA) (1:100 in 1:10 blockage buffer) at 4 °C. Then, they were washed again with phosphate buffer (3 x, 5 min each) and incubated for 1 h with the biotinylated anti-goat secondary antibody (1:500 in 1:10 blockage buffer) (Vector Laboratories, Burlingame, USA). Before and after the incubation with streptavidin Alexa 488 (1:1000 in 1:10 blockage buffer) (Invitrogen, Thermo Fisher Scientific, Waltham, USA) for 1 h, sections were washed again and rinsed with ultrapure water prior to mounting with Mowiol 4-88 (Carl Roth, Karlsruhe, Germany) supplemented with DAPI (0.15 µg/ml). Images were generated using an Axio Imager fluorescence microscope with a Plan-Neofluar 40x/1.30 Oil M27 objective (Carl Zeiss AG) and the Zen Software (Carl Zeiss Microscopy). For the quantitative evaluation of nanoparticle fluorescence in the RPE, the fluorescence area was gated, and the integrated fluorescence density of each gated area was quantified using ImageJ version 1.52. The respective other eye was used for the preparation of ultra-thin sections for transmission electron microscopy (TEM). To that end, eyes were embedded in London Resin white (L.R. white) (Serva, Garden City Park, NY) and finally ultra-thin sections (90 nm) were processed according to protocols published previously *(69)*. TEM imaging was performed, as previously described, using a Libra 120 electron microscope (Carl Zeiss AG) *(70)*.

### 4.6 Murine ROP Model

The animal experiments regarding the assessment of nanoparticle efficacy were carried out according to the national and institutional guidelines and were approved by the local authority (Regierung von Unterfranken, reference number: 55.2-2532-2-363). OIR was induced in mouse (129SV) pups according to a protocol previously established (*48*). In brief, at postnatal day 7 (P7), mouse pups and their nursing mothers were placed in a plexiglas incubator with an adjustable oxygen sensor and feedback system and exposed to hyperoxia (75 ± 1% oxygen) for 5 days. On P12, the pups were returned to room-air conditions for another 5 days until P17. Mice were treated at P12 directly after returning to normoxia with either 20 µl nanoparticle solution (RGD-LNCs or CsA RGD-LNCs 20 mg/ml), CsA solution (Sandimmun 50 mg/ml, Novartis, Basel, Switzerland) diluted with isotonic saline solution to a final concentration of 0.68 mg/ml or DPBS by injection via the vena jugularis after anesthesia with ketamine (125 mg per kg bodyweight) and xylazine (80 mg per kg bodyweight).

### 4.7 Assessment of ocular CsA content

To quantify the CsA content in the eye at P17 after the treatment with either CsA RGD-LNCs or free CsA on day P12, mice were killed through cervical dislocation, eyes were enucleated and the anterior parts including cornea and lens were discarded. Afterwards, the posterior parts of the eye were weighed and homogenized in 0.5 ml methanol using Ultra-Turrax tissue homogenizer (IKA) and ultrasonicated for 2 h. Prior to the centrifugation (2000 x g, 30 min, 20 °C), Cyclosporin D (CsD) was added as internal standard (0.02 µg/ml). Finally, the supernatant was analyzed and the CsA content determined using the same UHPLC-MS method as previously described *(68)*. Data handling and processing were done using Microsoft Excel 2019 and GraphPad Prism 6.0.

### 4.8 Quantification of Neovascularization

At P17, mice were weighed and underdeveloped mice (< 6 g) were excluded from further investigations. For the preparation of retina whole mounts, animals were anesthetized on day P17 with ketamine (125 mg per kg bodyweight) and xylazine (80 mg per kg bodyweight). The heart was exposed through the diaphragm and the left ventricle was injected with 1 ml of fluorescein isothiocyanate (FITC) dextran (TdB, Uppsala, Sweden) solution in DPBS (50 mg/ml). Afterwards, eyes were enucleated and placed in 4% PFA for 1 h. Eye cups were dissected, and retinal flat mounts created and examined using fluorescence microscopy (Axio Imager, Plan-Apochromat 20x/0.8 M27 objective). For quantitative analysis the whole retinal area and the area of vascular tortuosity, tufting and leakiness was determined randomized and blinded using the Zen Software (Carl Zeiss Microscopy) *(50)*.

### 4.9 Immunohistochemistry & Immunofluorescence

The immunofluorescent detection of VEGF-R2 and GFAP was performed using cryosections. For the preparation of cryosections, mice were anaesthetized at day P17 with ketamine (125 mg per kg bodyweight) and xylazine (80 mg per kg bodyweight) and killed through perfusion fixation with 4% PFA and afterwards, eyes were enucleated and processed as described above. For VEGF-R2 staining, cryosections were washed with phosphate buffer (0.1 m pH 7.4) prior to 1 h-blockage with 2% BSA supplemented with 0.2% CWFG. After the blockage, sections were washed (3 x, 5 min each) and incubated overnight with the primary polyclonal rabbit anti-VEGFR2 antibody (Cell Signaling Technology, Danvers, USA) (1:200 in 1:10 blockage buffer) at 4°C. Then they were washed (3 x, 5 min each) and incubated for 1 h with the biotinylated anti-rabbit secondary antibody (1:500 in 1:10 blockage buffer) (Vector Laboratories, Burlingame, USA). Before and after the incubation with streptavidin Alexa 488 (1:1000 in 1:10 blockage buffer) for 1 h, sections were washed again and rinsed with ultrapure water prior to mounting with Mowiol 4-88 supplemented with DAPI (0.15 µg/ml). For GFAP staining cryosections were washed with phosphate buffer (0.1 m pH 7.4) prior to the 1 h-blockage with 2% BSA supplemented with 0.2% CWFG and 0.1% Triton. After the blockage, sections were washed (3 x, 5 min each) and incubated overnight with the primary polyclonal chicken anti-GFAP antibody (LSBio, Seattle, USA) (1:1000 in 1:10 blockage buffer) at 4 °C. Then, they were washed (3 x, 5 min each) and incubated for 1 h with the Alexa 488 anti-chicken secondary antibody (1:1000 in 1:10 blockage buffer) (Abcam, Cambridge, UK). Finally, the sections were washed again and rinsed with ultrapure water prior to mounting with Mowiol 4-88 supplemented with DAPI (0.15 µg/ml). Images were generated using an Axio Imager fluorescence microscope with a Plan-Neofluar 40x/1.30 Oil M27 objective (Carl Zeiss AG) and the Zen Software (Carl Zeiss Microscopy). For the quantitative evaluation of immunofluorescence in the whole posterior eye section, the ocular area was gated, and the integrated fluorescence density of each gated area was quantified using ImageJ version 1.52.

### 4.10 VEGF Quantification

To assess the VEGF protein levels quantitatively, an Enzyme-linked Immunosorbent Assay (ELISA) for mouse VEGF (R&D systems, Minneapolis, USA) was used. For the generation of tissue samples, mice were killed through cervical dislocation, eyes were enucleated, and both the sensory retina and the RPE-choroid complex were collected. Samples were treated with 500 µl TRIzol (Invitrogen, Waltham, USA) and for protein isolation, the manufacturer's instructions were followed. Afterwards, 40 µl of sensory retina lysate or 100 µl RPE-choroid lysate respectively, were diluted with sample diluent provided by the manufacturer up to 200 µl. VEGF measurements were then performed according to the provided protocol. Fluorescence was measured using a FLUOstar Omega microplate reader and data were calculated using GraphPad Prism 6.0.

### 4.11 RT – qPCR

RNA samples from both the sensory retina and the RPE-choroid complex were extracted using TRIzol (Invitrogen, Waltham, USA) following the manufacturer's instructions for RNA isolation. After determining the RNA concentration using a NanoDrop spectrophotometer (Thermo Fisher Scientific, Waltham, USA), equal amounts of total RNA were reversed transcribed into first-strand cDNA using iScript cDNA Synthesis Kit (Bio-Rad, Hercules, USA) according to manufacturers' instructions. Quantitative real-time RT-PCR analyses were performed using the iQ5 Real-Time PCR Detection System (Bio-Rad). RNA that was not reverse transcribed served as negative control for real-time RT-PCR and for relative quantification GNB2L was used. Quantification and analysis were performed using BioRad iQ5 software (BioRad), data was processed using Microsoft Excel 2019 and GraphPad Prism 6.0. The primer sequences (Invitrogen, Waltham, USA) used were as follows:

5′-TCTGCAAGTACACGGTCCAG-3′; *Gnb2l* forward
5′-GAGACGATGATAGGGTTGCTG-3′; *Gnb2l* reverse
5′-GAACAAAGCCAGAAAATCACTGTG-3′; *Vegf-a-164* forward
5′-CGAGTCTGTGTTTTTGCAGGAAC-3′; *Vegf-a-164* reverse
5′-CAGTGGTACTGGCAGCTAGAAG-3′; *VegfR2* forward
5′-ACAAGCATACGGGCTTGTTT-3′; *VEGFR2* reverse
5′-TCTTCCGCTTGCAAAACC-3′; *Tgfbeta2* forward
5′-GTGGGAGATGTTAAGTCTTTGGA-3′; *Tgfbeta2* reverse
5′-AGAAGCCGCATGAAGTCTG-3′; *TgfbetaR2* forward
5′-GGCAAACCGTCTCCAGAGTA-3′; *TgfbetaR2* reverse
5′-AGTTGACCGACCCCAAAAG-3′; *Il-1beta* forward
5′-AGCTGCATGCTCTGATCAGG-3′; *Il-1beta* reverse

### 4.12 Morphological Examination

To detect morphological changes in the retina of mice caused by the therapeutic intervention, mice were anaesthetized at day P17 with ketamine (125 mg per kg bodyweight) and xylazine (80 mg per kg bodyweight) and killed through perfusion with 4% PFA. Then, eyes were enucleated, fixed for 24 h in Ito's fixative and embedded in Epon as previously described *(71)*. Semi-thin sections of 1.0 µm thickness were cut along the mid-horizontal (nasal-temporal) plane and stained by Richardson's stain. Afterwards, images were taken using light microscopy (Axio Imager, Plan-Neofluar 40x/1.30 Oil M27 objective; Carl Zeiss). For a quantitative assessment, the distance between ora serrata and optic nerve head was divided into tenths and the thickness of the outer nuclear layer (ONL) and inner nuclear layer (INL) was measured between each tenth using Zen Software (Carl Zeiss Microscopy) and ImageJ version 1.52. Data was further handled using Microsoft Excel 2019 and GraphPad Prism 6.0.

### 4.13 Statistical analysis

Data are expressed as mean ± SD. Statistical evaluation was performed using GraphPad Prism Software 6.0. Student's t-test for unpaired data, one-way ANOVA and two-way ANOVA with a Sidak's or Tukey's multiple comparison test were employed to evaluate statistical significance. Levels of statistical significance and "n" numbers for each experiment are indicated in figure legends. No statistical methods were used to predetermine sample size.

# References


(1) A.L. Solebo, L. Teoh, J. Rahi, Epidemiology of blindness in children, Archives of Disease in Childhood 102 (9) (2017) 853–857.
(2) S.R. Flaxman, R.R.A. Bourne, S. Resnikoff, P. Ackland, T. Braithwaite, M.V. Cicinelli, A. Das, J.B. Jonas, J. Keeffe, J.H. Kempen, J. Leasher, H. Limburg, K. Naidoo, K. Pesudovs, A. Silvester, G.A. Stevens, N. Tahhan, T.Y. Wong, H.R. Taylor, Global causes of blindness and distance vision impairment 1990–2020: A systematic review and meta-analysis, The Lancet Global Health 5 (12) (2017) e1221-e1234.
(3) A. Hellstrom, L.E. Smith, O. Dammann, Retinopathy of prematurity, The Lancet 382 (9902) (2013) 1445–1457.
(4) D.D. Antonetti, R. Klein, T.W. Gardner, Mechanisms of Disease - Diabetic Retinopathy, N. Engl. J. Med. (366) (2012) 1227–1239.
(5) P.T.V.M. de Jong, Age-related macular degeneration, N. Engl. J. Med. 355 (14) (2006) 1474–1485.
(6) J.R. Sparrrow, D. Hicks, C.P. Hamel, The Retinal Pigment Epithelium in Health and Disease, CMM 10 (9) (2010) 802–823.
(7) H. Xu, M. Chen, Targeting the complement system for the management of retinal inflammatory and degenerative diseases, European Journal of Pharmacology 787 (2016) 94–104.
(8) O. Strauss, The retinal pigment epithelium in visual function, Physiol. Rev. 85 (3) (2005) 845–881.
(9) I. Bhutto, G. Lutty, Understanding age-related macular degeneration (AMD): relationships between the photoreceptor/retinal pigment epithelium/Bruch's membrane/choriocapillaris complex, Mol. Aspects Med. 33 (4) (2012) 295–317.
(10) A. Urtti, Challenges and obstacles of ocular pharmacokinetics and drug delivery, Adv. Drug Deliv. Rev. 58 (11) (2006) 1131–1135.
(11) Q. Li, J. Weng, S.N. Wong, W.Y. Thomas Lee, S.F. Chow, Nanoparticulate Drug Delivery to the Retina, Mol. Pharm. (2020).
(12) N. Kuno, S. Fujii, Recent Advances in Ocular Drug Delivery Systems, Polymers 3 (4) (2011) 193–221.
(13) S.K. Sahoo, F. Dilnawaz, S. Krishnakumar, Nanotechnology in ocular drug delivery, Drug Discov. Today 13 (3-4) (2008) 144–151.
(14) S. Fouzdar Jain, H.H. Song, S.N. Al-Holou, L.A. Morgan, D.W. Suh, Retinopathy of prematurity: Preferred practice patterns among pediatric ophthalmologists, Clin. Ophthalmol. 12 (2018) 1003–1009.
(15) A.W. Stitt, T.M. Curtis, M. Chen, R.J. Medina, G.J. McKay, A. Jenkins, T.A. Gardiner, T.J. Lyons, H.P. Hammes, R. Simó, N. Lois, The progress in understanding and treatment of diabetic retinopathy, Prog. Retin. Eye Res. 51 (2016) 156–186.
(16) A.C. Bird, Therapeutic targets in age-related macular disease, J. Clin. Invest. 120 (9) (2010) 3033–3041.
(17) H.A. Mintz-Hittner, K.A. Kennedy, A.Z. Chuang, Efficacy of Intravitreal Bevacizumab for Stage 3+ Retinopathy of Prematurity, New England Journal of Medicine 364 (7) (2011) 603–615.
(18) M. Quresh, Management of Diabetic Retinopathy - A Systematic Review, Clinician's Corner (298) (2007) 902–916.
(19) D.F. Martin, M.G. Maguire, G. Ying, J.E. Grunwald, Ranibizumab and Bevacizumab for Neovascular Age-Related Macular Degeneration, N. Engl. J. Med. (364) (2011) 1897–1908.
(20) The CATT Research Group, Ranibizumab and Bevacizumab for Neovascular Age-Related Macular Degeneration, New England Journal of Medicine 364 (20) (2011) 1897–1908.
(21) H.H. Shen, E.C. Chan, J.H. Lee, Y.S. Bee, T.W. Lin, G.J. Dusting, G.S. Liu, Nanocarriers for treatment of ocular neovascularization in the back of the eye: new vehicles for ophthalmic drug delivery, Nanomedicine (Lond) 10 (13) (2015) 2093–2107.

(22) P.A. Keane, S.R. Sadda, Development of Anti-VEGF Therapies for Intraocular Use: A Guide for Clinicians, J. Ophthalmol. 2012 (2012) 483034.
(23) I. Yoshida, T. Shiba, H. Taniguchi, M. Takahashi, T. Murano, N. Hiruta, Y. Hori, H. Bujo, T. Maeno, Evaluation of plasma vascular endothelial growth factor levels after intravitreal injection of ranibizumab and aflibercept for exudative age-related macular degeneration, Graefes Arch. Clin. Exp. Ophthalmol. 252 (9) (2014) 1483–1489.
(24) K. Matsuyama, N. Ogata, M. Matsuoka, M. Wada, K. Takahashi, T. Nishimura, Plasma levels of vascular endothelial growth factor and pigment epithelium-derived factor before and after intravitreal injection of bevacizumab, British Journal of Ophthalmology 94 (9) (2010) 1215–1218.
(25) C.Y. Huang, R. Lien, N.K. Wang, A.N. Chao, K.J. Chen, T.L. Chen, Y.S. Hwang, C.C. Lai, W.C. Wu, Changes in systemic vascular endothelial growth factor levels after intravitreal injection of aflibercept in infants with retinopathy of prematurity, Graefes Arch. Clin. Exp. Ophthalmol. 256 (3) (2018) 479–487.
(26) R.L. Avery, D.J. Pieramici, M.D. Rabena, A.A. Castellarin, M.A. Nasir, M.J. Giust, Intravitreal bevacizumab (Avastin) for neovascular age-related macular degeneration, Ophthalmology 113 (3) (2006) 363-372.e5.
(27) R.L. Avery, J. Pearlman, D.J. Pieramici, M.D. Rabena, A.A. Castellarin, M.A. Nasir, M.J. Giust, R. Wendel, A. Patel, Intravitreal bevacizumab (Avastin) in the treatment of proliferative diabetic retinopathy, Ophthalmology 113 (10) (2006) 1695.e1-15.
(28) M. Tolentino, Systemic and ocular safety of intravitreal anti-VEGF therapies for ocular neovascular disease, Survey of Ophthalmology 56 (2) (2011) 95–113.
(29) K.G. Falavarjani, Q.D. Nguyen, Adverse events and complications associated with intravitreal injection of anti-VEGF agents: A review of literature, Eye 27 (7) (2013) 787–794.
(30) R.L. Avery, What is the evidence for systemic effects of intravitreal anti-VEGF agents, and should we be concerned? Br. J. Ophthalmol. 98 Suppl 1 (2014) i7-10.
(31) E. Blanco, H. Shen, M. Ferrari, Principles of nanoparticle design for overcoming biological barriers to drug delivery, Nat Biotechnol 33 (9) (2015) 941–951.
(32) N. Gordiyenko, M. Campos, J.W. Lee, R.N. Fariss, J. Sztein, I.R. Rodriguez, RPE Cells Internalize Low-Density Lipoprotein (LDL) and Oxidized LDL (oxLDL) in Large Quantities In Vitro and In Vivo, Invest. Ophthalmol. Vis. Sci. 45 (8) (2004) 2822.
(33) I.A. Pikuleva, C.A. Curcio, Cholesterol in the retina: The best is yet to come, Prog. Retin. Eye Res. 41 (2014) 64–89.
(34) K.C. Hayes, S. Lindsey, Z.F. Stephan, D. Brecker, Retinal pigment epithelium possesses both LDL and scavenger receptor activity, Invest. Ophthalmol. Vis. Sci. 30 (2) (1989) 225–232.
(35) D. Calvo, D. Gómez-Coronado, Y. Suárez, M.A. Lasunción, M.A. Vega, Human CD36 is a high affinity receptor for the native lipoproteins HDL, LDL, and VLDL, J. Lipid Res. 39 (4) (1998) 777–788.
(36) M. Kato, M. Mrksich, Using model substrates to study the dependence of focal adhesion formation on the affinity of integrin-ligand complexes, Biochemistry 43 (10) (2004) 2699–2707.
(37) M. Friedlander, C.L. Thehsfeld, M. Sugita, M. Fruttiger, M.A. Thomas, S. Chang, D.A. Cheresh, Involvement of integrins alphavbeta3 and alphavbeta5 in ocular neovascular diseases, Proceeding of the National Academy of Sience 1996 (93) 9764–9769.
(38) M. Mammen, S.K. Choi, G.M. Whitesides, Polyvalent Interactions in Biological Systems: Implications for Design and Use of Multivalent Ligands and Inhibitors, Angewandte Chemie International Edition 37 (20) (1998) 2754–2794.
(39) C.L. Modery-Pawlowski, A. Sen Gupta, Heteromultivalent ligand-decoration for actively targeted nanomedicine, Biomaterials 35 (9) (2014) 2568–2579. (40) J.F. Borel, C. Feurer, H.U. Gubler, H. Stähelin, Biological effects of cyclosporin A: A new antilymphocytic agent, Agents and Actions 43 (3) (1994) 179–186.
(41) D.J. Freeman, Pharmacology and pharmacokinetics of cyclosporine, Clinical Biochemistry 24 (1) (1991) 9–14.

(42) P. Rafiee, J. Heidemann, H. Ogawa, N.A. Johnson, P.J. Fisher, M.S. Li, M.F. Otterson, C.P. Johnson, D.G. Binion, Cyclosporin A differentially inhibits multiple steps in VEGF induced angiogenesis in human microvascular endothelial cells through altered intracellular signaling, Cell Communication and Signaling (2004) 1–22.
(43) S. Wilhelm, A.J. Tavares, Q. Dai, S. Ohta, J. Audet, H.F. Dvorak, W.C.W. Chan, Analysis of nanoparticle delivery to tumours, Nat Rev Mater 1 (5) (2016) 751.
(44) K. Pollinger, R. Hennig, A. Ohlmann, R. Fuchshofer, R. Wenzel, M. Breunig, J. Tessmar, E.R. Tamm, A. Goepferich, Ligand-functionalized nanoparticles target endothelial cells in retinal capillaries after systemic application, Proc. Natl. Acad. Sci. U. S. A. 110 (15) (2013) 6115–6120.
(45) F. Danhier, A. Le Breton, V. Préat, RGD-based strategies to target alpha(v) beta(3) integrin in cancer therapy and diagnosis, Mol. Pharm. 9 (11) (2012) 2961–2973.
(46) A. Scott, M. Fruttiger, Oxygen-induced retinopathy: A model for vascular pathology in the retina, Eye 24 (3) (2010) 416.
(47) J.C. Rivera, M. Holm, D. Austeng, T.S. Morken, T.E. Zhou, A. Beaudry-Richard, E.M. Sierra, O. Dammann, S. Chemtob, Retinopathy of prematurity: Inflammation, choroidal degeneration, and novel promising therapeutic strategies, J. Neuroinflammation 14 (1) (2017) 165.
(48) S. Rathi, S. Jalali, S. Patnaik, S. Shahulhameed, G.R. Musada, D. Balakrishnan, P.K. Rani, R. Kekunnaya, P.P. Chhablani, S. Swain, L. Giri, S. Chakrabarti, I. Kaur, Abnormal Complement Activation and Inflammation in the Pathogenesis of Retinopathy of Prematurity, Front. Immunol. 8 (2017) 1868.
(49) M. Chrzanowska, A. Modrzejewska, M. Modrzejewska, New insight into the role of the complement in the most common types of retinopathy-current literature review, Int. J. Ophthalmol. 11 (11) (2018) 1856–1864.
(50) K.M. Connor, N.M. Krah, R.J. Dennison, C.M. Aderman, J. Chen, K.I. Guerin, P. Sapieha, A. Stahl, K.L. Willett, L.E.H. Smith, Quantification of oxygen-induced retinopathy in the mouse: A model of vessel loss, vessel regrowth and pathological angiogenesis, Nat. Protoc. 4 (11) (2009) 1565–1573.
(51) B.A. Nacev, J.O. Liu, Synergistic inhibition of endothelial cell proliferation, tube formation, and sprouting by cyclosporin A and itraconazole, PLoS ONE 6 (9) (2011) e24793.
(52) Z.M. Bian, S.G. Elner, V.M. Elner, Regulation of VEGF mRNA expression and protein secretion by TGF-beta2 in human retinal pigment epithelial cells, Exp. Eye Res. 84 (5) (2007) 812–822.
(53) R.M. Kurtz, V.M. Elner, Z.M. Bian, R.M. Strieter, S.L. Kunkel, S.G. Elner, Dexamethasone and cyclosporin A modulation of human retinal pigment epithelial cell monocyte chemotactic protein-1 and interleukin-8, Invest. Ophthalmol. Vis. Sci. 38 (2) (1997) 436–445.
(54) M. Rutar, K. Valter, R. Natoli, J.M. Provis, Synthesis and propagation of complement C3 by microglia/monocytes in the aging retina, PLoS ONE 9 (4) (2014) e93343.
(55) D. Dahl, The radial glia of Müller in the rat retina and their response to injury. An immunofluorescence study with antibodies to the glial fibrillary acidic (GFA) protein, Exp. Eye Res. 28 (1) (1979) 63–69.
(56) A.M. Sofias, Y.C. Toner, A.E. Meerwaldt, M.M.T. van Leent, G. Soultanidis, M. Elschot, H. Gonai, K. Grendstad, Å. Flobak, U. Neckmann, C. Wolowczyk, E.L. Fisher, T. Reiner, C.d.L. Davies, G. Bjørkøy, A.J.P. Teunissen, J. Ochando, C. Pérez-Medina, W.J.M. Mulder, S. Hak, Tumor Targeting by αvβ3-Integrin-Specific Lipid Nanoparticles Occurs via Phagocyte Hitchhiking, ACS Nano 14 (7) (2020) 7832–7846.

(57) B.K. Clifford, A.P. D'Amore, K.M. Connor, Revisiting the mouse model of oxygen-induced retinopathy, Eye Brain 8 (2016) 67–79.
(58) M.Y. Hsu, Y.C. Hung, D.K. Hwang, S.C. Lin, K.H. Lin, C.Y. Wang, H.Y. Choi, Y.P. Wang, C.M. Cheng, Detection of aqueous VEGF concentrations before and after intravitreal injection of anti-VEGF antibody using low-volume sampling paper-based ELISA, Sci. Rep. 6 (2016) 34631.
(59) J.I. Greenberg, D.J. Shields, S.G. Barillas, L.M. Acevedo, E. Murphy, J. Huang, L. Scheppke, C. Stockmann, R.S. Johnson, N. Angle, D.A. Cheresh, A role for VEGF as a negative regulator of pericyte function and vessel maturation, Nature 456 (7223) (2008) 809–813.
(60) A.S. Maharaj, M. Saint-Geniez, T.E. Walshe, E. Sekiyama, T. Kurihara, B. Tucker, M. Young, P.A. D'Amore, VEGF Is Required for Neuroretina Survival and Function, Invest. Ophthalmol. Vis. Sci. 49 (13) (2008) 5836.
(61) N. Ferrara, H.P. Gerber, J. LeCouter, The biology of VEGF and its receptors, Nature Medicine 9 (6) (2003) 669.
(62) G.E. Quinn, Retinopathy of prematurity blindness worldwide: Phenotypes in the third epidemic, Eye Brain 8 (2016) 31–36.
(63) S.J. Kim, A.D. Port, R. Swan, J.P. Campbell, R.V.P. Chan, M.F. Chiang, Retinopathy of prematurity: A review of risk factors and their clinical significance, Survey of Ophthalmology 63 (5) (2018) 618–637.
(64) B. Heurtault, P. Saulnier, B. Pech, A Novel Phase Inversion-Based Process for the Preparation of Lipid Nanocarriers, Pharmaceutical Research (19) (2002) 875–880.
(65) M. Bohley, A. Haunberger, A. Goepferich, Intracellular availability of poorly soluble drugs from lipid nanocapsules, European Journal of Pharmaceutics and Biopharmaceutics 139 (2019) 23–32.
(66) M.S. Bohley, E. Birch, F.J. Baumann, A.E. Dillinger, E.R. Tamm, A.M. Goepferich, Design of dye and superparamagnetic iron oxide nanoparticle loaded lipid nanocapsules with dual detectability in vitro and in vivo, Int. J. Pharm. 585 (2020) 119433.
(67) T. Perrier, P. Saulnier, F. Fouchet, N. Lautram, J.-P. Benoît, Post-insertion into Lipid NanoCapsules (LNCs): From experimental aspects to mechanisms, Int. J. Pharm. 396 (1-2) (2010) 204–209.
(68) C. Luschmann, W. Herrmann, O. Strauss, K. Luschmann, A. Goepferich, Ocular delivery systems for poorly soluble drugs: an in-vivo evaluation, Int. J. Pharm. 455 (1-2) (2013) 331–337.
(69) K.C. Richardson, L. Jarett, E.H. Finke, Embedding in epoxy resins for ultrathin sectioning in electron microscopy, Stain Technol. 35 (1960) 313–323.
(70) B. Braunger, V.S. Leimbeck, A. Schlecht, C. Volz, H. Jägle, E. Tamm, Deletion of ocular transforming growth factor β signaling mimics essential characteristics of diabetic retinopathy, Am. J. Pathol. 185 (6) (2015) 1749–1768.
(71) B.M. Braunger, A. Ohlmann, M. Koch, N. Tanimoto, C. Volz, Y. Yang, M.R. Bösl, A. Cvekl, H. Jägle, M.W. Seeliger, E.R. Tamm, Constitutive overexpression of Norrin activates Wnt/β-catenin and endothelin-2 signaling to protect photoreceptors from light damage, Neurobiology of Disease 50 (2013) 1–12.

# Chapter 5 – Supporting Information

---

# Targeted Lipid Nanoparticles for the Treatment of Neovascular Ocular Diseases

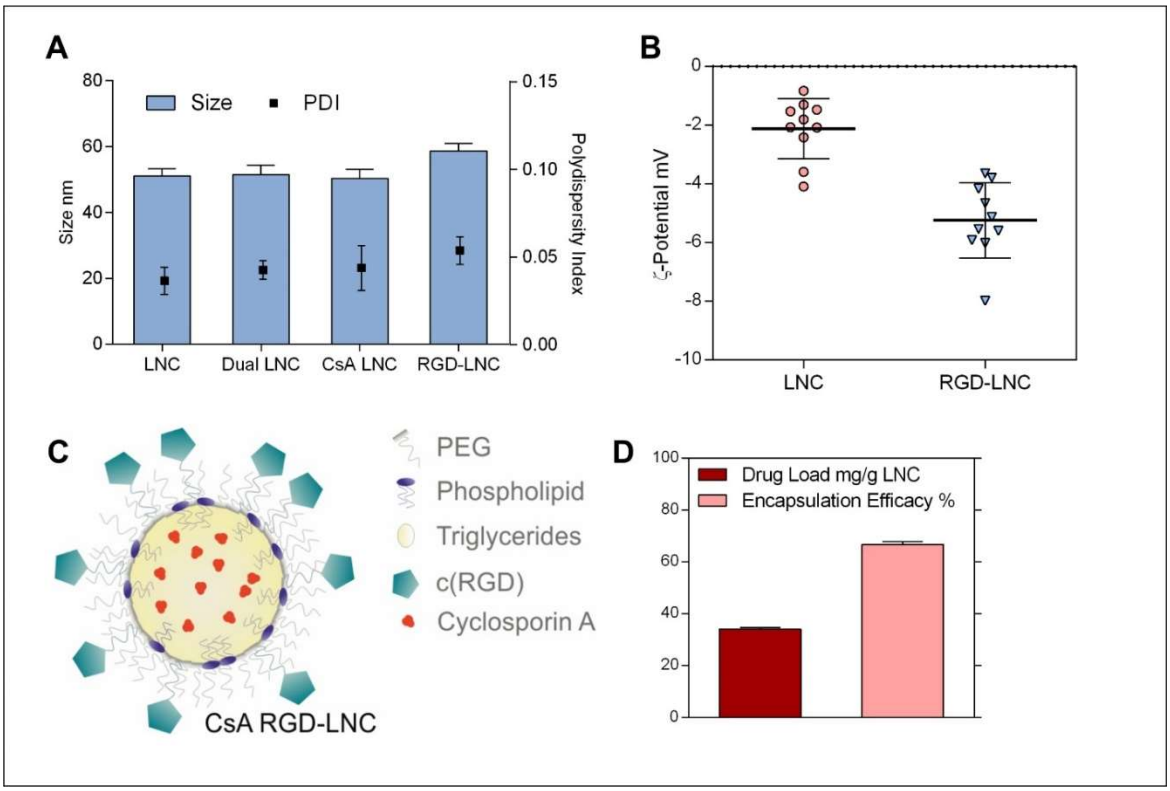


***Figure S1. Nanoparticle characterization.***

*(**A**) Hydrodynamic diameter and polydispersity index (PDI) of different LNC and RGD-LNC formulations. (**B**) ς -potential of LNCs and RGD-LNCs. (**C**) Schematic illustration of CsA loaded RGD-LNCs. (**D**) Absolute drug-load in mg CsA per g LNC dispersion and percentage encapsulation efficacy (experimental drug payload/theoretical drug payload). Results are presented as mean ± SD of n = 10 (**A** and **B**) and n = 3 (**D**) independent experiments.*

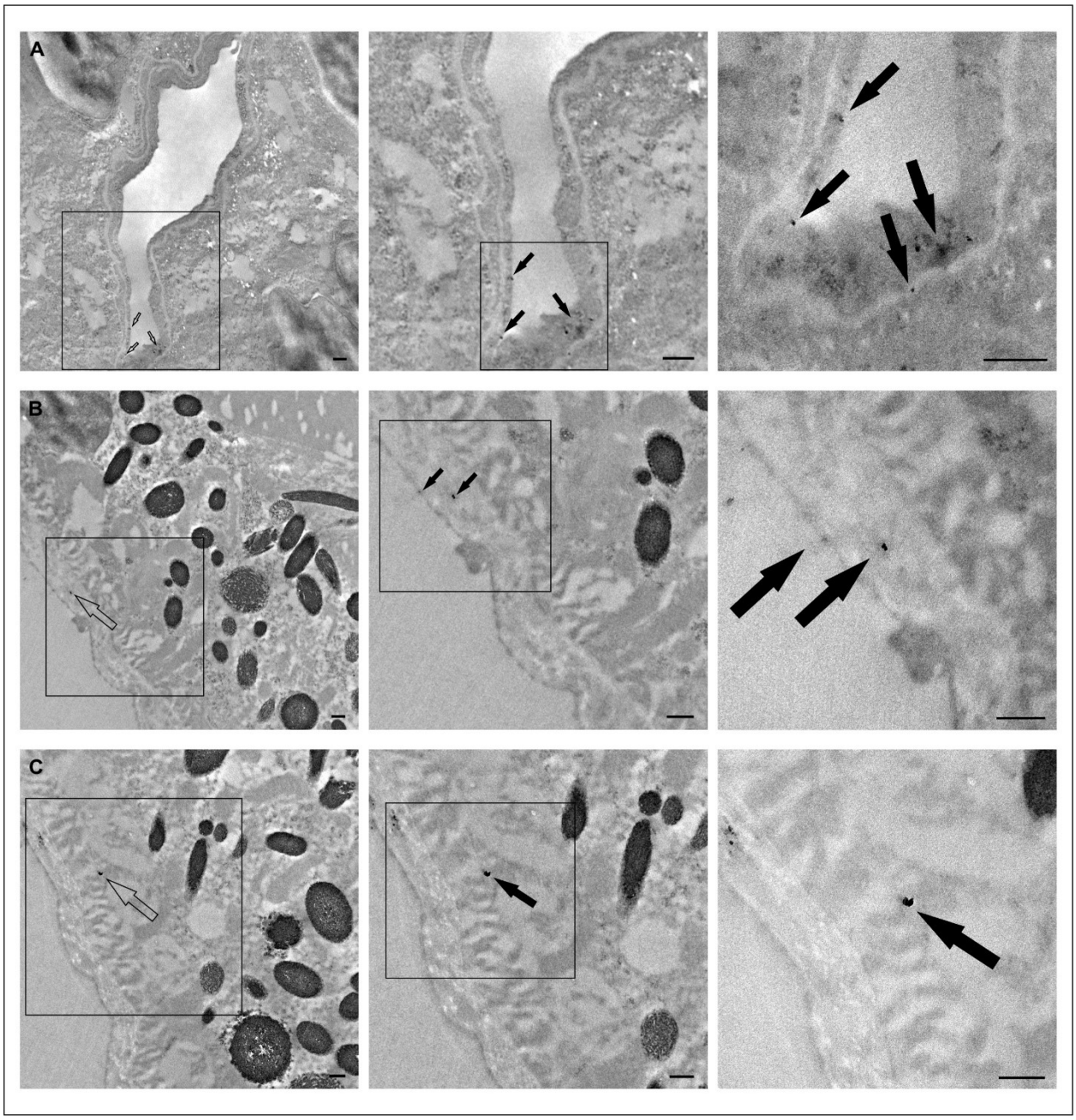


**Figure S2. TEM images of RGD-LNCs' *in vivo* route to the RPE.**

TEM images of nanoparticle targeting in the posterior eye 1 h after administration. (**A**) RGD-LNCs being associated with endothelial cells. (**B**) RGD-LNCs adjacent to and migrating in the Bruch's Membrane. (**C**) RGD-LNCs in the RPE cell. Arrows indicating electron dense SPION and dye loaded Dual LNCs. From left to right squared out regions are shown as magnifications. Scale bars: 250 nm. Representative images of at least n = 5 biologically independent samples.

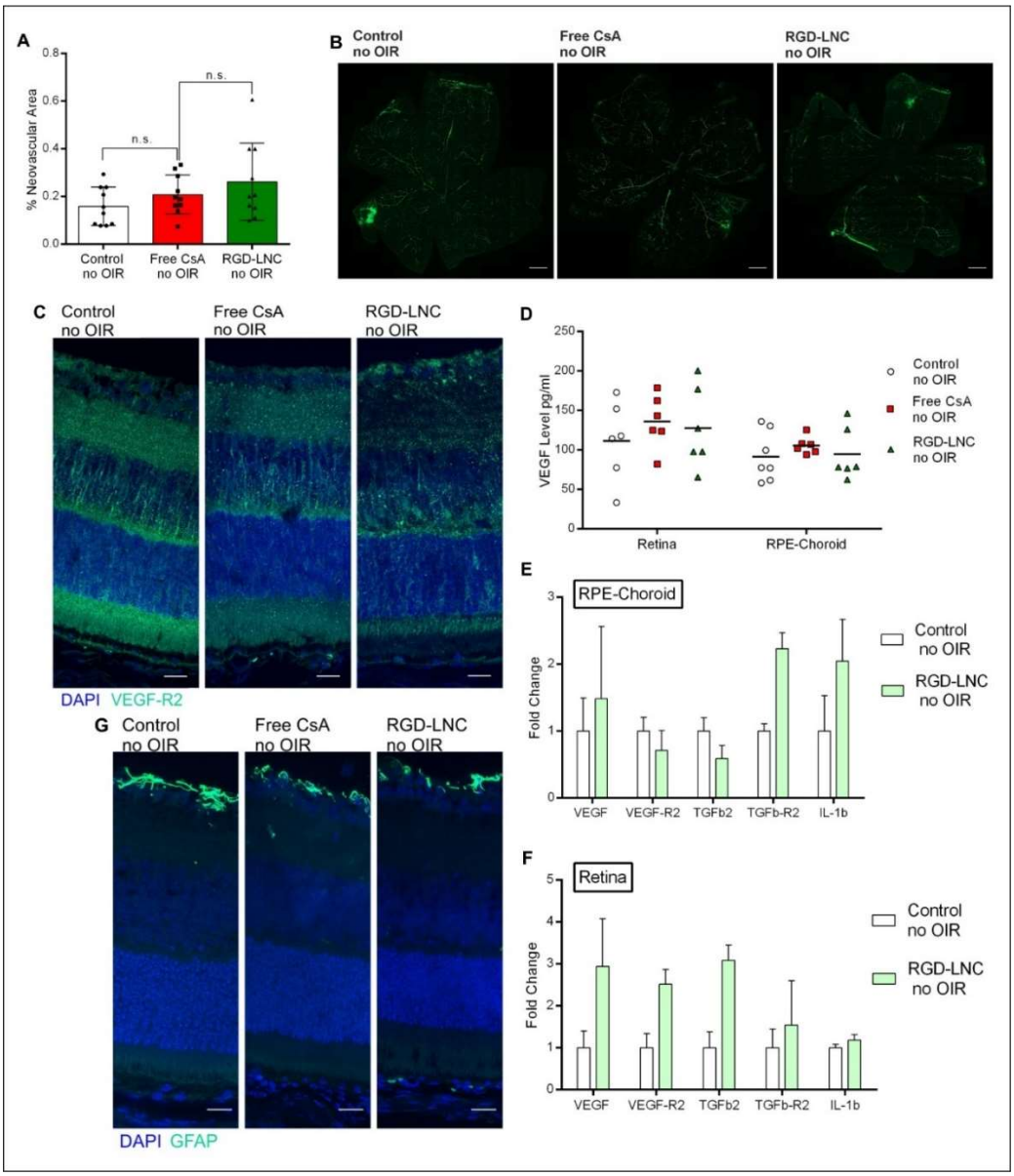


**Figure S3. Effects of free CsA and RGD-LNCs on mice without OIR.**

(**A**) Quantification of the relative neovascular area of mice without OIR at P17. (**B**) Representative images of retina whole mounts showing the retinal vasculature at P17. Green: FITC-Dextran. Scale bars: 500 µm. (**C**) Imaging of VEGF-R2 expression in the posterior eye. Scale bars: 20 µm. Blue: DAPI staining of cell nuclei; green: VEGF-R2. (**D**) Assessment of VEGF protein levels in the retina or RPE-choroid complex. (**E** and **F**) Representation of mRNA level fold change of VEGF, VEGF-R2, TGFb2, TGFb-R2 and IL-1β in either the retina or RPE-choroid complex. (**G**) Imaging of GFAP expression in the posterior eye of mice without OIR. Scale bars: 20 µm. Blue: DAPI staining of cell nuclei; green: GFAP. Results are presented as mean ± SD of at least n = 10 (**A**), n = 6 (**D**) and n = 5 (**E** and **F**) mice per treatment group. Levels of statistical significance are indicated as * $P \leq 0.05$, ** $P \leq 0.01$, *** $P \leq 0.001$, **** $P \leq 0.0001$ and n.s.: non-significant. P values determined by one-way ANOVA (**A**) and two-way ANOVA (**D** to **F**).

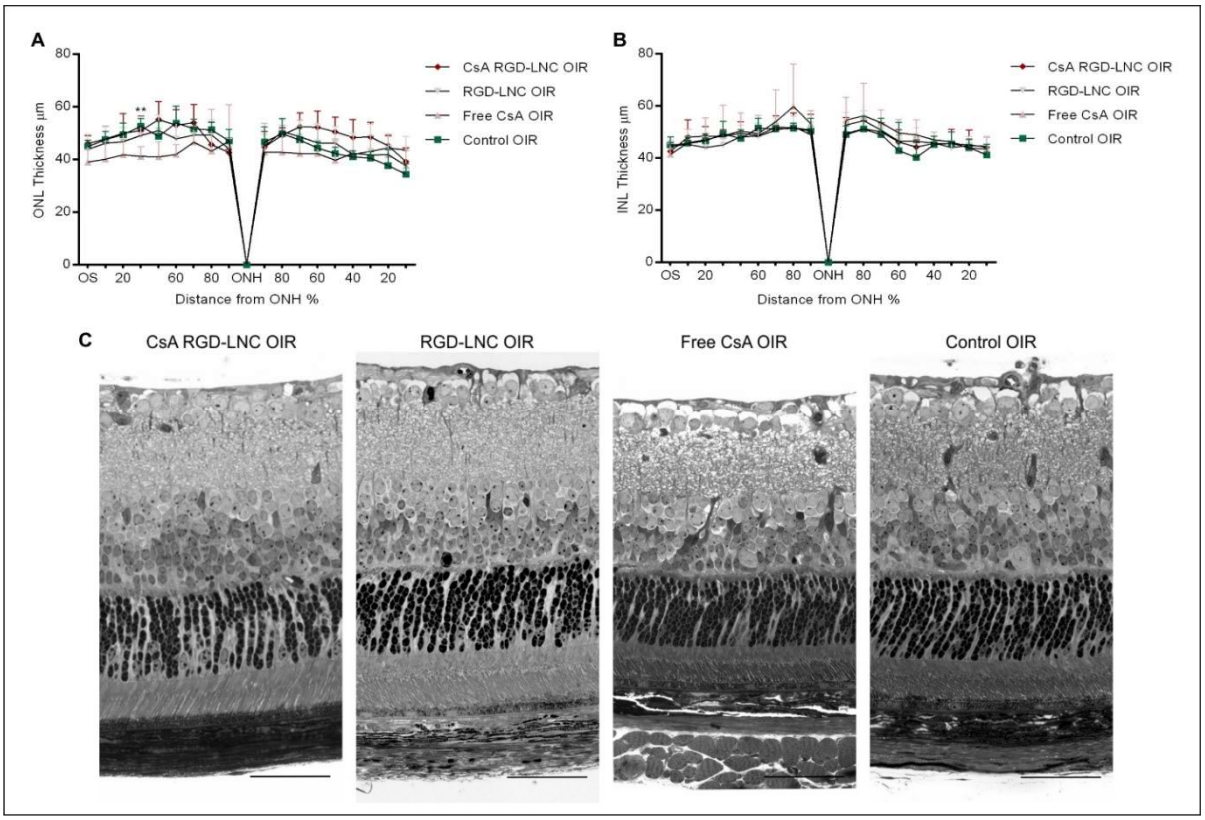


**Figure S4. Therapeutic intervention causes no morphological changes.**

Retinal topography of mice at P17. ONH: optic nerve head. (**A**) Outer nuclear layer (ONL) thickness measurements. ** Comparison of Control OIR and Free CsA OIR. (**B**) Inner nuclear layer (INL) thickness measurements. (**C**) Representative images of the morphologic appearance of photoreceptors and RPE in the central retina of mice at P17 with and without OIR treated with CsA RGD-LNCs, RGD-LNCs or free CsA at P12 compared to control. Level of statistical significance is indicated as ** $P \leq 0.01$, P values determined by one-way ANOVA (**A**), Scale bars: 500 µm.

# Chapter 6

# Summary and Conclusion

# Summary

Research continuously improves our understanding of diseases and promising new pharmacological targets pave the way for novel drugs. Many highly promising drug candidates, however, show limited efficacy due to the inability to sufficiently reach the retina (*1*). While nanoparticle mediated drug delivery could enhance the bioavailability of a plethora of drugs, for various drug classes including small molecules and nucleic acids, targeted delivery to the retina remains challenging (*2*). One key reason is that the retina is a highly conserved tissue shielded from blood circulation by the retinal-blood barrier. To bypass the obstacle present by the retinal-blood barrier, most nanoparticle approaches aiming for retinal drug delivery rely on intravitreal administration of the nanotherapeutic (*3*). However, even though being favorable in terms of enhanced ocular bioavailability, limited off-target distribution and systemic side effects, nanoparticles must first diffuse through the vitreous, penetrate through limiting membranes of the retina, escape retinal immune cells and ultimately specifically address target cells (**Chapter 1**). Furthermore, intravitreal injections are invasive interventions and therefore often come along with serious side effects like intraocular infections, bleedings, and retinal detachment. More so, by being accompanied with patient discomfort, pain, and enormous therapeutic costs, intravitreal therapy often results in lack of patient compliance and are further not available or economically feasible in many parts of the world (*4, 5*).

Since intravenous nanotherapy can improve compliance, safety and therapeutic efficacy, we developed a systemic nanotherapeutic for retinal delivery of Cyclosporin A (CsA), which has been suggested to be a promising drug candidate for ocular diseases (**Chapter 3**): CsA has been associated with an enormous potential for the treatment retinal diseases, due to its synergistic effects on neovascularization, inflammation, and immune system activation. Furthermore, CsA is able to inhibit vascular endothelial growth factor (VEGF) signaling pathways at different intracellular sites in both retinal pigment epithelial (RPE) cells and retinal endothelial cells, counteract transforming growth factor-β (TGF-β) mediated VEGF production in RPE cells and additionally suppress inflammatory and immune responses by interference with cytokine and complement expression (*6–8*). Therefore, endothelial and RPE cell specific CsA drug delivery would bear enormous potential for the treatment of multifactorial degenerative retinal diseases like retinopathy of prematurity (ROP), diabetic retinopathy (DR) and age-related macular degeneration (AMD).

Since enhanced on-site availability of the drug depends on successful internalization of the nanoparticle into target cells, we modified nanoparticles with the αvβ3 integrin-specific ligand cyclo(-Arg-Gly-Asp-D-Phe-Cys) (RGD), to facilitate receptor-mediated uptake into target cells. As intracellular availability of CsA is reflected by therapeutic efficacy of the drug, we investigated the *in vitro* anti-angiogenic efficiency regarding endothelial cell proliferation, growth factor expression and endothelial tube formation. However, even though free CsA revealed distinct anti-angiogenic effects, CsA loaded lipid nanoparticles lacked *in vitro* efficacy, presumable due to limited intracellular availability of the drug. This, however, does not render the nanotherapeutic ineffective, given low *in vitro – in vivo* correlation of nanoparticle formulations due to completely different framework conditions (*9, 10*).

Since most nanoparticle formulations fail to significantly enrich at the target site, consequently lacking therapeutic efficacy, the capability of the designed targeted nanoparticles to efficiently reach the retina and target endothelial as well as RPE cells upon systemic injection was assessed. To further elucidate the route nanoparticles take to reach the RPE, LNCs were simultaneously loaded with fluorescent dye and superparamagnetic iron oxide nanoparticles (Dual LNCs) allowing for complementary broad range imaging and quantification (**Chapter 4**). Dual LNCs were successfully prepared without altering substantial LNC characteristics like size, zeta potential, integrity, and cellular internalization. Therefore, allowing to visualize Dual LNCs in organic tissues after intravenous administration to mice using both fluorescence and transmission electron microscopy.

Accumulation of RGD-LNCs in the eye as well as off-target tissues was assessed accordingly, revealing targeted accumulation of nanoparticles in ocular tissues. By use of fluorescence microscopy, cell specific enrichment in both RPE and retinal endothelial cells after systemic administration to healthy mice was observed (**Chapter 5**). More so, using transmission electron microscopy, it was possible to elucidate the transport mechanism leading to accumulation of RGD-LNCs in RPE cells. However, as LNCs generally mimic characteristics of natural lipoproteins like very low-density and low-density lipoprotein (VLDL and LDL), they follow the same route from the blood-circulation to the RPE (*11, 12*). Like their natural counterparts the 50 - 60 nm LNCs consist of a triglyceride core and a phospholipid shell that binds to lipoprotein receptors like the scavenger receptor CD36 on RPE cells triggering nanoparticle uptake (*13, 14*). Modified with a targeting ligand to facilitate uptake into endothelial cells, RGD-LNCs were able to extravasate from the choriocapillaris, diffuse through the extracellular matrix (Bruch's Membrane) and are finally taken up into adjacent RPE cells. The tremendous potential of RGD-LNCs for retinal drug delivery was further demonstrated by exclusive and cell specific accumulation in RPE and retinal endothelial cells. More so, RGD-LNCs had a distinct residence time in the RPE with substantial nanoparticle amounts being present for at least 5 days after the intravenous injection.

This nanoparticle depot formation in the RPE is another advantage for the delivery of drugs since rapid tissue clearance would be counterbalanced by long-term drug release and enhanced on-site availability. It is hypothesized that CsA loaded RGD-LNCs can be a highly promising tool for the treatment of various retinal diseases, including ROP, DR and AMD in particular given combinatory effects of versatile drug CsA and the drug delivery system able to efficiently target cells vital for pathogenesis.

To investigate exactly this therapeutic potential an ROP mouse model was used (*15*). This model mimics not only the pathogenesis of human ROP, but also the multifactorial pathomechanism consisting of neovascularization, inflammation and immune system activation. In **Chapter 5**, it was shown that one intravenous injection of CsA RGD-LNCs was able to suppress neovascularization, while an identical dose of CsA injected as aqueous solution revealed no effects. A single injection of CsA RGD-LNCs administered directly after the oxygen treatment results in effective prevention of ROP initiation and progression and it was demonstrated that this can be attributed to targeting effects. More so, CsA RGD-LNC treatment significantly decreased elevated VEGF and VEGF receptor levels to physiological levels. Furthermore, CsA RGD-LNCs normalized exaggerated levels of pro-inflammatory cytokines and dampened retinal immune cell reactivity and activation.

Thus, its concrete therapeutic rational, the simplicity of administration and the need of a single application would make this nanotherapeutic a precious tool to fight ROP more efficiently, prophylactically, safer and more costs efficient. This is particularly advantageous for middle- and low-income countries, where the prevalence of ROP is high and the diagnostic and therapeutic capabilities are rather low (*16, 17*). More so, as the nanotherapeutic exerts synergistic therapeutic effects on multiple mechanisms involved in ROP pathophysiology, these findings are further paving the way for comprehensive and causal treatment of various other retinal diseases, including the chronic and progressive DR and AMD.

# Conclusion

This work has elucidated the potential of bio-inspired lipid nanoparticles for targeted retinal drug delivery. The functionalization of lipid nanocapsules (LNCs) with an αvβ3 integrin-specific ligand endowed the particles with the ability to not only target retinal endothelial cells but evade from the systemic circulation and accumulate in RPE cells upon systemic administration. By loading these particles with CsA, therapeutic effects on neovascularization and inflammation were achieved *in vivo*, even though *in vitro* efficacy was lacking. Taken all together, the described findings demonstrate the distinct potential of bio-inspired lipid nanoparticles for retinal drug delivery, as the use of targeted nanoparticles was required to obtain therapeutic effects. It is believed that these findings have the potential to pave the way for the development of a single dose intravenous treatment for ROP. Even though, further research and development is needed to successfully translate the nanotherapeutic into clinics, the nanotherapeutic approach could represent a paradigm shift in neonatal care to a future in which a single intravenous injection of drug loaded nanoparticles is a standard treatment for millions of infants at risk for ROP and further points towards a future of comprehensive and causal therapies for a plethora of degenerative retinal diseases.

# References


1. E. M. del Amo, A.-K. Rimpelä, E. Heikkinen, O. K. Kari, E. Ramsay, T. Lajunen, M. Schmitt, L. Pelkonen, M. Bhattacharya, D. Richardson, A. Subrizi, T. Turunen, M. Reinisalo, J. Itkonen, E. Toropainen, M. Casteleijn, H. Kidron, M. Antopolsky, K.-S. Vellonen, M. Ruponen, A. Urtti, Pharmacokinetic aspects of retinal drug delivery. *Progress in retinal and eye research* **57**, 134–185 (2017).
2. Q. Li, J. Weng, S. N. Wong, W. Y. Thomas Lee, S. F. Chow, Nanoparticulate Drug Delivery to the Retina. *Molecular pharmaceutics* (2020).
3. X. Huang, Y. Chau, Intravitreal nanoparticles for retinal delivery. *Drug discovery today* **24**, 1510–1523 (2019).
4. F. G. Holz, R. Tadayoni, S. Beatty, A. Berger, M. G. Cereda, R. Cortez, C. B. Hoyng, P. Hykin, G. Staurenghi, S. Heldner, T. Bogumil, T. Heah, S. Sivaprasad, Multi-country real-life experience of anti-vascular endothelial growth factor therapy for wet age-related macular degeneration. *The British journal of ophthalmology* **99**, 220–226 (2015).
5. N. Ferrara, A. P. Adamis, Ten years of anti-vascular endothelial growth factor therapy. *Nature reviews. Drug discovery* **15**, 385–403 (2016).
6. P. Rafiee, J. Heidemann, H. Ogawa, N.A. Johnson, P.J. Fisher, M.S. Li, M.F. Otterson, C.P. Johnson, D.G. Binion, Cyclosporin A differentially inhibits multiple steps in VEGF induced angiogenesis in human microvascular endothelial cells through altered intracellular signaling. *Cell Communication and Signaling*, 1–22 (2004).
7. B. A. Nacev, J. O. Liu, Synergistic inhibition of endothelial cell proliferation, tube formation, and sprouting by cyclosporin A and itraconazole. *PloS one* **6**, e24793 (2011).
8. C. Esposito, A. Fornoni, F. Cornacchia, N. Bellotti, G. Fasoli, A. Foschi, I. Mazzucchelli, T. Mazzullo, L. Semeraro, A. Dal Canton, Cyclosporine induces different responses in human epithelial, endothelial and fibroblast cell cultures. *Kidney international* **58**, 123–130 (2000).
9. K. Park, Facing the truth about nanotechnology in drug delivery. *ACS nano* **7**, 7442–7447 (2013).
10. D. Rosenblum, N. Joshi, W. Tao, J. M. Karp, D. Peer, Progress and challenges towards targeted delivery of cancer therapeutics. *Nat Commun* **9**, 1410 (2018).
11. N. Gordiyenko, M. Campos, J. W. Lee, R. N. Fariss, J. Sztein, I. R. Rodriguez, RPE Cells Internalize Low-Density Lipoprotein (LDL) and Oxidized LDL (oxLDL) in Large Quantities In Vitro and In Vivo. *Invest. Ophthalmol. Vis. Sci.* **45**, 2822 (2004).
12. I. A. Pikuleva, C. A. Curcio, Cholesterol in the retina. *Progress in retinal and eye research* **41**, 64–89 (2014).
13. B. Heurtault, P. Saulnier, B. Pech, A Novel Phase Inversion-Based Process for the Preparation of Lipid Nanocarriers. *Pharmaceutical Research*, 875–880 (2002).
14. K C Hayes, S Lindsey, Z F Stephan, D Brecker, Retinal pigment epithelium possesses both LDL and scavenger receptor activity. *Invest. Ophthalmol. Vis. Sci.* **30**, 225–232 (1989).
15. K. M. Connor, N. M. Krah, R. J. Dennison, C. M. Aderman, J. Chen, K. I. Guerin, P. Sapieha, A. Stahl, K. L. Willett, L. E. H. Smith, Quantification of oxygen-induced retinopathy in the mouse. *Nature protocols* **4**, 1565–1573 (2009).
16. G. E. Quinn, Retinopathy of prematurity blindness worldwide. *Eye and brain* **8**, 31–36 (2016).
17. S. J. Kim, A. D. Port, R. Swan, J. P. Campbell, R. V. P. Chan, M. F. Chiang, Retinopathy of prematurity. *Survey of Ophthalmology* **63**, 618–637 (2018).

# Appendix

# Abbreviations

| | |
|---|---|
| A2E | Pyridinium bis-retinoid N-retinylidene-N-retinylethanolamine |
| AGE | Advanced glycosylation end products |
| AMD | Age-related macular degeneration |
| ARPE-19 | Human retina pigment epithelial cells |
| BM | Bruch's membrane |
| BM | Endothelial cell basal medium MV |
| BRB | Blood-retinal-barrier |
| BSA | Bovine serum albumin |
| C | Complement component |
| CLSM | Confocal laser scanning microscopy |
| CNTF | Ciliary neurotrophic factor |
| CsA | Cyclosporin A |
| CsD | Cyclosporin D |
| DAPI | 4′,6-diamidino-2-phenylindole |
| DHA | Docosahexaenoic acid |
| DiD | 1,1-dioctadecyl-3,3,3′,3′-tetramethylindodicarbocyanine perchlorate |
| DiI | 1,1-Dioctadecyl-3,3,3',3'-tetramethylindocarbocyanine perchlorate |
| DiO | 3,3-Dioctadecyloxacarbocyanine perchlorate |
| DLS | Dynamic light scattering |
| DMSO | Dimethyl sulfoxide |
| DNA | Deoxyribonucleic acid |
| DPBS | Dulbecco’s phosphate buffered saline |
| DR | Diabetic retinopathy |
| ELISA | Enzyme-linked immunosorbent assay |

| | |
|---|---|
| EMEM | Eagle's minimal essential medium |
| FACS | Fluorescent-activated flow cytometry |
| FCS | Fetal calf serum |
| FGF | Fibroblast growth factors |
| FRET | Fluorescence resonance energy transfer |
| GFAP | Glial fibrillary acidic protein |
| GM | Endothelial cell growth medium MV |
| HDMECs | Human dermal microvascular endothelial cells |
| i.v. | intravenous |
| ICP-OES | Inductively coupled plasma optical emission spectroscopy |
| IGF | Insulin-like growth factor |
| IL | Interleukin |
| ILM | Inner limiting membrane |
| It | Itraconazole |
| L. R. white | London Resin white |
| LDL | Low-density lipoprotein |
| LEDGF | Lens epithelium-derived growth factor |
| LNC | Lipid nanocapsule |
| MCT | Miglyol® 812 (medium chain triglycerides) |
| MHC | Major histocompatibility complex |
| MRI | Magnetic resonance imaging |
| MS | Mass spectrometry |
| MTT | 3-(4,5-Dimethyl-2-thiazolyl)-2,5-diphenyl-2H-tetrazolium bromide |
| NP | Nanoparticle |
| OIR | Oxygen induced retinopathy |
| OLM | Outer limiting membrane |

| | |
|---|---|
| P | Postnatal day |
| PBS | Phosphate buffered saline |
| PDGF | Platelet-derived growth factor |
| PEDF | Pigment epithelium-derived factor |
| PFA | Paraformaldehyde |
| PLGA | Poly-(lactide-co-glycolide) |
| PVR | Proliferative vitreoretinopathy |
| qdots | Quantum dots |
| RC | Regenerated cellulose |
| RGD | cyclo(-Arg-Gly-Asp-D-Phe-Cys) |
| RNA | Ribonucleic acid |
| ROP | Retinopathy of prematurity |
| ROS | Reactive oxygen species |
| RPE | Retinal pigment epithelium |
| RT-qPCR | Real-time quantitative polymerase chain reaction |
| SDS | Sodium dodecyl sulfate |
| SPION | Superparamagnetic iron oxide nanoparticle |
| TEM | Transmission electron microscopy |
| TGF-β | Transforming growth factor-β |
| TNF-α | Tumor necrosis factor-α |
| UHPLC | Ultra high-performance liquid chromatography |
| VEGF | Vascular endothelial growth factor |
| VEGF-R2 | Vascular endothelial growth factor receptor type 2 |
| VLDL | Very low-density lipoprotein |
| ZP | Zeta potential |

# Curriculum Vitae

| | |
|---|---|
| **Name:** | Marilena Sabine Bohley |
| **Date of birth:** | 6th of July 1991 |
| **Place of birth:** | Coburg (Germany) |
| **Nationality:** | German |

**Scientific education and work experience**

| | |
|---|---|
| 07/2017 – 08/2021 | **PhD Candidate/Research Assistant**<br>Department of Pharmaceutical Technology<br>University of Regensburg |
| 07/2017 – 08/2021 | **Structured doctorate program**<br>Graduate school ChemPharm<br>Faculty of Chemistry and Pharmacy<br>University of Regensburg |
| 12/2016 | **Licensure as Pharmacist** |
| 05/2016 – 11/2016 | **Practical Training**<br>Einhorn Apotheke, Nuremberg |
| 11/2015 – 04/2016 | **Practical Training**<br>Dr. Pfleger Arzneimittel GmbH, Bamberg |
| 07/2015 | **Research Intern/ DAAD scholarship**<br>Hoshi University, Tokyo |
| 03/2015 | **Research Intern**<br>Chair for Drug formulation and delivery<br>Julius-Maximilians University Würzburg |
| 04/2014 – 04/2015 | **Undergraduate Research Assistant/Tutor**<br>**I**nstitute for Pharmacy and Food Chemistry<br>Julius-Maximilians University Würzburg |
| 10/2011 – 10/2015 | **Study of Pharmacy**<br>Julius-Maximilians University Würzburg |

**School Education**

| | |
|---|---|
| 04/2011 | **Abitur/A levels** |
| 09/2002 – 04/2011 | **Grammar School**<br>Arnold Gymnasium, Neustadt b. Coburg |

# List of Publications

**Peer-reviewed publications**

1. **M. Bohley**, E. Birch, F. Baumann, A. Dillinger, E. Tamm, A. Goepferich: Design of dye and superparamagnetic iron oxide nanoparticle loaded lipid nanocapsules with dual detectability in vitro and in vivo. In: International Journal of Pharmaceutics 2020, 585, 119433 (**Chapter 4**)

2. **M. Bohley**, A. Haunberger, A. Goepferich: Intracellular availability of poorly soluble drugs from lipid nanocapsules. In: European Journal of Pharmaceutics and Biopharmaceutics 2019,139, 23-32 (**Chapter 3**)

**Conference abstracts**

1. **M. Bohley**, A. Goepferich: Targeted cyclosporin A nanoparticles enable cell-specific anti-VEGF therapy. PRO RETINA Research Colloquium Potsdam, Germany, 2021.

2. **M. Bohley**, E. Birch, F. Baumann, A. Goepferich: Design of Dye and SPION loaded Lipid Nanocapsules for dual detectability. World Meeting on Pharmaceutics, Biopharmaceutics and Pharmaceutical Technology, 2021.

3. **M. Bohley**, A. Goepferich: Cyclosporin A loaded lipid nanoparticles for the intravenous treatment of retinopathy of prematurity. European and Global CLINAM-Summit, 2020.

4. **M. Bohley**, A. Goepferich: RGD-peptide grafted Lipid Nanocapsules (LNC) for drug delivery to the posterior eye. Controlled Release Society Annual Meeting & Exposition, Valencia, Spain, 2019.

5. **M. Bohley**, A. Goepferich: Intracellular availability of poorly soluble drugs from lipid nanocapsules. Controlled Release Society German Chapter Meeting, Leipzig, Germany, 2019.

**Patent**

1. **M. Bohley**, A. Goepferich. 2020. A nanoparticle for use in the treatment of an ocular disease. Submitted as European Patent, EP20162277. Patent pending.

# Acknowledgements

First and foremost I would like to express my deepest gratitude to Professor Achim Göpferich for giving me the opportunity to be part of his research group and for entrusting me with this engaging project. I am deeply thankful for his unconditional support, his continued enthusiasm for this project, his valuable intellectual contributions, the many fruitful discussions we had and for providing me with the opportunity to attend several meetings, conferences, and trainings. I appreciate all his contributions of time and ideas while at the same time he gave me the freedom to pursue my own ideas and make my own mistakes. More so, his incomparable ability to put things in a new light always inspired me to "think out of the box", finding novel solutions, hypotheses, and scientific questions. During the last four years, he encouraged me to continuous growth, which I am deeply thankful for and certainly will miss.

Furthermore, I want to thank Professor Ernst Tamm for his invaluable guidance as my graduate school mentor and during our research cooperation. I thank him for the opportunity to be a part of his research group, surrounded by exceptional people. His profound expertise provided extremely helpful scientific input for my work, facilitated my continuous learning about the eye and heightened the motivation for the project.
In this regard I'd like to thank Dr. Andrea Dillinger, for being an exceptional cooperation partner, postdoc and friend. Her fascination and motivation for research always inspired and motivated me. I appreciate her open nature that made me feel at home at the Department of Human Anatomy and Embryology. I am deeply thankful for the always productive meetings and chats which decisively contributed to the success of the project and further made me truly enjoy our time working together.

I express my deep gratitude to all my former and present colleagues in the research group of Pharmaceutical Technology. They created an atmosphere of companionship and made the 'Lab' feel like a second home. In this regard, a special 'thanks' goes out to:

> Moritz Graf and Christian Ziegler for being the perfect lab-mates, creating a very enjoyable work atmosphere, helping me out in countless situations and being always enjoyable conversation partners.
>
> Sebastian Beck and Dr. Sara Maslanka Figueroa for hilarious, inspiring, and motivating conversations in- and outside the lab.

Dr. Stefanie Thalhauser for our numerous fantastic conversations, our coffee strolls, and our lasting friendship, which I truly value.

And a very special thanks goes to Monika Stahl, for her unconditional support and friendship, our endless and always up-lifting conversations, lunch breaks and wine dates. I am truly thankful that we've met.

Moreover, I'd like to thank Emily Birch for her passion, patience, and dedication to our project. I am very grateful for becoming friends and keeping in touch with each other.

I also want to thank all my former and present cooperation-colleagues in the research group of Human Anatomy and Embryology for always having an open ear and a helping hand whenever I struggled with 'Biology'. Thank you for letting me be part of the team.

Furthermore, I thank Eva Wrobel for her amazing organization skills and her caring nature.

I am truly grateful for the excellent technical assistants I had the pleasure to work with during the last years. I especially would like to thank Renate Liebl for sharing her cell culture expertise with me and her invaluable support with the cell culture experiments during my first year. Furthermore, I thank Silvia Babl, Elke Stauber and Angelika Back for their excellent technical advice and support and our cheerful chats.

The German Research Foundation (DFG) is acknowledged for providing financial support for my project.

Additionally, I'd like to thank the Girls Squad for their endless support, trust, and love and for never letting me down.

A very special thanks goes to M&P, without whom this would not have been possible, for their never-ending support, encouragement to be myself and unconditional love and for being the most loving parents one could imagine.

And lastly, I'd like to give a special 'thank you' to P for introducing me in the fascinating world of natural science, for encouraging me to never stop asking questions and always striving to find the answers - and thank you for always reminding me 'Kommt Zeit, kommt Rat'.

# Declaration in lieu of an oath

I hereby declare that I have completed the dissertation presented without the impermissible help of third parties, without the use of resources other than those indicated, and that any data and concepts stemming directly or indirectly from other sources are indicated with citations to the literature.

No further persons were involved with the creation of the contents of the dissertation presented. In particular, I have not made use of the assistance of a doctoral consultant or other person in return for payment. No-one has received payment in kind either directly or indirectly for work which is associated with the content of the dissertation submitted.

The dissertation has not been submitted in the same or similar form to another examining authority, neither in Germany nor abroad.

Regensburg, 05.08.2021 _____

(Marilena Bohley)